MODELING AND CONTROL OF THE SOLID-LIQUID INTERFACE SHAPE DURING CRYSTAL GROWTH

A Dissertation

Presented to

The Graduate Faculty of The University of Akron

In Partial Fulfillment

of the Requirements for the Degree

Doctor of Philosophy

Arvind Srinivasan

December 1994

MODELING AND CONTROL OF THE

SOLID-LIQUID INTERFACE SHAPE

DURING CRYSTAL GROWTH

Arvind Srinivasan

Dissertation

Approved:

Advisor

Committee Member

Committee Member

Committee Member

Committee Member

Committee Member

Accepted:

Department Head

Dean of the College

Dean of the Graduate School

01 Dec 1994

Date

ABSTRACT

This dissertation proposes "feedback control" techniques to achieve the desirable solid-liquid interface shape during crystal growth to produce high quality material. The feedback controller is designed utilizing a state-space model of the crystal-growth process. This model is obtained by lumping the governing equations determined using the apparent heat capacity formulation through finite-elements.

To gain insight into the control design procedures, the heat conduction problem with no phase change is first considered. Here, a controller is designed using the standard design techniques to improve the transient response and to establish a desirable temperature distribution inside the material. A similar approach is taken to design controllers that would establish an arbitrary temperature distribution and, hence, the interface shape for heat conduction problems with phase change. Some general conditions are derived for the existence of a boundary control to establish a given temperature distribution in the steady-state.

The proposed control method is used to establish a certain distribution on a simulated heat conduction system. Control simulation results are presented for the heat-conduction system with no phase change and then for the system with phase-change problem.

The system designed by the proposed technique is able to translate the interface at the desired rate while maintaining the desired interface shape. The results validate the use of feedback control techniques for the boundary control of a diffusion dominated crystal growth problem.

ACKNOWLEDGMENTS

I would like to take this opportunity to thank Dr. Celal Batur, for guiding me in all my research efforts, for shaping and provoking my thought process, and for taking the efforts to find me financial support during this graduate study. It gives me a great pleasure to be able to thank Mr. Bruce Rosenthal for providing me with all necessary resources, and software packages to conduct research at NASA Lewis Research Center and for constantly working with the badge control office to provide me the access to the facilities at NASA. The cooperation extended to me by the dissertation committee members: Dr. De-Abreu, Dr. Duval, Dr. Hartley, Dr. Padovan, Dr. Veillette, Dr. Young is commendable and I am grateful for their constructive criticisms, encouragement's, and suggestions. There are several others who have made positive effect during my graduate studies at Akron. One of them is Dr. T. Srivatsan who has always extended his support to me in all possible ways. Others include Dr. Balasubramaniam for providing valuable insights, Ram for helping me to communicate with the committee members, Dr. Kassemi for his valuable suggestion during the start of this dissertation, and Mr. Natrajan Ramachandran for believing in my abilities. I am very grateful to all my friends who have made this study period fun and memorable. Though redundant, I thank my parents and my brothers for their love and affection. Finally, I would like to thank NASA Lewis Research Center, Processing Science Technology Branch for providing me financial support during the course of this study.

TABLE OF CONTENTS

LIST OF TABLES

LIST OF FIGURES

CHAPTER I

INTRODUCTION

In recent years, there has been a considerable interest in the directional solidification processing technique to develop materials with improved structural properties. In this approach, the molten material enclosed in an ampoule is subjected to a temperature gradient that includes its solidification temperature. An important objective is to produce material with desirable structural properties consistently. Examples of desired structural properties are reduced residual thermal stress, higher yield strength, material toughness, and a homogenous refractive index.

One way to achieve the desired objective is to measure the structural property "on-line" and modify the process parameters, i.e., the temperature gradient and translation rate of the ampoule accordingly. However, the implementation of this procedure poses several practical problems:

(a) On-line measurements of the structural property are not possible.

(b) The relationship between the structural property and the axial temperature gradient, translation rate in the furnace is not known. Hence, even if the measurements are available, it would be difficult to use them for controlling the process.

(c) It is difficult to maintain an arbitrary temperature gradient around the ampoule.

There are other intermediate quantities that are related to the structural property. The interface shape during solidification determines the crystal quality. Another important parameter that controls the growth rate of the material is the translation rate of the ampoule. For example, a flat interface would yield reduced thermal stresses in the material. Hence, the crystal quality can be significantly improved by varying the

temperature gradient and setting the translation rate optimally inside the furnace to produce the desirable interface shape during the crystal growth process. The statements (a), (b), and (c) given above are pertinent as discussed in the rest of this Section.

Regarding the issue in (a), the interface shape can be directly measured through X-rays in the case of non-transparent material or by image processing techniques for transparent furnaces. Also, it is possible to predict the interface shape by measuring auxiliary quantities such as the ampoule surface temperature. A mathematical model obtained by considering the physics of the problem can be used for this purpose.

With respect to the issue in (b), it is difficult to find the furnace temperature gradient and the translation rate that would yield the desirable interface shape. In the past, the furnace operator would tune the temperature gradients and the translation rate to achieve this. More recently, an optimization approach [1] has been taken to determine the temperature gradient. This approach cannot take advantage of any on-line measurements to correct any modeling errors. In control terminologies, this approach just yields "open-loop" temperature gradients. This work proposes a new approach to determine the furnace temperature gradient by using the on-line measurements to establish a desired interface shape and the grow the crystal at a desired translation rate.

Regarding the issue in (c), the furnace provides the hardware to establish the temperature gradient that is requested by the controller. Many types of furnaces are available, of which the multi-zone furnaces allow for a variety of temperature profiles inside the furnace. Here, an increased number of zones can implement the required temperature profile across the ampoule more accurately.

1.1 Proposed Technique

A new approach is proposed to model the crystal growth process and control the shape of the interface and the crystal growth rate by making use of all available

measurements. The ultimate aim of this research is to achieve the desired interface shape and growth rate by altering the temperature profile at the boundary. The heat transfer process that determines the interface shape is modeled using the Finite Element (FE) technique. This model is utilized to predict the interface shape (in situations where the interface cannot be directly measured) and also to determine the required temperature gradients.

1.2 Crystal Growth Modeling

The crystal growth problem can be modeled through a set of Partial Differential Equations (PDE) with appropriate Boundary Conditions (BC). The interface shape during crystal growth is determined by conduction, convection and radiation heat transfer modes. Depending on the materials, one mode of heat transfer is significantly more dominant than the other. For example, in the case of the electronic and photonic materials, heat conduction is the dominant mode due to high magnitude of thermal conductivity. This work attempts to demonstrate some of the capabilities of feedback controls. In an effort to keep the problem simple, only the conduction heat transfer mode is assumed to determine the temperature distribution inside the material.

The heat conduction process is described by a set of PDEs and in control terminology represents a Distributed Parameter System (DPS). In the controls area, it is customary to describe a system by a set of Ordinary Differential Equations (ODE). The PDEs, conceptually, can be considered as infinite dimensional ODEs. Thus, this research addresses into the topic of DPS or infinite dimensional systems. Research in these areas has been very active in the last decade, especially, with regard to space structures.

Most of the existing techniques handle this problem by approximating (lumping) the infinite dimensional system with a finite dimensional system. In this dissertation, a spatially lumped model of the system is obtained through FE technique. This model is in

the standard state-space form and can be directly used to determine the necessary temperature gradients. The nodal temperatures are the state variables, the parameterized temperature gradients are the inputs and all available measurements, such as the ampoule surface temperature, and interface location, form the output of the system.

1.3 Controller Design

The FE based state-space model can be used to determine the necessary inputs (temperature gradients) so that a desired temperature distribution (interface shape) is established inside the material. The model has many state variables and relatively few inputs and measurements. Hence, it is natural to expect some of the state variables (nodal temperatures) to be completely/weakly controllable or observable. These state variables cannot be used for feedback and hence the controller is designed using a reduced order model. The controller designed using the reduced order model may not be able to produce an arbitrary temperature distribution inside the material (interface shape). Some necessary and sufficient conditions for the requested temperature distribution to be achievable are derived in this dissertation.

1.4 Organization of the Dissertation

The need for interface shape control is motivated by the objective of producing materials with improved structural properties. A method for controlling the shape of the interface is proposed in this work. In Chapter II, a brief study of various crystal growth modeling techniques is provided. Also, the developments in the modeling and control of Distributed Parameter Systems (DPS) are summarized. In Chapter III, the approach to solving the interface-shape control problem is presented. The finite element based state-space modeling of a general heat conduction PDE with arbitrary boundary conditions is presented in Chapter IV. Necessary and sufficient conditions for setting up an achievable distribution inside the continuum are derived in Chapter V. The FE formulation for the

phase change problem is presented in Chapter VI. Results associated with the control of interface shape using the FE model is presented in Chapter VII. A summary of this dissertation is provided in Chapter VIII.

CHAPTER II

BACKGROUND STUDY

Crystals can be grown by subjecting the pure molten compound encapsulated inside an ampoule to a temperature profile which includes its solidification temperature. Continuous solidification of the melt can be achieved by one of the two techniques: In the first approach, a Stationary Temperature Gradient (STG) is established inside the furnace and the ampoule is translated axially at a constant speed across the gradient. In the second method known as Electro Dynamic Gradient (EDG) control [2], the ampoule is held stationary and the temperature gradient is translated along the vertical axis of the furnace. In either case, the furnace is used to establish the temperature gradient around the ampoule. In the next section, various furnace construction techniques are reviewed.

2.1 Furnace Construction Techniques

The original Bridgman furnace developed in 1925 by Bridgman to directionally solidify crystal is shown in Figure 2.1. This furnace has only one heating zone and is heated to a temperature higher than the material's melting point. A wire and a translation mechanism is used to support and translate the ampoule from the hot zone to room temperature. The achievable temperature gradient of this furnace is limited and can be varied by changing the temperature of the heating zone.

The Stockbarger furnace developed in 1936 improved the capabilities of the Bridgman furnace by introducing a controllable cold zone. The crucible is supported by a pedestal and lowered out of the bottom of the furnace. The temperature gradient is a

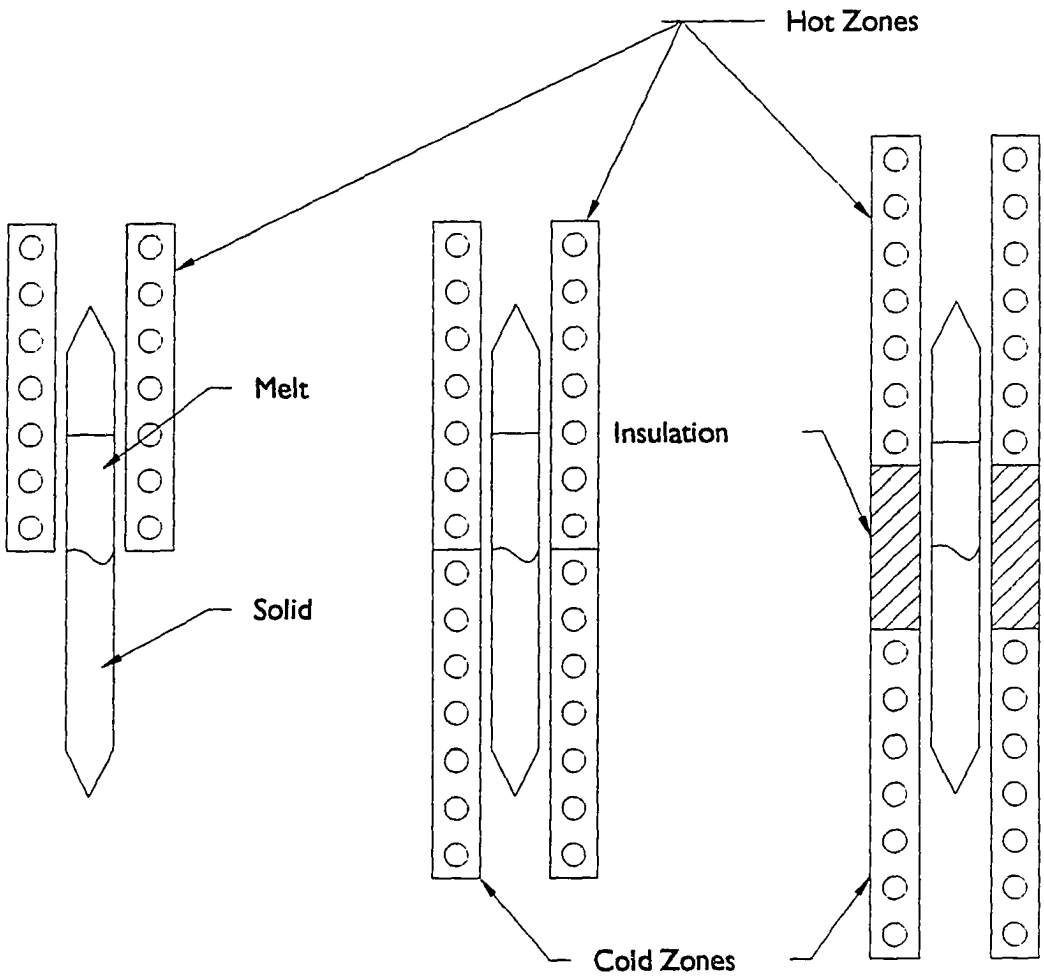

Figure 2.1. Various crystal growth furnaces

function of the temperature difference between the hot and cold zones and the heat transfer out of the bottom of the pedestal. Under this configuration, the furnace can maintain a steeper temperature gradient than the original Bridgman furnace and therefore gives an improved crystal growth rate.

In the modified Bridgman-Stockbarger furnace, a section of insulating material is placed between the hot and cold zones of the Stockbarger furnace to increase the controllability of the temperature gradient during the crystal growth. The temperature gradient inside the furnace is determined by the length of the insulation and the temperature difference between the hot and cold zones.

One of the latest furnace designs known as the Mellen EDG furnace emulates the growth characteristics of the Bridgman-Stockbarger furnace with many small heating zones. Each heating zone contains four radial heaters in order to control both the radial and longitudinal temperature profile.

Currently, there is a trend towards using multi-zone furnaces. Multi-zone furnaces allow for a variety of temperature profiles inside the furnace. An increased number of zones provides better control of the temperature profiles. Multi-zone furnaces can be constructed to operate as STG or EDG. In the case of EDG, more zones are needed to translate the temperature profile in a smooth fashion.

The furnace provides the hardware to establish the temperature gradient. The following Sections review furnace temperature control techniques.

2.2 Furnace Temperature Control Techniques

The initial Bridgman, Stockbarger furnaces have been controlled by open loop gain controller. The Bridgman-Stockbarger furnace has been controlled by open loop proportional gain and feedback Proportional Integral Derivative (PID) controllers. In the case of the Mellen EDG furnace, each zone has been independently controlled by a PID

controller with temperature feedback. In all these cases, control parameters have been found either by trial and error or by some kind of ad-hoc techniques and then fine tuned to improve performance of the controller.

The open loop system may experience an unrecoverable error, and the PID controller may produce sub-optimal transients. The sub-optimal transients may include undesirable temperature fluctuations or prolonged reference errors. To overcome this, self-tuning controllers using Single Input Single Output (SISO) and Multi Input Multi Output (MIMO) input-output models have been used to control the furnace [3], [4], [5]. More recently, low-order output-feedback controllers have been designed using a state-space model of the furnace through the projective control approach [6], [7].

The reference zone-temperature must be selected in such a way that the solidified crystals have certain desirable properties, such as low thermal stresses, and few crystalline imperfections. The shape of the solid-liquid interface is related to the crystal properties. Chang and Wilcox [8] showed that a planar solid-liquid interface minimizes the residual thermal stresses and crystalline imperfections. Singh et.al [9] have shown that the shape of the interface is determined by the magnitude of the imposed temperature gradient and the translational velocity of the ampoule. Hence, the reference zone-temperature must be selected to produce the desired interface shape.

To accomplish this, Taghavi and Duval, [10] solved the inverse heat transfer problem for a simplified furnace analytically to determine a furnace temperature profile that would result in a flat interface. Dantzig et. al [1] used a FE model of the furnace to find the necessary furnace temperature profile for a flat interface. The necessary furnace zone temperatures in their case are found as a solution to an optimization problem. These two methods can be used to determine the necessary temperature profile off-line. However, owing to inevitable modeling errors, this solution may not produce the desirable

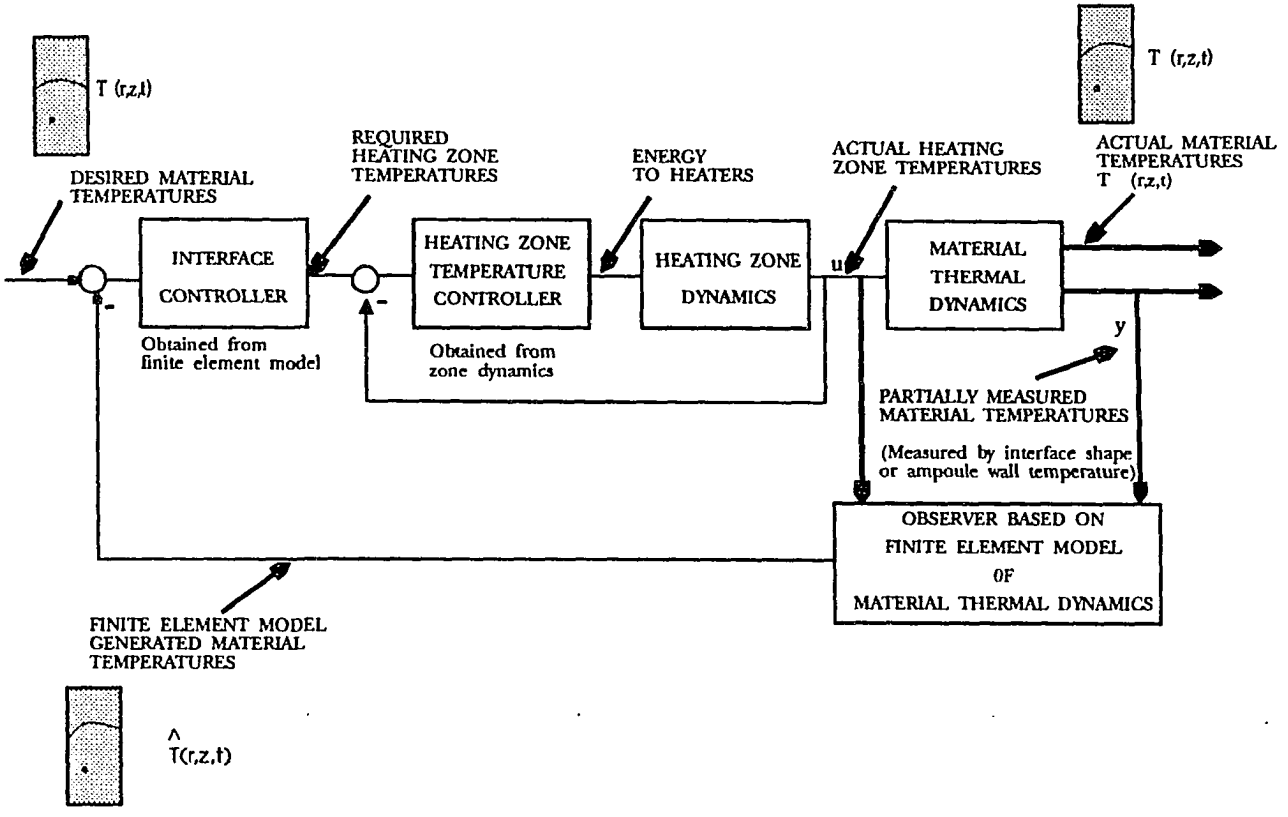

Figure 2.2 Proposed method to control the shape of the interface.

interface shape. The control philosophy to overcome such problems is to use on-line measurements for feedback. In this work, a controller is designed that makes use of measurements to determine the necessary temperature gradient as in Figure 2.2. The proposed method requires a model of the crystal growth process. This modeling of the process is considered in the following section.

2.3 Modeling of Crystal Growth

The interface shape during crystal growth is determined by conduction, convection and radiation heat transfers modes. Depending on the materials, one mode of heat transfer is significantly more dominant than others. For example, in the case of the electronic and acousto-optic materials, under certain conditions, heat conduction is the dominant mode [42]. The main idea in this dissertation is to solve the inverse problem to establish a desired interface shape. This is a difficult problem, accounting for all dynamics will make it almost impossible to solve with the available resources. Therefore, as a first cut, we consider heat-conduction as the primary mode of heat-transfer and ignore all other phenomena.

The dynamics for the crystal interface shape inside an ampoule is assumed to be primarily governed by the conduction equation

$$\rho c \frac{\partial T}{\partial t} = \nabla \cdot (k \nabla T), \tag{2.1}$$

where ρ is the density, c is the heat capacity, k is the thermal conductivity of the material and T is the temperature. In any crystal growth problem, the material is undergoing a phase change. The material properties are usually different for the solid and the liquid region. In addition when solidification occurs, energy due to latent heat of fusion is released. This introduces an additional energy equation for the interface region. The mathematical model for the heat conduction problem with phase change, also known as the Stefan's problem, includes two heat conduction equations; one each for solid and liquid

regions and a solid/liquid interface condition. The model is described by the following set of equations [11]

$$\begin{aligned} \rho_l c_l \frac{\partial T}{\partial t} &= \nabla \cdot (k_l \nabla T) && \text{Liquid region,} \\ \rho_s c_s \frac{\partial T}{\partial t} &= \nabla \cdot (k_s \nabla T) && \text{Solid region,} \\ k_s \frac{\partial T}{\partial n} - k_l \frac{\partial T}{\partial n} &= \rho L v_n && \text{At the Interface,} \end{aligned} \tag{2.2}$$

where the subscript '*l*' corresponds to properties of the material in the liquid region and subscript '*s*' corresponds to material properties in the solid region. n is in the unit normal into the liquid region, v_n is the velocity of the interface along the unit normal, and L is the latent heat of solidification. There are additional boundary conditions that depend on the geometry of the ampoule, and the type of furnace. These boundary conditions usually make the problem more complicated.

The interface shape during crystal growth is determined by conduction, convection and radiation heat transfers modes. Depending on the materials, one mode of heat transfer is significantly more dominant than others. For example, in the case of the electronic and photonic materials, heat conduction is the dominant mode due to high magnitude of thermal conductivity.

Other phenomena such as convection and radiation affect the crystal growth dynamics. Inside the liquid region, the fluid move around due to convection affecting the temperature distribution. Simulation and experimental studies on the effect of convection over the interface shape can be found in [12], [13]. In [12], it is shown that convection has significant effect on the interface shape for horizontal furnaces. However, for semi-conductor materials inside a vertical multi-zone furnace the effect of convection on the interface shape is not significant due to the magnitude of thermal conductivity coefficients.

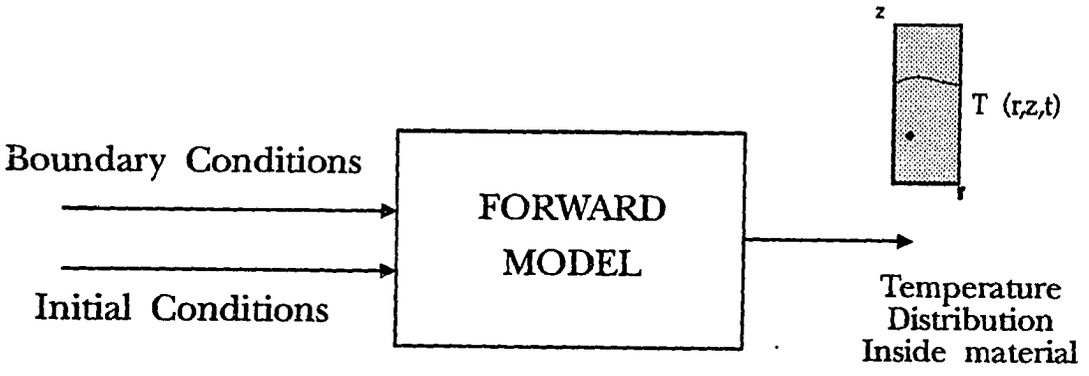

Figure 2.3 Representation of forward problem.

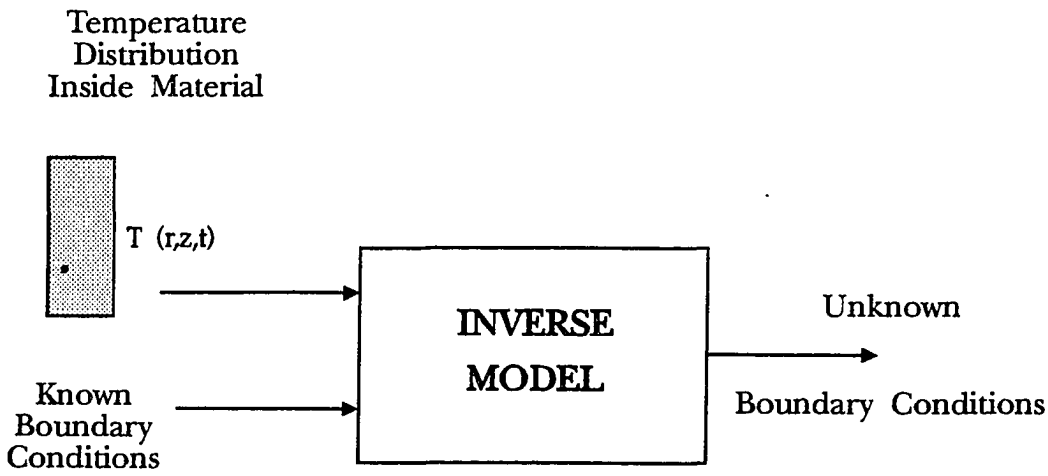

Figure 2.4 Representation of inverse problem.

This fact coupled with the idea of keeping the problem simple, it is assumed that only conduction heat-transfer affects the interface shape. All other effects are neglected.

Phase change occurs in different forms depending on the type of material involved [14]. In pure materials, the phase change region has distinct solid and liquid regions separated by a smooth and continuous interface. For metal alloys, the interface is mushy, i.e., the interface has a complex shape and is not necessarily smooth and continuous. In materials like wax or polymers, the solid and liquid phases are fully dispersed throughout the region with no distinct interface. In this dissertation, as we are dealing with pure materials, it is assumed that there is a smooth and continuous interface with a distinct solid and liquid phases.

2.4 Definition of the Forward and Inverse Problems

It is imperative to find the temperature distribution or the interface location for the given boundary conditions and initial conditions as illustrated in Figure 2.3. Within this dissertation, this is referred to as the "forward" problem. In a similar fashion, the "inverse problem" corresponds to finding the necessary BC for a desired temperature distribution or interface location, and is given in Figure 2.4.

2.5 Solutions to Forward Problem

A number of research articles have appeared in the last few years to solve the forward problem. The main difficulty in solving the forward problem is the movement of the interface surface. The rate at which this movement occurs depends on the heat removal rate at the interface surface region. The heat removal rate is dependent on the material's properties, which are usually temperature dependent or at least depend on the state[1] of the material. This phenomenon introduces non-linearities in the problem.

---

[1] solid or liquid

Further, the rate of travel of the interface is not known *a priori*. This rate is needed to make a heat balance across the interface to solve for the temperature distribution. Hence, an iterative scheme is needed to solve the forward problem. This introduces yet another non-linearity.

2.5.1 Analytical and Semi-Analytical Methods

Many analytical solutions are available in the literature to solve the 1-D Stefan problem with specific boundary conditions [15], [16]. Sukanek [17], [18] found an approximate quasi steady-state solution to the 1-D Stefan problem in a Bridgman-Stockbarger furnace using the perturbation technique. A few results are available for the 2-D case with simplified geometries and BC's [19], [20]. Even for the simplified geometries, most of the analytical results provide only the steady-state solution. It is very difficult to obtain analytical solutions for the transient problem even for simple geometries and BC's. In these situations, the solution is found using numerical techniques.

2.5.2 Numerical Methods

The numerical techniques depending on the choice of dependent variables can be broadly classified into two categories: frontal tracking methods, and fixed grid techniques [21].

2.5.2.1 Frontal Tracking Methods

In the frontal tracking method [11], valid for phase change problems with a distinct interface, the temperature is the sole dependent variable. Conduction energy equations are written for the solid and liquid regions. The boundaries of the solid and the liquid region are determined by the interface location, which is unknown. To overcome this problem, the interface position is assumed and the conduction equation is solved to determine the temperature distribution using either Finite Element Method (FEM) [22] or Finite Difference Method (FDM) [23]. Using the temperature information, the assumed

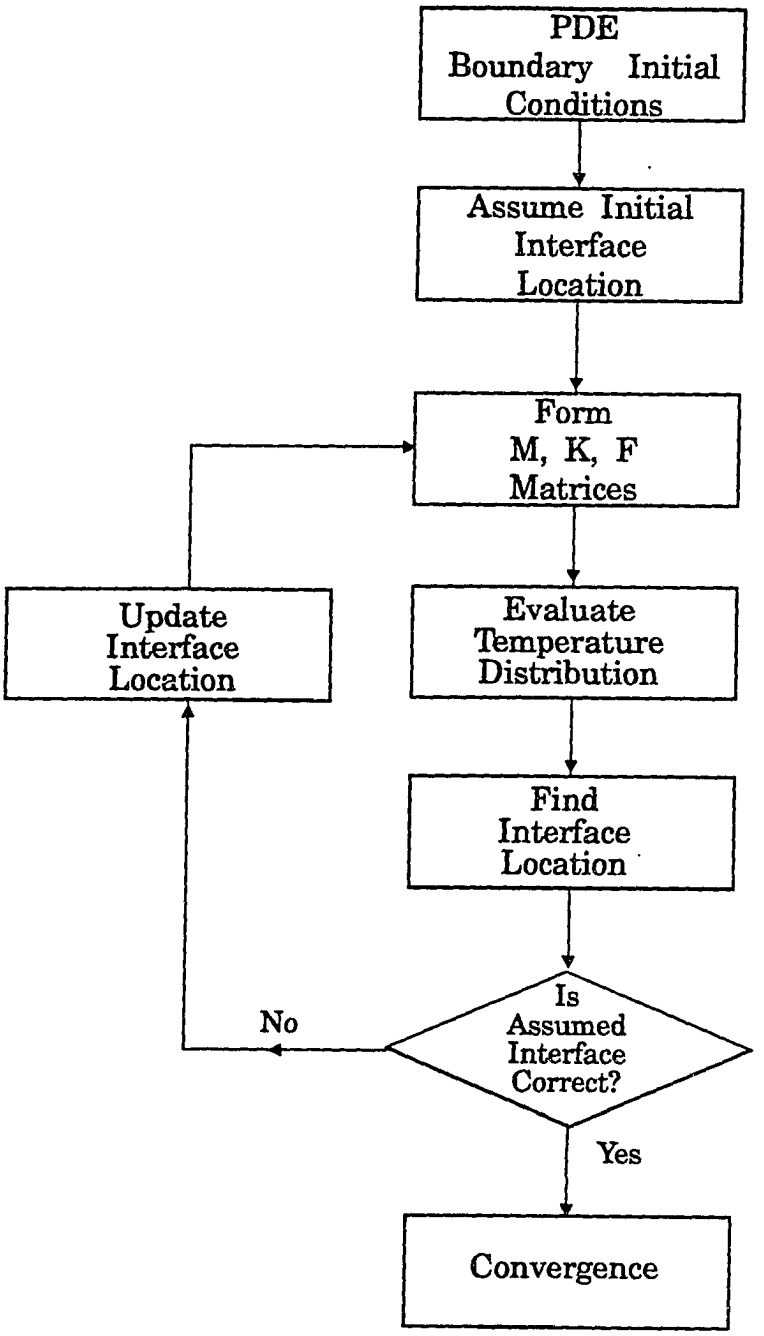

Figure 2.5 Iterative scheme to locate the interface shape and location.

interface position is adjusted. This process is repeated until convergence occurs. The general procedure can be seen in Figure 2.5. The FEM or the FDM essentially discretizes the solid and liquid regions. It is very difficult to accurately describe the shape of the interface with this procedure. In order to obtain more accurate results, the region around the interface is more finely discretized than the other regions.

2.5.2.2 Fixed Grid Technique

Here, the enthalpy is used as the dependent variable along with the temperature. The released latent heat during solidification is accounted for in the governing energy equation through the definition of total enthalpy. This way the interface shape and location are not used for computing the temperature distribution, rather, the interface shape and location are found using the computed temperature distribution.

A comprehensive survey of the fixed grid techniques is given by Voller and co-workers [14]. The total enthalpy is defined as

$$H(T) = \int_{T_{ref}}^{T} \rho c \, d\theta + \rho g(T) L \quad , \tag{2.3}$$

where H is the total enthalpy dependent on the temperature T, T_{ref} is the arbitrary reference temperature and $g(T)$ for problems with distinct interface is the Heaviside step function given by

$$g(T) = \begin{cases} 0, & T < T_m \\ 1, & T > T_m \end{cases} , \tag{2.4}$$

where T_m is the melting point of the material. A modification in $g(T)$ is necessary to use this procedure to solve the mushy phase change problem.

2.5.2.2.1 Basic Enthalpy Method

In the basic enthalpy formulation, the governing equation for the phase change problem is given by

$$\frac{\partial H}{\partial t} = \nabla \cdot (k \nabla T) \quad (2.5)$$

The properties ρ, c at any spatial location are dependent on the state[2] of the material and are given by

$$\rho = (1 - g(T))\rho_s + g(T)\rho_l$$
$$c = (1 - g(T))c_s + g(T)c_l \quad (2.6)$$

The enthalpy formulation given by (2.5) is equivalent to the conduction energy formulation given by (2.2). The proof to the general 3-D case can be found in [21].

Standard FEM or FDM discretization can be used to solve for enthalpy in (2.5) [24], [25]. In this method, the enthalpy is the primary variable and the temperature is computed using the enthalpy definition in (2.3) directly or an approximated version of (2.3) as in [26].

2.5.2.2.2 Apparent Heat Capacity Methods

In apparent heat capacity methods [27], the temperature is the primary variable. According to (2.5), the enthalpy is a function of temperature only and hence the rate of change of enthalpy is given by

$$\frac{\partial H}{\partial t} = \frac{\partial H}{\partial T}\frac{\partial T}{\partial t} \quad (2.7)$$

Further from (2.3),

$$c^A(T) \equiv \frac{\partial H}{\partial T} = \rho c + \rho L \delta(T - T_m) \quad (2.8)$$

where c^A is the Apparent Heat Capacity (AHC), δ(.) is the delta-dirac function. Using (2.7) and (2.8), the basic enthalpy formulation Equation (2.5) is transformed to

[2]solid or liquid

$$c^A(T)\frac{\partial T}{\partial t} = \nabla \cdot (k \nabla T) \tag{2.9}$$

Note that the above governing equation is similar to the conduction energy equation in (2.1). The AHC is temperature dependent; hence, the above equation is non-linear. Further, the AHC function defined in (2.8) has a singularity at $T = T_m$.

Two schemes have been proposed to approximate the singularity, namely, the linear approximation [27] and the homographic approximation [28]. These methods are described in Chapter VI. With these approximations, the well-known FEM or FDM discretization techniques can be used to solve for the temperature distribution. The resulting temperature distribution is a good approximation of reality for small time steps. If a large time step is used, the nodal points may solidify[3] without releasing the latent heat, as AHC does not take the peak value. This problem is termed as 'jumping of the latent heat peak' [29]. To overcome this, many approximations to the AHC have been proposed. A classification of these approximations are provided in [14]. In general, two classes of approximations are available, namely the ones based on spatial averaging [30] and the ones based on temporal averaging [31]. These approximation techniques can be used in connection with both explicit and implicit integration schemes and provide a reasonable solution when the time step is not too large. Several other modifications to the above approximations are also found in the literature [26], [32], [29].

In summary, the apparent heat capacity method is one of the most appealing techniques because of its simplicity. This method works well for small integration steps and can be used to solve the multi-dimension transient problem. In this dissertation, a simplified version of this technique is used for simulating the crystal growth process.

---

[3]go past the melting temperature

2.5.2.2.3 Source Methods

In this technique [33], the latent heat evolution is accounted for in the definition of a source term. The total enthalpy is split into an effective specific heat component and a latent heat component as

$$H(T) = \underbrace{h(T)}_{\substack{\text{specific heat} \\ \text{component}}} + \underbrace{\rho g(T) L}_{\substack{\text{Latent heat} \\ \text{component}}}, \tag{2.10}$$

where

$$h(T) = \int_{T_{ref}}^{T} \rho c \, d\theta \,. \tag{2.11}$$

Defining the specific heat c^s as

$$c^s = \rho c, \tag{2.12}$$

the rate of change of the enthalpy is given by

$$\frac{\partial H}{\partial t} = \frac{\partial H}{\partial T}\frac{\partial T}{\partial t} = c^s \frac{\partial T}{\partial t} + \rho L \frac{dg}{dt}. \tag{2.13}$$

Substituting the above relation into the basic enthalpy governing Equation (2.5) yields

$$c^s(T)\frac{\partial T}{\partial t} = \nabla \cdot (k \nabla T) + S, \tag{2.14}$$

with S being the non-linear source term given by

$$S = -\rho L \frac{dg}{dt}. \tag{2.15}$$

The problem with this method is that the location of the interface is unknown and hence it is difficult to compute the source term S. To overcome this, Voller [33] used iterative schemes in connection with FDM discretization to solve for the temperature distribution. However, the iterative scheme does not have the same stabilizing mechanism found in the

apparent heat capacity method [14]. Voller [34] linearized the nonlinear source term to obtain improved results.

2.6 Inverse Problem

The inverse problem is generally more difficult to solve than the forward problem. Some results regarding inverse heat conduction problems can be found in [35]. Even for simple heat conduction problems, the inverse problems are ill-conditioned. Taghavi and Duval, [10] analytically solved the inverse heat transfer problem for a simplified furnace to determine a furnace temperature profile that would result in a flat interface. Dantzig et. al [1] used an enthalpy-based FE model of the furnace to find the necessary temperature profile for a flat interface. The necessary furnace zone temperatures in their case are found as a solution to an optimization problem. These two methods can be used to determine the necessary temperature profile off-line. However, due to inevitable modeling errors, this solution will not produce the desirable interface shape. Some of the modeling errors arise from the inexact knowledge of the material properties, from heat transfer coefficients, and boundary conditions that only approximate the reality.

In the control's area, the shortcomings associated with the use of the inverse solution is very well understood. The main shortcoming is that the inverse solution does not achieve the desirable temperature distribution and there is no standard technique to correct for such errors. A control's approach to overcome such a difficulty is to use on-line measurements to compensate for modeling errors. For the crystal growth problem, the on-line measurements are used to determine the necessary temperature gradient to produce the desired interface shape. Clearly, to implement such an idea, it is necessary to have sensors for the sake of measurements and actuators to obtain the necessary temperature gradient around the ampoule. A procedure to determine the necessary

temperature gradient on-line by making use of all available measurements is proposed in this work.

A significant amount of research has been reported in the control's areas to solve problems similar to crystal growth. This area is known as "Distributed Parameter Systems (DPS)." A survey of the developments in the modeling and control of DPS is provided in the next Section.

2.7 Distributed Parameter System

A DPS is a system in which the variables of interest are a function of both space and time. This definition classifies almost all physical systems to be intrinsically distributed. The mathematical model of a DPS is derived from fundamental laws such as the conservation of mass, energy and momentum. In general, the model is usually represented by Partial Differential Equations (PDEs). Alternative forms of representation includes Integral Equations and Integro-Differential Equations. Examples of DPSs include the crystal growth furnace, casting processes, heat exchangers, transmission lines, space structures, distillation processes, nuclear and chemical reactors.

The modeling and control of DPSs have been a topic of research for several years. Wang [36] has defined several notions regarding the modeling and control of distributed systems as early as 1964. Balas [37] has summarized the trends in the control of a specific DPS, namely, large space structures. A good overview of the approximation schemes and the observability concepts as related to the DPSs can be found in [38]-[39].

In classical control, the system to be controlled is represented in the form of Ordinary Differential Equations (ODE). The model of the system is usually described in either the Laplace domain or the state-space domain. The DPSs, on the other hand, are characterized by PDEs, which conceptually can be thought of as an infinite system of ODEs. For this reason, DPSs are also known as infinite dimensional systems. The DPS

theory can be broadly divided into two main groups: modeling and control. The modeling aspect includes obtaining a model to perform controller design or perform system simulation. The control aspect of DPS includes issues such as stability, controllability, observability, stabilizability, detectability, and control design techniques.

2.7.1 Modeling of DPS

There are two basic approaches to model DPS: the exact or the analytical approach, and the approximate approach.

2.7.1.1 Exact Approach

In the exact approach, the transfer function between the input and output is used to model the DPS. The transfer function is obtained by finding the Green's function as in [40] . However, even for a simple problem, the resulting transfer functions are complicated and are never rational like those of lumped systems. These transfer functions have an infinite number of poles. For systems with complicated boundary conditions, such as the crystal growth furnaces, it is not feasible to find the transfer functions between the inputs and outputs.

2.7.1.2 Approximate Approach

Most of the practical approaches approximate the distributed system, which is theoretically an infinite dimensional system, by a set of finite dimensional systems. FDM is a spatial lumping technique which transforms the original distributed system to a set of difference equations. Many applications of FDM can be found in [41], [70]. Another method is to obtain a finite rational transfer function by performing an infinite product expansion of the transfer function and truncating the higher order terms [43]. In the modal approximation technique, the system is approximated by a few dominant eigenfunctions [44], [45]. The number of modes can be fixed by comparing the norms of the approximated and the original systems [46]. In the method of weighted residuals, the

solution is approximated by a set of basis functions [47] and the resulting spatially weighted residual is minimized. This transforms the distributed system into a set of Ode's. The FEM is a special type of weighted residual technique in which the basis and weight functions are non-zero on a small part of the spatial domain [41], [17]. The FEM has been used to determine optimal controllers as [85], [86]].

Almost all practical controller design methodologies for distributed systems approximate the system by one of the many techniques described above. The most popular technique is the FDM. The main attraction behind FDM is that the approximated system is in the state-space form and therefore, many of the multi-variable control techniques [49] may be readily used for this purpose. However, the FDM provides a solution at the nodal points only and it is difficult to use FDM on complicated geometries.

On the other hand, FEM provides a solution everywhere in the domain and can be used for complicated geometries with very little extra effort. There have been some applications of FEM in the space-structures controller design [50]. The major problem with FEM is that a state-space model is not readily available, especially for systems that are controlled from the boundary. The boundary conditions are embedded in the force term and there is no direct way to find the boundary conditions that would yield the desirable conditions inside the continuum. In this dissertation, a new approach is proposed to overcome this limitation and modify the FE formulation to obtain a lumped state-space model of the DPS. This formulation is presented in Chapter IV.

2.7.2 Control Issues

2.7.2.1 Stability

The stability definition for Finite Dimensional Continuous Linear Time Invariant (FDCLTI) systems is given by any one of the following statements [51], [52]:

(a) A continuous linear system is stable if its output remains bounded for every bounded input (BIBO stable).

(b) A FDCLTI system is stable if $\int_0^\infty |h(\tau)|\,d\tau < \infty$, where $h(\tau)$ is the impulse response of the system.

(c) A FDCLTI system is stable if all the poles of the transfer function lie in the open left half of the s-plane.

(d) A FDCLTI system is stable if all the eigenvalues of the A matrix have negative real parts, where A is the system matrix in the state-space representation of the system given by

$$\dot{x} = Ax + Bu$$
$$y = Cx. \tag{2.16}$$

(e) A FDCLTI system is stable if there exist two positive constants M and α such that $\|e^{At}\| \le Me^{-\alpha t}$, for all $t \ge 0$ where $\|\cdot\|$ is any norm of the matrix (Exponential stability).

All of the five definitions stated above are equivalent for the FDCLTI systems. Several stability tests have been developed for finite dimensional systems. Some of them are the Nyquist method, the Routh technique, and the Lyapunov technique [53].

Many of the results valid for finite dimensional systems have been extended to the linear time invariant DPS or to infinite dimensional linear system. A necessary and sufficient condition for BIBO stability of DPS is given by Vidyasagar [54]. The condition is exactly the same as (b). Condition (c), i.e., a stable system has all its poles in the left half of the s-plane, readily extends to linear DPS. This has been stated as a fact in [54]. In [55], the infinite dimensional state-space system is defined and is given by

$$\dot{x} = Ax + Bu$$
$$y = Cx, \tag{2.17}$$

where $A: X \to X, B: U \to X, C: X \to Y$ are infinite dimensional linear operators with X, U and Y being real Banach spaces. Further, the operator A is assumed to be a generator of a continuous semigroup denoted by $\{e^{At}\}_{t>0}$. This assumption is an extension of the finite-dimensional state-transition matrix to the infinite-dimensional case, i.e., the infinite-dimensional analog of the matrix exponential. Exponential stability in this domain is defined exactly the same way as in (e), i.e.,. the system is stable if there exist positive constants M and α such that $\|e^{At}\| \leq Me^{-\alpha t}$ for all $t \geq 0$, where $\|\cdot\|$ is an appropriate norm defined on the Banach space X.

Many stability tests, valid for finite dimensional system have been extended to DPS. Desoer and Wang [56], and Chait and Racliffe [57] have extended the Nyquist stability criterion to DPS. Pourki and Shoureshi [58], [59] have applied the Lyapunov technique to analyze the stability of a class of DPS. Though many tests have been proposed similar to those for finite dimensional systems, the task of determining the stability of a general linear DPS is very difficult. All the techniques require either the state-space representation or the transfer function of the DPS. These are not, unlike the lumped case, generally available. Usually only approximate (lumped) models of any general DPS can be obtained. However, a stability analysis on the approximate model will not yield accurate information about the stability of the original system.

2.7.2.2 Controllability

Insights on controllability of DPS can be obtained by considering the definition for finite-dimensional systems. For finite dimensional continuous linear system, controllability is defined as follows: "A system is said to be controllable if there exist a finite control sequence $u(t)$, $t \geq 0$ that transforms the system from any initial state $x(0)$ to any other state $x_T = x(T)$ in a finite time $T > 0$." To verify controllability, one of the following tests can be used

(a) A FDCLTI system is controllable (also observable) if there are no pole-zero cancellations in the transfer function and this is valid for SISO system only.

(b) A FDCLTI system is controllable if the matrix Ω_c defined as

$$\Omega_c = \begin{bmatrix} B & AB & A^2B & \cdots & A^{n-1}B \end{bmatrix}, \tag{2.18}$$

has full row rank. Here A and B are state-space matrices as defined in (2.16), and n is the number of states.

(c) A FDCLTI system is controllable if $v^T B \neq 0$, where v is any eigenvector of A^T.

(d) A FDCLTI system is controllable if the controllability Grammian P defined by

$$P = \int_0^\infty e^{At} B B^T e^{A^T t}\, dt \tag{2.19}$$

is positive definite.

All four tests described above are equivalent. Note the integral given by (2.19) exists only if all the eigen values of system matrix A is in the open half plane. Therefore the test (d) is not always equivalent to others.

The concept of controllability is much more complicated for DPS. In fact, for DPS there are two types of controllability, namely, exact controllability, and approximate controllability [55]. "A system is said to be exactly controllable if there exists a finite control sequence $u(t)$, $t \geq 0$ that transforms the system from any initial state $x(0)$ to any other state $x_T = x(T)$ in a finite time $T > 0$, where $x(.)$ resides in an infinite dimensional space (Hilbert space)." The exact equality is very difficult to achieve in practice and therefore most distributed systems are not exactly controllable. An approximate controllability concept is defined as follows: "A system is said to be approximately controllable if there exists a finite control sequence $u(t)$, $t \geq 0$ that transforms the system from any initial state $x(0)$ to any other state $x(T)$ in a finite time $T > 0$ such that $\|x(T) - x_T\| \leq \varepsilon$ for all $\varepsilon > 0$, where x_T is any arbitrary state."

Unlike the finite-dimensional case, there are no criteria that can be used to check the controllability of DPS. If the transfer function of the DPS is available, then it is possible to check controllability by finding out if there are any pole-zero cancellations (SISO). This is not practical as there are infinitely many poles and probably infinitely many zeros. Delfour and Mitter [60] employed functional analysis to derive conditions on the state-input operator, $S: u \varepsilon U \rightarrow x \varepsilon X$, where U is the input space and X is the infinite-dimensional state-space (Hilbert space), to check for controllability. One of the main results is that "the image of the operator S must be dense in the state-space X for the system to be controllable." More recently, Lions [61] developed conditions for exact controllability of a wave equation with both Dirichlet and Neuman boundary conditions.

In many control system application, the location of the actuators is to be selected by the designers. The concept of "strategic actuators" [62] is developed for this purpose. Actuators residing at the given locations are said to be "strategic actuators" if the resulting control system is weakly controllable. Some of the controllability conditions can be used to find the optimal actuator locations.

2.7.2.3 Stabilizability

Consider the question "if the given system is uncontrollable, is it possible to design a controller?" This question can be answered using the concept of stabilizability. As in the previous sections, let us first consider the finite-dimensional case. Given a system, the state-space X can be divided into two subspaces; namely the controllable subspace and the uncontrollable subspace. The uncontrollable subspace contains all the modes that are not controllable. "A system is stabilizable if the entire uncontrollable space is stable." Hence if a system is stabilizable, it is possible to design a controller to meet reasonable

specifications[4]. The stabilizability of a finite-dimensional system can be checked by one of the three equivalent methods given below:

(a) A system is stabilizable if $v^T B \neq 0$,where v is any eigenvector of A^{T} corresponding to a non-negative eigenvalue.

(b) A system is stabilizable if the controllability Grammian P given by (2.19) is positive definite.

(c) A system is stabilizable, if there exists a gain matrix K such that the matrix $(A\text{-}BK)$ is Hurwitz, i.e, has all eigenvalues with negative real parts.

The stabilizability definition for DPS can be defined in the same way as in the finite-dimensional case. However, for a particular DPS, the infinite-dimensional state-space X may not be decomposable into controllable and uncontrollable subsystems. Thus, to overcome this technical difficulty, the formal definition of the stabilizability of DPS is given as follows: "An infinite dimensional state-space system (A, B) is said to be stabilizable if there exists a bounded linear operator $K: X \rightarrow U$ such that $A\text{-}BK$ generates a continuous stable semi-group denoted by $\left\{e^{(A-BK)t}\right\}_{t>0}$."[63]. Rebarber and Knowles [64] have shown that if a system is stabilizable then there are only finitely many unstable modes (right half plane eigenvalues). A similar result for joint stabilizability/detectability (defined later) can be found in [63]. Thus stabilizability of an infinite-dimensional system is essentially finite-dimensional.

2.7.2.4 Observability

Observability is the dual concept of controllability. For continuous time finite-dimensional systems, observability is defined as follows: "A system is said to be observable

---

[4]The choice of the design specifications is less when compared to a controllable system. This can be seen in the section on trackability in Chapter V.

if any initial state $x(0)$ can be determined uniquely through the knowledge of $y(t)$, $u(t)$, $0 \le t \le T$, where T is finite." Just as controllability, the observability of the state-space system can be verified by one of the following equivalent tests:

(a) System is observable if matrix Ω_0 defined as

$$\Omega_o = \left[C^T \quad (CA)^T \quad (CA^2)^T \quad \cdots \quad (CA^{n-1})^T \right]^T, \tag{2.20}$$

has full column rank. Here A, and C are state-space matrices as defined in (2.16), and n is the number of states.

(b) A FDCLTI system is observable if $Cv \neq 0$, where v is any eigenvector of A.

(c) Assuming stability, a FDCLTI system is observable if the observability Grammian Q defined by

$$Q = \int_0^\infty e^{A^T t} C^T C e^{At}\, dt \tag{2.21}$$

is positive definite.

Observability concept of DPS is older than controllability due to developments in the area of identification of DPS. Two types of observability that are important from the controls view point are defined in this section; namely, exact and approximate observability. There are other types of observability such as G-K observability, N-node observability [65] which shall not be discussed here. "A DPS is said to be strictly observable if any initial state x can be uniquely determined from the knowledge of u and the measurements y". In [62] this is defined mathematically as follows: The DPS is exactly (continuously) observable, if there exists a $\gamma > 0$ such that

$$\left\| Ce^{A\tau} x(0) \right\|_{0 \le \tau \le T} \ge \gamma \|x(0)\| \quad \forall x(0). \tag{2.22}$$

Note $\{e^{A\tau}\}$ is the continuous semigroup generated by A. The exact observability definition is satisfied by very few DPS and many times, it is not necessary to have exact observability

to design and implement controllers. Hence a weaker or approximate observability is defined as follows: "The DPS is approximately observable if

$$\left\| Ce^{At} x(0) \right\|_{0 \le t \le T} = 0 \Rightarrow x(0) = 0 \text{ "} \tag{2.23}$$

Just like controllability, there are very few criteria that may be used to check observability of a general DPS. If the transfer function of DPS has no pole-zero cancellation the DPS is observable and controllable. However, as stated before, this is not practical because there are infinitely many pole and possibly infinitely many zeros. Functional analysis has been used in [60] to derive some general conditions for observability.

2.7.2.5 Detectability

There are many systems that may not be observable. To design controllers to meet reasonable specifications, the concept of detectability is used. The state-space X can be partitioned into an observable subspace and an unobservable subspace. Detectability of a finite-dimensional linear system or linear DPS is defined as follows: " A system is detectable if the entire unobservable subspace is stable". Thus if a particular mode is unobservable, we know that mode does not cause instability. The concept of detectability is dual to that of stabilizability. For continuous time finite-dimensional systems the detectability can be verified by one of the following conditions:

(a) A FDCLTI system is detectable if $Cv \neq 0$, where v is any eigenvector of A corresponding to a non-negative eigenvalue.

(b) A FDCLTI system is detectable if the observability Grammian Q given by (2.21) is positive definite.

(c) A FDCLTI system is detectable if there exist a gain matrix L such that the matrix $(A\text{-}LC)$ is Hurwitz.

For DPS, a more practical definition of detectability is given in [63] as "An infinite dimensional state-space system (A, C) is said to be detectable if there exists a bounded linear operator $L: Y \rightarrow X$ such that A-LC generates a continuous stable semi-group denoted by $\left\{e^{(A-LC)t}\right\}_{t>0}$." Using the duality concept, it is possible to show that detectability of an infinite-dimensional system is essentially finite-dimensional.

2.7.2.6 Control Design Techniques

In this section, a brief review of different control design techniques is made. The coprime factorization technique [54], and H^{∞} control technique [66], [67] are two of several approaches that utilize the transfer function of the system to design controllers. The transfer function is obtained by analytically solving the PDE including the BC's. A robust multivariable PID controller using an infinite-dimensional state-space model is designed in [68]. Many control design problems have been formulated as a regulator problem such that the control action minimizes a quadratic performance index [69]. There are very few practical control design applications that make use of the infinite dimensional state-space or the transfer functions. This is because of the difficulty of obtaining such models for general DPS.

Most practical control of DPS is performed using a lumped model of the DPS. Some of them are: state-space design techniques using FDM [70], state-space design technique using reduced-order FE based models [50], adaptive control using FE based model [71], and modal control [72]. The designed controller may have satisfactory performance with respect to the lumped model; however, in some situations, this controller may not stabilize the original DPS. This is known as the spill-over effect [72]. This usually occurs when there are modes close to the $j\omega$ axis that are not included in the lumped models. One way to overcome this problem is to include all such modes in the lumped model and then design the controller. This may not be always feasible as in the

case of flexible systems, where there are infinitely many modes close to the $j\omega$ axis. Another method is to design a robust controller that stabilizes all the nearby systems (in some norm sense) as in [73]. The heat conduction equation is inherently very stable and so the system dealt with in this dissertation most probably will not have any spill-over problems.

2.7.3 On Lumped Model Representation of DPS

Many times, the applied control is also distributed. In this situation, there are two options. In the first option, a lumped model of the system is used to design a lumped controller which in turn is used to construct the distributed controller. The second option is to include the controller into the distributed model and lumping is done to solve for the controller. The authors in [74] argue that the second option would yield better controllers as the distributed nature of the system is retained in the control design equations. Unfortunately, solving the distributed control design equation is not easy. Therefore, most practical control implementation utilize a lumped model of DPS. This raises the following question: "Does such an approximation preserve the stability, controllability, and observability of the original DPS?" The answer to this question depends on the type of the approximating method. As stated before, if a system is jointly stabilizable/detectable then the number of unstable modes is finite. Hence, the approximated model must at the least contain all of the unstable modes. This is essential to design a stabilizing controller.

For some approximating methods, it is possible to obtain an error bound. Let the input-output mapping of the DPS be given by $H: u \in U \rightarrow y \in Y$ and the approximate input output map be given by H_n. The infinity norm error bound denoted by $\|H - H_n\|_\infty$ can be found for certain approximation schemes (modal approximations) given in [75], [76]. This knowledge gives us an estimate of the infinity norm of the uncertain/unmodeled

portion of the system and the controller designed through robust control design technique can guarantee some performance on the infinite-dimensional closed-loop system.

For spatial lumping techniques such as FDM or FEM, there are some bounds on the error of approximation for the steady-state linear problems [77, pg. 268]. However, there are no such error bounds for the transient problem with general BC. It is known that increasing the number of nodes will increase accuracy. Also, for simple problems, the nodal solution of the unknown variables is exact. Thus, if the distribution is not wild, then the spatially lumped model based solution is a good representation of the exact solution. With this in mind, it is reasonable to expect approximate preservation of stability, controllability and observability.

2.8 Summary

In this chapter, it is concluded that conduction is the main mode of heat transfer that determines the shape of the interface. A brief survey of different methods to solve the phase change problem is contained in this chapter. The most attractive method for controller design is the apparent heat capacity method, in which the moving boundary value problem is modified into a non-linear fixed domain problem. Developments in the area of DPS is used to gain insight into the inverse problem. Several control issues, such as stability, controllability, observability, stabilizability, and detectability pertaining to DPS are discussed. The next chapter proposes a method to solve the inverse problem.

CHAPTER III

PROPOSED METHOD

The main objective of this dissertation is to control the shape of the interface by varying the furnace zone temperatures. This is achieved by first constructing a model for the crystal-growth process and then using it to design a controller. The modeling of the crystal growth process dynamics is discussed in the following section.

3.1 Heat Transfer Modeling

The dynamics of interface shape during crystal growth process inside an ampoule is assumed to be primarily governed by the conduction heat-transfer. The mathematical model for the heat conduction problem with phase change includes two heat conduction equations, one for the solid region and another for the liquid region and a solid-liquid interface condition accounting for the release of latent heat as given in (2.2). This problem is a moving boundary value problem as the location of the interface is changing with time. Enthalpy formulation can be used to transform the moving boundary value type problem to a non-linear heat conduction problem without change of phase through the definition of total enthalpy.

3.1.1 Modeling of a General Heat Conduction Problem

The general heat conduction problem is described in terms of a PDE along with appropriate boundary conditions. In the inverse problem, it is required to determine the controllable BC[5] that would set up a desired temperature distribution inside the region of

[5]The required BC are set up by a command to the heater temperature control system.

interest. The FEM can be used to obtain a lumped model of the heat conduction problem including the BC's and is given by

$$M\dot{T} + KT = F, \tag{3.1}$$

where M, K, and F are the mass, stiffness, and force matrices respectively and T is a vector containing the temperature at certain key points (nodes). The above equation can be used to determine the solution to the forward problem. However, solving the inverse problem is difficult using Equation (3.1) as the relation on how the BC's affect the temperatures is embedded in the force matrix F.

In this dissertation, a state-space model of the heat conduction energy equation is obtained by lumping the partial differential equation using the FE approximation. In this approach, the three main BC's namely the insulation BC, the convection BC, and the Dirichlet BC are parameterized and the variable parameters are included in the input vector u_1 and all other uncontrollable parameters in u_2. The resulting state-space model is given by

$$\dot{T} = \tilde{A}T + \tilde{B}_1 u_1 + \tilde{B}_2 u_2, \tag{3.2}$$

where $\tilde{A}$, $\tilde{B}_1$, and $\tilde{B}_2$ are matrices of appropriate dimensions and T is the temperature at the nodes. Any temperature measurements can be described in terms of the nodal temperature as

$$y = \tilde{C}T + \tilde{D}_1 u_1 + \tilde{D}_2 u_2. \tag{3.3}$$

This formulation can be seen in Chapter IV.

3.1.2 Heat Conduction Problem with Phase Change

The AHC method can be used to obtain a PDE that models the phase change problem. This PDE has a form similar to that of the regular heat-conduction problem, with temperature dependent specific heat and heat conductivity coefficients. Hence, a

similar procedure described in the previous section is used to obtain a state-space model of the system. However, the matrices $\tilde{A}$, $\tilde{B}_1$, and $\tilde{B}_2$ are temperature dependent and thus make the state-space model non-linear.

3.2 Controller Design

3.2.1 Control of a Heat Conduction Problem

A controller is designed using the state-space model. The dynamics of the controlled system (closed-loop system) must have the following properties: stability, reasonable transient response, and tracking of a specified temperature distribution. State-feedback is the most general linear control law and is given as

$$u_1 = K_s T, \tag{3.4}$$

where K_S is the state-feedback gain matrix. With the above control-law, the transient response of the lumped system can be shaped to satisfy reasonable design requirements. Setting up an arbitrary constant temperature distribution can be accomplished by adding a bias input u_b as

$$u_1 = K_s T + u_b. \tag{3.5}$$

The existence of a bias input that will produce a desired temperature distribution depends on the actuator locations. A necessary and sufficient condition for the existence of such a bias input is derived in Chapter V.

To implement the control law in (3.5), it is necessary to know the states, i.e., the nodal temperatures T. Only a few of the states[6] are measured and therefore all other states are reconstructed from these measurements. This is feasible if the system is observable. The control law in (3.5) is modified as

---

[6]or linear combinations of states

$$u_1 = K_s \hat{T} + u_b, \tag{3.6}$$

where $\hat{T}$ is the estimated state, found by simulating the system

$$\dot{\hat{T}} = \tilde{A}\hat{T} + \tilde{B}_1 u_1 + \tilde{B}_2 u_2 + L(y - \tilde{C}\hat{T} - \tilde{D}_1 u_1 - \tilde{D}_2 u_2). \tag{3.7}$$

Here L is the observer gain matrix which is selected by the designer to shape the estimated state transient response.

Further, when the system is stabilizable and detectable but not observable or controllable, the temperature distribution that can be established inside the material is limited. It is possible that depending on the location of actuators, the desired temperature distribution cannot be established by any input. In this situation, the temperature distribution can be implemented only in a least-squares sense. In Chapter V, necessary and sufficient conditions are developed for the existence of inputs so that a desired temperature distribution can be established in the steady-state.

3.2.2 Control of a Heat Conduction Problem with Phase Change

The main objective here is to control the shape of the interface and grow the crystal at a desired rate. This objective is equivalent to setting up a desired temperature distribution inside the material and translating it at a desired rate. The state-space model of this system is similar to the general heat conduction problem except that the state-space matrices are temperature (state) dependent and therefore is non-linear. The task of designing a controller (linear or non-linear) for a general non-linear system is a very difficult proposition. A standard approach is to linearize the non-linear system and utilize the linear control design procedures. This would result in finding a linear controller. The linearization procedure is described in Chapter VII. The linearized model is used to a controller in the same way as in the previous section to establish the appropriate temperature distribution that corresponds to the desired interface shape.

The translation of the interface is achieved by requesting a temperature distribution that moves at the desired translation rate. If the controller can keep up with this request and establish the temperature distribution at every instance, the desired translation rate is achieved. More details on this subject can be found in Section 7.3.2.

3.3 Summary

A method is proposed to control the shape of the interface, the dynamics of which are governed by conduction heat transfer. A new technique is formulated to obtain a state-space model of a general linear heat-conduction equation controlled from the boundary using FEM. The same procedure is used to obtain a state-space model of the heat-conduction equation with phase change. An observer based state-feedback controller with an additional bias input is used to establish the desired temperature distribution inside the material and translate the distribution at the desired rate.

In the next chapter, the FE formulation of a general heat conduction problem with arbitrary BC's is presented.

CHAPTER IV

STATE-SPACE MODELING OF BOUNDARY CONTROLLED HEAT CONDUCTION EQUATION

One of the main ideas of this dissertation is the use of the FEM to develop a state-space model of the distributed system. In this chapter, the formulation is presented for an axi-symmetric linear heat conduction problem. This formulation can be generalized to a general 3-D problem, and to other DPSs. Later on in Chapter VI, we will extend this modeling approach in this chapter to diffusion dominated phase change problems.

4.1 Boundary Control of Axi-Symmetric Heat Conduction Equation: Problem Statement

The temperature distribution inside a material due to conduction heat transfer is determined by the partial differential equation

$$k\nabla^2 T = \rho c_p \frac{\partial T}{\partial t}, \tag{4.1}$$

where k is the thermal conductivity, ρ is the density, c_p is the specific heat and T is the temperature. The condition of axi-symmetry is assumed for this formulation to reduce the complexity of the problem. However, the formulation derived in this chapter can be generalized to problems that do not satisfy the axi-symmetry assumption. An example problem is illustrated in Figure 4.1. Three different boundary conditions are possible; namely the insulation, convection and Dirichlet boundary condition. These are given as

$$\begin{aligned} &\text{Insulation} && \left.\frac{\partial T}{\partial n}\right|_{\Gamma_i} = 0 \\ &\text{Convection} && \left. k\frac{\partial T}{\partial n} + h(T - T_b^i)\right|_{\Gamma_i} = 0 \\ &\text{Dirichlet} && T|_{\Gamma_i} = T_{\Gamma_i} \end{aligned}, \tag{4.2}$$

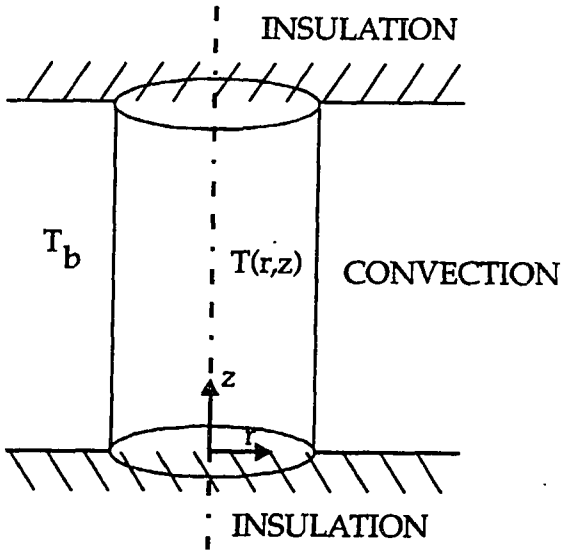

Figure 4.1 Illustration of a simple axi-symmetric heat conduction problem.

where Γ_i denotes the either the insulation, or convection or the Dirichlet boundary surface, T_b^i denotes the boundary temperature in the convection boundary condition, and h denotes the convection coefficient. The control problem is to determine the boundary temperature T_b^i in the convection equation and/or the surface temperature T_{Γ_i} in the Dirichlet BC so that an appropriate temperature can be established either at certain key points or at every point inside the material.

4.2 Finite Element Formulation

The heat conduction equation given by (4.1) in a cylindrical coordinate system with the axi-symmetry condition takes the following form

$$k\left(\frac{\partial^2 T}{\partial r^2}+\frac{1}{r}\frac{\partial T}{\partial r}+\frac{\partial^2 T}{\partial z^2}\right)=\rho c_p\frac{\partial T}{\partial t}, \tag{4.3}$$

where (r,ϕ,z) are the cylindrical coordinates. Because of the assumption of axi-symmetry, the ϕ term is not included in the above equation; it is sufficient to find the temperature for the surface $\phi = 0$ as shown in Figure 4.2. Along with this simplification, it is necessary to introduce an insulation BC on the axi-symmetric axis as given by

$$\left.\frac{\partial T}{\partial r}\right|_{r=0}=0 \tag{4.4}$$

The temperature profile $T(r,z)$ can be found by solving the weighted residual equation

$$\iint_{\Omega} w(r,z)\left(k\left(\frac{\partial^2 T}{\partial r^2}+\frac{1}{r}\frac{\partial T}{\partial r}+\frac{\partial^2 T}{\partial z^2}\right)-\rho c_p\frac{\partial T}{\partial t}\right)2\pi r\,dr\,dz=0, \tag{4.5}$$

where Ω is the domain of integration, and w is the weighting function satisfying certain smoothness conditions. The weighting functions belong to the Sobolev space [77] and are zero at Dirichlet BC locations (at which temperatures are fixed). A variational form of Equation (4.5) is given by

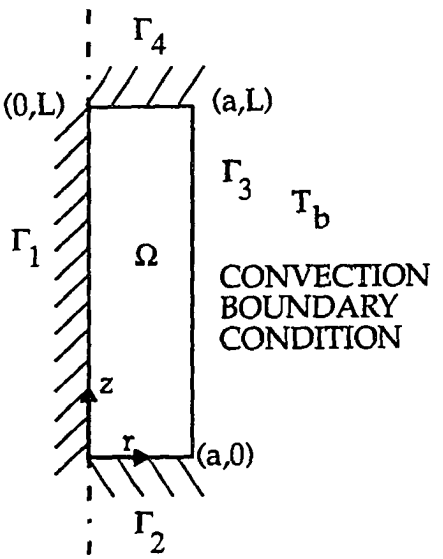

Figure 4.2. Implementation of axi-symmetry condition.

$$\iint_{\Omega} w\rho c_p \frac{\partial T}{\partial t} r dr dz + \iint_{\Omega} k\left(\frac{\partial T}{\partial r}\frac{\partial w}{\partial r} + \frac{\partial T}{\partial z}\frac{\partial w}{\partial z}\right) r dr dz = \int_{\Gamma} kw\left(\frac{\partial T}{\partial r} n_r + \frac{\partial T}{\partial z} n_z\right) r d\Gamma \quad , \quad (4.6)$$

where Γ is the bounding surface of the domain Ω. n_r and n_z are the r and z components of the unit outward normal vector to Γ. The first term in (4.6) corresponds to the mass term, while the second corresponds to the stiffness term and the term on the right hand side is due to the BC and makes up the force term. The variational form is a simpler equation to solve as the equation is first order in terms of the unknown temperature. The finite element procedure uses the variational form in (4.6) to solve for the temperature inside the continuum. Proofs to equivalence of solutions of Equations (4.5) and (4.6) can be found in [77]. In the next section, the Galerkin approximation technique to solve Equation (4.6) is discussed.

4.2.1 Galerkin Approximation Technique

A finite-dimensional approximation is obtained by assuming the weight and temperature function as

$$w \approx w^h = \sum_{A=1}^{n} w_A N_A \quad , \quad (4.7)$$

$$T \approx T^h = \sum_{A=1}^{n} T_A N_A \quad , \quad (4.8)$$

where w^h and T^h are the finite dimensional approximations of w and T. N_A's are the shape or the interpolation functions and are defined as

$$N_A : \Omega \rightarrow \Re[0,1] \quad , \quad (4.9)$$

where w_A, and T_A are constants. The shape functions are usually non-zero only on a small region of Ω and are defined such that the constants T_A's typically correspond to temperatures at certain key points known as the nodes (see Figure 4.3). From (4.7) and (4.8), the mass term of (4.6) can be written as

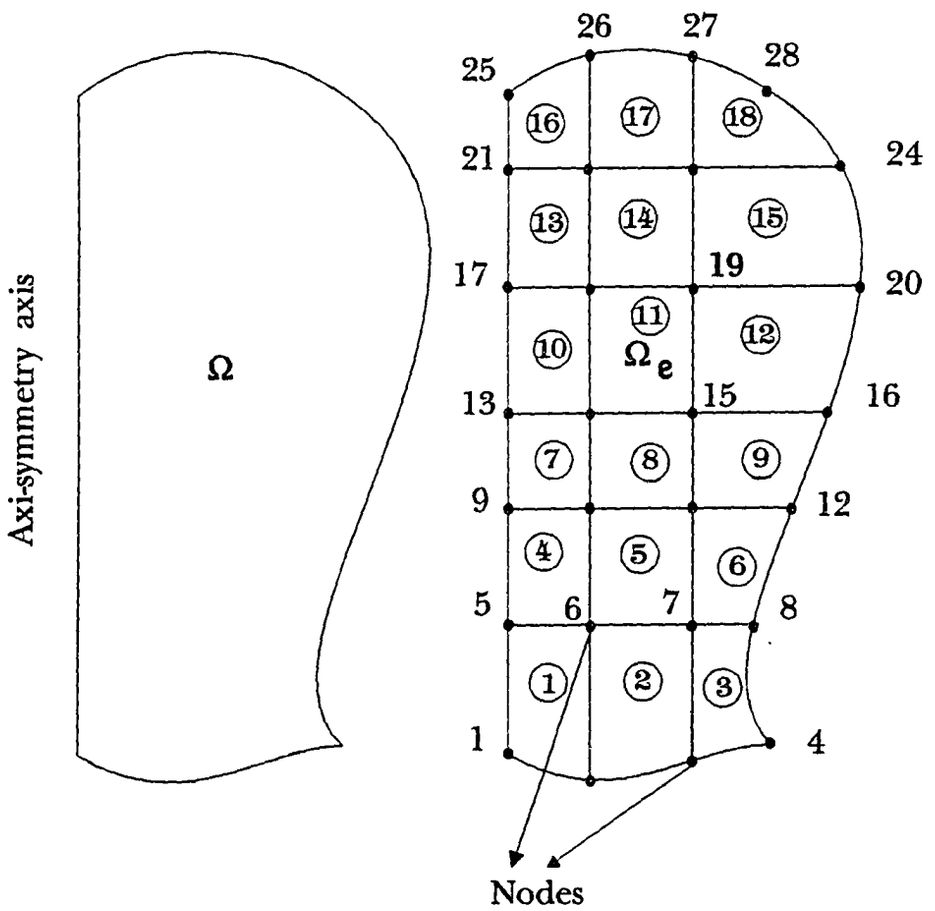

Figure 4.3. Discretization of an arbitrary axi-symmetric geometry.

$$\iint_{\Omega} w^h \rho c_p \frac{\partial T^h}{\partial t} r dr dz = \sum_{A=1}^{n} \sum_{B=1}^{n} w_A [M_{AB}] \dot{T}_B \quad , \tag{4.10}$$

where

$$M_{AB} = \iint_{\Omega} \rho c_p N_A N_B r dr dz \quad . \tag{4.11}$$

Similarly, the stiffness term reduces to

$$\iint_{\Omega} k \left(\frac{\partial T^h}{\partial r} \frac{\partial w^h}{\partial r} + \frac{\partial T^h}{\partial z} \frac{\partial w^h}{\partial z} \right) r dr dz = \sum_{A=1}^{n} \sum_{B=1}^{n} w_A [K_{AB}] T_B \tag{4.12}$$

with

$$K_{AB} = \iint_{\Omega} k \left(\frac{\partial N_A}{\partial r} \frac{\partial N_B}{\partial r} + \frac{\partial N_A}{\partial z} \frac{\partial N_B}{\partial z} \right) r dr dz \quad . \tag{4.13}$$

The force term becomes

$$\int_{\Gamma} k w^h \left(\frac{\partial T^h}{\partial r} n_r + \frac{\partial T^h}{\partial z} n_z \right) r d\Gamma = \sum_{A=1}^{n} w_A [F_A] \quad , \tag{4.14}$$

where

$$F_A = \int_{\Gamma} k N_A \left(\frac{\partial T^h}{\partial r} n_r + \frac{\partial T^h}{\partial z} n_z \right) r \, d\Gamma \quad . \tag{4.15}$$

Note T^h in F_A is not expanded in terms of the shape function. Later, the BC's in (4.2) and (4.4) will be implemented in (4.15) to make up the force term. Introducing Equations (4.10)-(4.15) into the variation form of the problem given by (4.6), we get

$$\sum_{A=1}^{n} \sum_{B=1}^{n} w_A [M_{AB}] \dot{T}_B + \sum_{A=1}^{n} \sum_{B=1}^{n} w_A [K_{AB}] T_B = \sum_{A=1}^{n} w_A [F_A] \quad . \tag{4.16}$$

Equation (4.16) must hold for all possible w^h and hence for all w_A. This is true only when

$$\sum_{B=1}^{n} [M_{AB}] \dot{T}_B + \sum_{B=1}^{n} [K_{AB}] T_B = [F_A] \quad \forall A \in \{1, 2 \ldots, n\} \quad . \tag{4.17}$$

4.2.2 Implementation of Boundary Conditions

The finite element system of equations given by (4.17) can be used to obtain the temperatures inside the domain. However, the force matrix whose elements are given in (4.15) cannot be computed without imposing boundary conditions. In the next three sections, implementations of three BC, namely the insulation BC, the convection BC and the Dirichlet BC into the FE formulation are illustrated. In the simple problem given by Figure 4.2, there are four boundary surfaces and Equation (4.15) is computed as

$$F_A = \int_{\Gamma} kN_A \left(\frac{\partial T^h}{\partial r} n_r + \frac{\partial T^h}{\partial z} n_z \right) r d\Gamma = \int_{\Gamma_1} \cdots d\Gamma_1 + \int_{\Gamma_2} \cdots d\Gamma_2 + \int_{\Gamma_3} \cdots d\Gamma_3 + \int_{\Gamma_4} \cdots d\Gamma_4 \tag{4.19}$$

4.2.2.1. Insulation BC

The general insulation condition is given as

$$\left. \frac{\partial T^h}{\partial n} \right|_{\Gamma_i} = 0 \quad , \tag{4.20}$$

where n is the outward unit normal to the line (surface) defined by Γ_i. The contribution of this BC to the force matrix elements is

$$F_A|_{\Gamma_i} = \int_{\Gamma_i} kN_A \left(\frac{\partial T^h}{\partial r} n_r + \frac{\partial T^h}{\partial z} n_z \right) r d\Gamma_i = \int_{\Gamma_i} kN_A \frac{\partial T^h}{\partial n} r d\Gamma_i = 0 \tag{4.21}$$

4.2.2.2 Convection BC

At any convection boundary Γ_i,

$$k \frac{\partial T^h}{\partial n} + h(T^h - T_b^i)\big|_{\Gamma_i} = 0 \quad , \tag{4.22}$$

where n is the same as before and T_b^i is the outside temperature. Thus from (4.15), the force matrix contribution becomes

$$F_A|_{\Gamma_i} = \int_{\Gamma_i} kN_A \frac{\partial T^h}{\partial n} r\, d\Gamma_i = \int_{\Gamma_i} hN_A T_b^i\, r d\Gamma_i - \int_{\Gamma_i} hN_A T^h r\, d\Gamma_i \quad . \tag{4.23}$$

Introducing the expression for T^h given by (4.8) into the above equation gives

$$F_A|_{\Gamma_i} = \int_{\Gamma_i} hN_A T_b^i\, r d\Gamma_i - \sum_{B=1}^{n} \int_{\Gamma_i} hN_A N_B\, r d\Gamma_i T_B = \int_{\Gamma_i} hN_A T_b^i r\, d\Gamma_i - \sum_{B=1}^{n} \left[K_{AB}^{f_i}\right] T_B \tag{4.24}$$

with

$$K_{AB}^{f_i} = \int_{\Gamma_i} hN_A N_B\, r d\Gamma_i \quad . \tag{4.25}$$

Note $K_{AB}^{f_i}$ is multiplied by the nodal temperatures T_B as in the case of the stiffness term in Equation (4.17). Hence, this term is added to the stiffness matrix and this is shown later. In conventional FEM, the temperatures inside the domain are found for a given set of BC's. Hence T_b^i is known and F_A is computed using Equation (4.24) and the resulting temperature distribution from Equation (4.17). However, solving the inverse problem, i.e., finding T_b^i for a given temperature distribution inside the domain, is difficult using Equation (4.17) as the relation on how T_b^i affects the temperatures are embedded in the force matrix F. This corresponds to knowing (Bu) but not (B) itself of a standard state-space model

$$\dot{x} = Ax + Bu \,. \tag{4.26}$$

In order to overcome this problem, parametrization of the boundary temperature is done. This parametrization is made in the same fashion as the weights and temperatures and is given as

$$T_b^i = \sum_{D=1}^{n_{b_i}} N_{b_D}^i T_{b_D}^i \,, \tag{4.27}$$

where $N_{b_D}^i$ can be thought as a basis or shape function similar to the shape functions used for temperature or weights. n_{b_i} is the number of boundary shape functions used for

approximating T_b^i and is equal to the number of nodes on the bounding surface Γ_i. Each boundary shape function typically attains a value one at the nodes on Γ_i and is non-zero in regions that contains the node as shown in Figure 4.4. Hence, $T_{b_D}^i$ are actually the boundary temperatures at key points.

Now substituting the definition for T_b^i in the equation for determining F_A given by (4.24), we get

$$F_A\big|_{\Gamma_i} = \sum_{D=1}^{n_{b_i}} \left[B_{AD}^{f_i}\right] T_{b_D}^i - \sum_{B=1}^{n} \left[K_{AB}^{f_i}\right] T_B \tag{4.28}$$

with

$$B_{AD}^{f_i} = \int_{\Gamma_i} hN_A N_{b_D}^i \, rd\Gamma_i \tag{4.29}$$

The definition of $N_{b_D}^i$ is such that the integration limits for each element of B^{f_i} need not be the whole boundary surface, rather the small region in which N_A's and $N_{b_D}^i$ are non-zero. The definition also conforms with the requirements of the usual finite-element computation procedure where the actual integrals are computed on an element by element basis.

4.2.2.3 Dirichlet BC

This BC corresponds to a certain fixed temperature profile T_{Γ_i} on the bounding surface Γ_i and is formally stated as

$$T(r,z)\big|_{\Gamma_i} = T_{\Gamma_i}. \tag{4.30}$$

From our initial approximation of temperature given by (4.8), we get

$$T(r,z)\big|_{\Gamma_i} = T_{\Gamma_i} \approx T^h\big|_{\Gamma_i} = \sum_{A=1}^{n} T_A N_A \Big|_{\Gamma_i} = \sum_{A \in \Gamma_A} T_A N_A \tag{4.31}$$

The Dirichlet BC can be implemented by forcing all the nodal temperatures of this set Γ_A to be equal to the imposed profile's temperature, T_{Γ_i}.

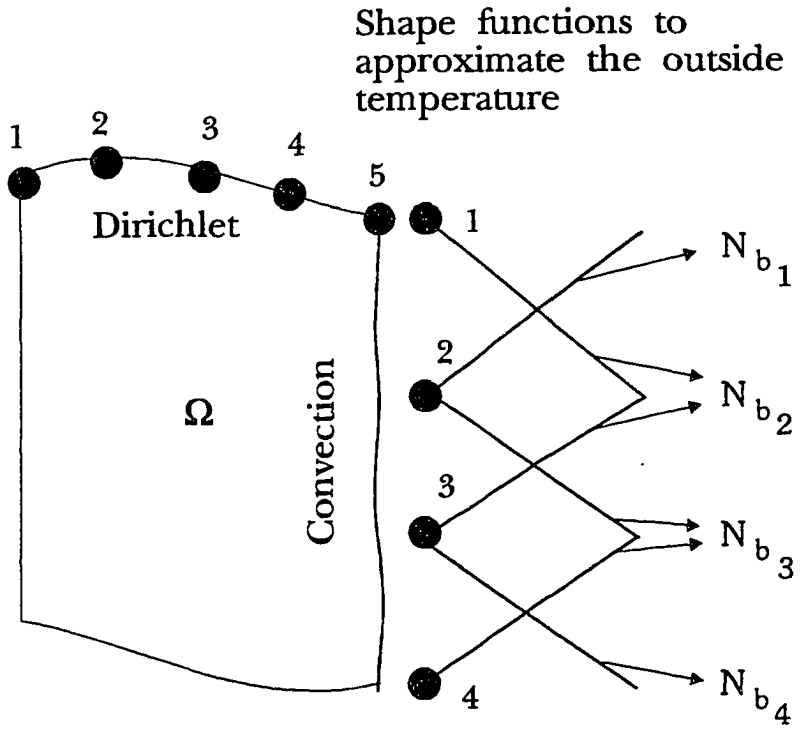

Figure 4.4. Parameterization of convection and Dirichlet BC's.

The nodal temperatures at the boundary are known and hence it is only required to find the other unknown temperatures, i.e., Equation (4.17) is solved for a reduced set of unknowns as given below

$$\sum_{B=1}^{n}[M_{AB}]\dot{T}_B+\sum_{B=1}^{n}[K_{AB}]T_B=[F_A]\quad \forall A\in\{\Gamma_{A_i}\}^c, \tag{4.32}$$

where $\{\Gamma_{A_i}\}^c=\{1,2,\cdots,n\}-\{\Gamma_{A_i}\}$. Now Equation (4.32) can be decomposed into knowns and unknowns variables and this results in

$$\sum_{B\in\{\Gamma_{A_i}\}^c}[M_{AB}]\dot{T}_B+\sum_{B\in\{\Gamma_{A_i}\}^c}[K_{AB}]T_B=-\sum_{B\in\{\Gamma_{A_i}\}}[M_{AB}]\dot{T}_B-\sum_{B\in\{\Gamma_{A_i}\}}[K_{AB}]T_B+[F_A]\quad \forall A\in\{\Gamma_{A_i}\}^c. \tag{4.33}$$

In the next section, all the different boundary conditions are combined and a general force matrix is obtained.

4.2.3 Generalization of all Boundary Conditions

Suppose there are N_I insulation boundary surfaces, N_C convection boundary surfaces, and N_D Dirichlet boundary surfaces, then the generalized FEA model is found as follows. The insulation BC does not contribute to the force term. The convection BC alters the force matrix and indirectly alters the stiffness matrix as will be shown later in this Section. The contribution to the force matrix due to all the convection BC's is given by

$$F_A|_{ConvectionBC}=\sum_{i=1}^{N_c}\sum_{D=1}^{n_{b_i}}[B_{AD}^{f_i}]T_{b_D}^i-\sum_{B=1}^{n}\left(\sum_{i=1}^{N_c}[K_{AB}^{f_i}]\right)T_B. \tag{4.34}$$

Since the insulation and Dirichlet BC's do not affect the force matrix, we substitute the final force matrix into the general finite element equation given by (4.17) to obtain

$$\sum_{B=1}^{n}[M_{AB}]\dot{T}_B+\sum_{B=1}^{n}[K_{AB}]T_B=\sum_{i=1}^{N_c}\sum_{D=1}^{n_{b_i}}[B_{AD}^{f_i}]T_{b_D}^i-\sum_{B=1}^{n}\left(\sum_{i=1}^{N_c}[K_{AB}^{f_i}]\right)T_B\quad \forall A\in\{1,2\ldots,n\}. \tag{4.35}$$

Combining convection stiffness terms into the general stiffness term in the above equation, we get

$$\sum_{B=1}^{n}[M_{AB}]\dot{T}_B+\sum_{B=1}^{n}\left[K_{AB}+\sum_{i=1}^{N_c}\left[K_{AB}^{f_i}\right]\right]T_B=\sum_{i=1}^{N_c}\sum_{D=1}^{n_{b_i}}\left[B_{AD}^{f_i}\right]T_{b_D}^{i}\quad \forall A\in\{1,2\ldots,n\} \tag{4.36}$$

The Dirichlet BC reduces the number of unknowns as shown earlier. The effect of multiple Dirichlet boundary conditions on the above equation is given as

$$\sum_{B\in\{\Gamma_A\}^c}[M_{AB}]\dot{T}_B+\sum_{B\in\{\Gamma_A\}^c}\left[K_{AB}+\sum_{i=1}^{N_c}\left[K_{AB}^{f_i}\right]\right]T_B=-\sum_{B\in\{\Gamma_A\}}[M_{AB}]\dot{T}_B-\sum_{B\in\{\Gamma_A\}}\left[K_{AB}+\sum_{i=1}^{N_c}\left[K_{AB}^{f_i}\right]\right]T_B$$
$$+\sum_{i=1}^{N_c}\sum_{D=1}^{n_{b_i}}\left[B_{AD}^{f_i}\right]T_{b_D}^{i}\quad \forall A\in\{\Gamma_A\}^c \tag{4.37}$$

with

$$\{\Gamma_A\}=\bigcup_{i=1}^{N_D}\{\Gamma_{A_i}\} \tag{4.38}$$

At this point, it is advantageous to introduce the following matrix notations

$$T=\{T_B\} \qquad B\in\{\Gamma_A\}^c$$
$$M=[M_{AB}] \qquad A,B\in\{\Gamma_A\}^c$$
$$K=[K_{AB}]+\sum_{i=1}^{N_c}\left[K_{AB}^{f_i}\right] \qquad A,B\in\{\Gamma_A\}^c$$
$$T^f=\{T_B\} \qquad B\in\{\Gamma_A\}$$
$$M^f=[M_{AB}] \qquad A\in\{\Gamma_A\}^c,B\in\{\Gamma_A\}$$
$$K^f=[K_{AB}]+\sum_{i=1}^{N_c}\left[K_{AB}^{f_i}\right] \qquad A\in\{\Gamma_A\}^c,B\in\{\Gamma_A\}$$
$$T_b^i=\left\{T_{b_D}^i\right\} \qquad D\in\left\{1,2\cdots,n_{b_i}\right\}$$
$$B^{f_i}=\left[B_{AD}^{f_i}\right] \qquad A\in\{\Gamma_A\}^c,D\in\left\{1,2\cdots,n_{b_i}\right\} \tag{4.39-4.46}$$

Using the above matrix notations into the general finite element equations given by (4.37), we get the matrix equation

$$M\dot{T}+KT=-M^{f}\dot{T}^{f}-K^{f}T^{f}+\sum_{i=1}^{N_c}B^{f_i}T_b^i \quad , \tag{4.47}$$

where M and K are referred to as global mass and stiffness matrices respectively. In the present formulation, we don't have a conventional force matrix; instead the force matrix is composed of three distinct terms. The mass matrix M and the stiffness matrix K are usually banded matrices. The mass matrix can be converted to a diagonal form using lumped mass approximations[7] [77], [78] and hence taking the inverse of the rather large mass matrix is not expensive. This allows us to write the general finite element equations in the following state-space like form

$$\dot{T}=-M^{-1}KT-M^{-1}M^{f}\dot{T}^{f}-M^{-1}K^{f}T^{f}+M^{-1}\sum_{i=1}^{N_c}B^{f_i}T_b^i \quad . \tag{4.48}$$

The vector T^f, its derivative and all T_b^i's are the inputs to the system, some of which may be exogenous. As an initial step in the development, we assume all of them to be inputs to the system and we obtain

$$\dot{T}=\tilde{A}T+\tilde{B}u \tag{4.49}$$

with

$$\tilde{A}=-M^{-1}K$$

$$\tilde{B}=\begin{bmatrix}-M^{-1}M^{f} & -M^{-1}K^{f} & M^{-1}B^{f_1} & \cdots & M^{-1}B^{f_{N_c}}\end{bmatrix}$$

$$u=\begin{Bmatrix}\left(\dot{T}^{f}\right)^{T} & \left(T^{f}\right)^{T} & \left(T_b^{1}\right)^{T} & \cdots & \left(T_b^{N_c}\right)^{T}\end{Bmatrix}^{T} \tag{4.50-4.52}$$

---

[7]This additional approximation reduces the number of computations significantly.

Note that the input vector u is composed of the nodal temperature on the Dirichlet boundary, its derivative, and the nodal temperature just outside the convection boundary (see Figure 4.4). We can decompose the vector u into a set of regular inputs u^c and a set of exogenous inputs u^e such as disturbances and accordingly, $\tilde{B}$ can be decoupled to satisfy

$$\tilde{B}u = \tilde{B}^c u^c + \tilde{B}^e u^e . \tag{4.53}$$

Substituting the above relation into the state-space finite element model given by Equation (4.49) yields

$$\dot{T} = \tilde{A}T + \tilde{B}^c u^c + \tilde{B}^e u^e \tag{4.54}$$

Note that the states are the temperatures at the nodal points. Let there be q temperature measurements at the locations (r_i, z_i). The q measurements are represented by a measurement vector y. All the measurements can be determined as a linear combination of the nodal temperatures and thus any measurement y_i is given as

$$y_i = \sum_{B=1}^{n} C_{iB} T_B \quad i \in \{1,2,\cdots,q\}, \tag{4.55}$$

with

$$C_{iB} = N_B(r_i, z_i) \tag{4.56}$$

If there are Dirichlet BCs, it is possible that some of the nodal temperatures are actually inputs to the system rather than the states of the system, and hence writing y_i in terms of states and inputs yields

$$y_i = \sum_{B \in \{\Gamma_A\}^c} C_{iB} T_B + \sum_{B \in \{\Gamma_A\}} C_{iB} T_B \qquad i \in \{1,2,\cdots,q\} . \tag{4.57}$$

Define the matrices

$$y=\{y_i\} \qquad i\in\{1,2,\cdots,q\}$$
$$\tilde{C}=[C_{iB}] \qquad i\in\{1,2,\cdots,q\}, B\in\{\Gamma_A\}^c$$
$$\tilde{D}=\begin{bmatrix} 0^{q\times n_{\Gamma_A}} & [C_{iB}] & 0^{q\times n_{b_1}} & \cdots & 0^{q\times n_{b_{N_c}}} \end{bmatrix} \qquad i\in\{1,2,\cdots,q\}, B\in\{\Gamma_A\}, \quad (4.58\text{-}4.60)$$

where n_{Γ_A} is the number of elements in the set Γ_A. All other quantities are the same as defined before. Implementing the matrix notations defined in (4.58)-(4.60) into the output equation given by (4.57), we get

$$y=\tilde{C}T+\tilde{D}u. \qquad (4.61)$$

As before the input u can be divided into two sets: a set of control inputs u^c and a set of exogenous inputs u^e. Decoupling $\tilde{D}$ appropriately to satisfy

$$\tilde{D}u=\tilde{D}^c u^c+\tilde{D}^e u^e, \qquad (4.62)$$

allows the output vector y to be written as

$$y=\tilde{C}T+\tilde{D}^c u^c+\tilde{D}^e u^e. \qquad (4.63)$$

4.3 Finite Element Implementation

The mass, stiffness and the force matrices are computed by solving the appropriate integrals. Earlier, it has been stated that the shape functions are defined in such a way that the integrals can be computed in an element by element basis. In the following section, these issues are examined.

4.3.1 Geometry Discretization

The domain Ω is discretized into small non-overlapping regions or elements. In Figure 4.3, an arbitrary domain is discretized into 18 elements. In 2-D, elements are either triangular or quadrilateral. There are certain key points on the elements known as the nodes. These points occur more frequently on the inter-element boundary and less often

inside the element. In Figure 4.3, each element has 4 nodal points[8]. In the remaining of this section, all developments are made on the 4-node quadrilateral element.

The discretization may yield elements of different size and shape. Consequently, the integral limits are different for each element which makes the computation of the stiffness, mass and force terms cumbersome. To overcome this, a transformation is done so that any element is of a desired shape and size. Figure 4.5 depicts global to local transformation of an element in Figure 4.3. The 4-node element in the local coordinates is a square. The transformation is defined in terms of the shape functions. A shape function is attached to each node. The actual global coordinates at any local location for the 4-node quadrilateral element is given by

$$r(\xi,\eta)=\sum_{a=1}^{4}N_a(\xi,\eta)r_a$$
$$z(\xi,\eta)=\sum_{a=1}^{4}N_a(\xi,\eta)z_a \quad , \tag{4.64}$$

The shape function must be selected so that the approximation is exact at the nodal points. One way to guarantee this is to define the shape function N_a 's inside the element such that it takes a value of 1 at the node to which it is attached and 0 at all other nodal points[9]. The shape functions are assumed to be piece-wise polynomials. There are 4 constraints

---

[8]The element is known as the 4-node quadrilateral element. There are other types of elements such as the 9-node quadrilateral element, 3-node triangular element, etc. More nodes in an element can accommodate more complicated geometries within the element while increasing the number of equations (states).

[9]This need not be the case for some elements such as the 5-node quadrilateral element.

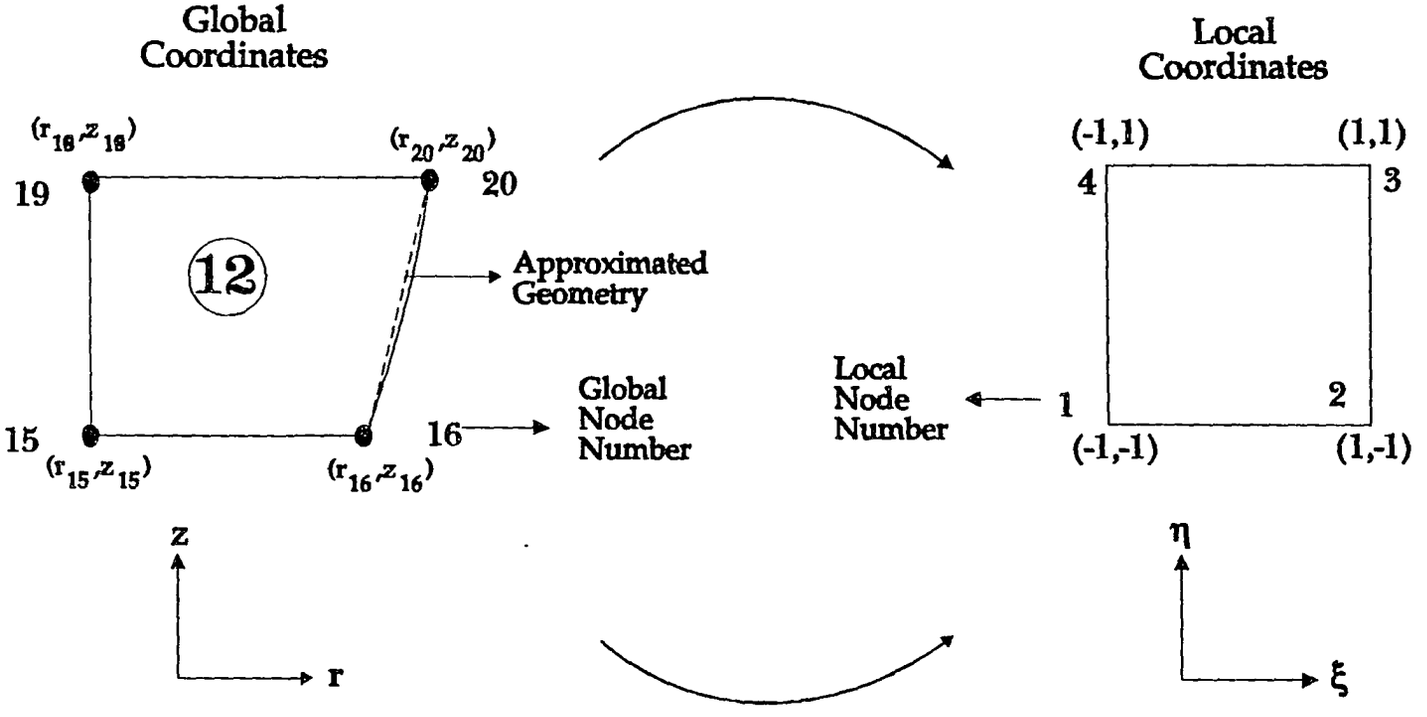

Figure 4.5. An arbitrary element in global and local co-ordinates.

and hence the polynomial can have four unknowns. The assumed polynomials have the form[10]

$$N_a(\xi,\eta) = b_o^a + b_1^a\xi + b_2^a\eta + b_3^a\xi\eta \tag{4.65}$$

The four constraints can be represented by the following matrix equation

$$\begin{pmatrix} b_o^1 & b_1^1 & b_2^1 & b_3^1 \\ b_o^2 & b_1^2 & b_2^2 & b_3^2 \\ b_0^3 & b_1^3 & b_2^3 & b_3^3 \\ b_0^4 & b_1^4 & b_2^4 & b_3^4 \end{pmatrix} \begin{pmatrix} 1 & 1 & 1 & 1 \\ -1 & 1 & 1 & -1 \\ -1 & -1 & 1 & 1 \\ 1 & -1 & 1 & -1 \end{pmatrix} = \begin{pmatrix} 1 & 0 & 0 & 0 \\ 0 & 1 & 0 & 0 \\ 0 & 0 & 1 & 0 \\ 0 & 0 & 0 & 1 \end{pmatrix} \tag{4.66}$$

The above equation is solved to yield the shape function for the 4-node element as

$$\begin{aligned} N_1(\xi,\eta) &= \frac{1}{4}(1-\xi)(1-\eta) \\ N_2(\xi,\eta) &= \frac{1}{4}(1+\xi)(1-\eta) \\ N_3(\xi,\eta) &= \frac{1}{4}(1+\xi)(1+\eta) \\ N_4(\xi,\eta) &= \frac{1}{4}(1-\xi)(1+\eta) \end{aligned} \tag{4.67}$$

Note that with this definition, the shape function is zero when the corresponding nodal point is not a part of the element.

The bounding surface Γ_i are made up of several elements boundaries (see Figure 4.6). This surface is approximated by piece-wise polynomials using the shape functions attached to the nodes on the element boundary surface. To see this, consider an arbitrary element boundary between node 16 and 20 in Figure 4.5. On this element boundary, ξ=1 at every point. Using (4.67), the shape functions N_1 and N_4 are identically zero. This is not surprising as the local nodes 1 and 4 are not on the element bounding surface.

---

[10]The polynomial form must satisfy certain completeness conditions [77, pg. 117].

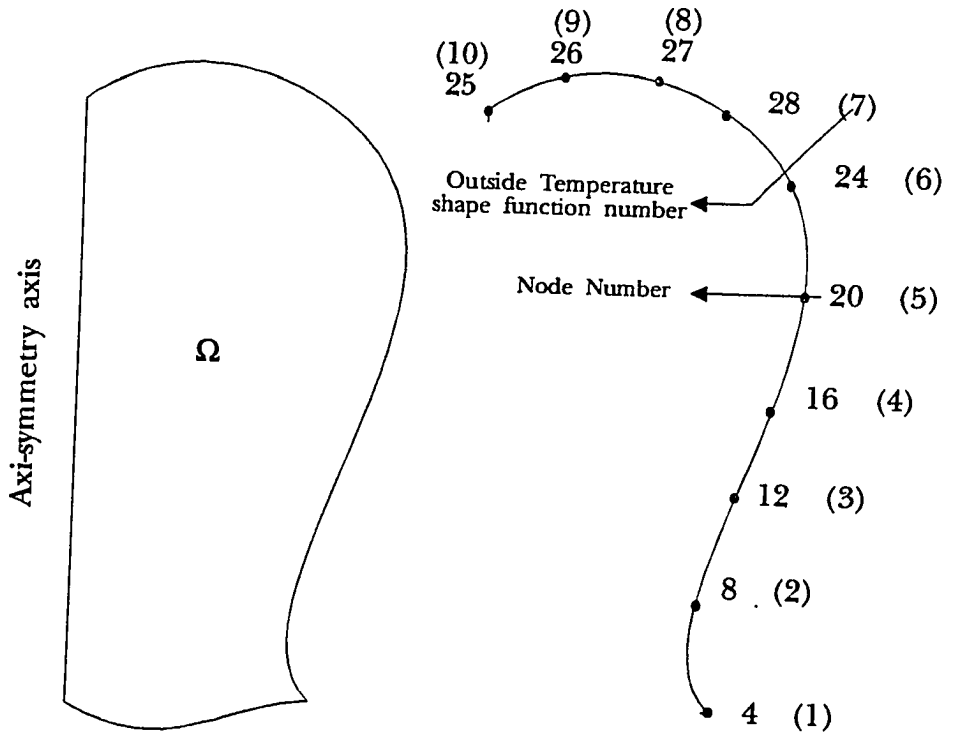

Figure 4.6 Discretization of a bounding surface of figure 4.3.

4.3.2 Approximation of Temperature Distribution and Boundary Conditions

The temperature distribution inside an element is approximated by employing the isoparametric concept. Here, shape functions defined in (4.67) to approximate the geometry are also used to define the temperature distribution within the element. The temperature distribution inside the element is assumed as

$$T(\xi,\eta) \approx \sum_{a=1}^{4} N_a(\xi,\eta) T_a \,, \tag{4.68}$$

where T_a is the nodal temperature at the local node 'a' of the element.

The insulation BC across any bounding surface Γ_i is represented exactly to the extent to which the bounding surface itself is represented by the discretized geometry. For the convection BC, as stated earlier, the outside temperature T_b^i on the boundary surface Γ_i is approximated by defining additional shape functions for each node on the bounding surface. Each boundary surface Γ_i is made up of n_i^e non-overlapping elemental boundary surfaces $\Gamma_{e_j}^i$ as in Figure 4.6 such that

$$\Gamma_i = \bigcup_{j=1}^{n_i^e} \Gamma_{e_j}^i \,. \tag{4.69}$$

The global to local transformation mapping of an elemental bounding surface is shown in Figure 4.7. Across each elemental bounding surface over which convection BC exist, the outside temperature in local coordinates is approximated by

$$T_b^i\Big|_{\Gamma_{e_j}^i} \approx \sum_{d=1}^{2} N_{b_d} T_{b_d} \,, \tag{4.70}$$

where T_{b_d} is the outside temperature very near the d th local node of the element bounding surface and N_{b_d} is the additional shape function associated with the same node. The additional shape functions are defined such that the approximated outside temperature are exact very near the nodal points. The simplest shape function that satisfy this requirement is given by

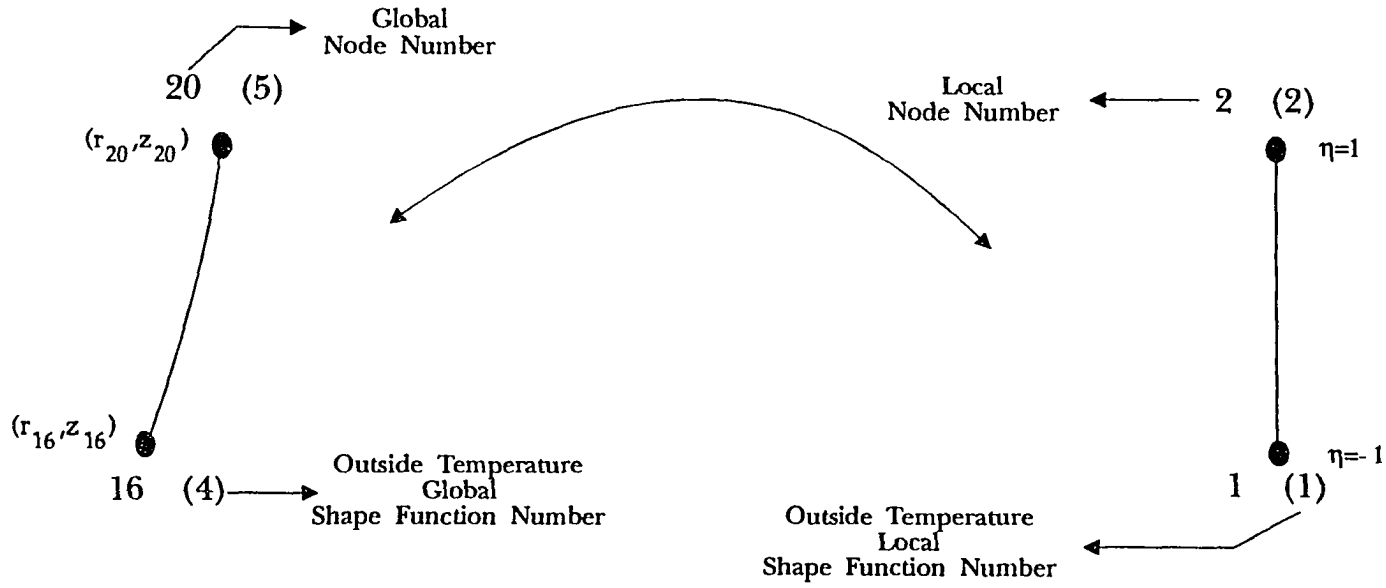

Figure 4.7 An arbitrary element bounding surface in global and local coordinates.

$$N_{b_1}(\xi) = \frac{1}{2}(1-\xi)$$
$$N_{b_2}(\xi) = \frac{1}{2}(1+\xi) \tag{4.71}$$

In the case of Dirichlet BC, the temperature on the boundary surface Γ_i is equal to a known T_{Γ_i}. The temperature inside any element is approximated by (4.68). Therefore, the temperature profile on any elemental boundary can be best approximated by

$$T(\xi,\eta)\big|_{\Gamma_i} = \sum_{a=1}^{4} N_a(\xi,\eta) T_a \Big|_{\Gamma_i}. \tag{4.72}$$

4.3.3 Gauss Quadrature Rule

Integration in the local domain is needed to compute the stiffness, mass and force terms. The integrals to be evaluated have the form

$$\int_{-1}^{1} g(\xi)\, d\xi \tag{4.73}$$

in one dimension and

$$\int_{-1}^{1}\int_{-1}^{1} g(\xi,\eta)\, d\xi\, d\eta \tag{4.74}$$

in two dimensions. These integrations are performed numerically. The most common numerical integration method is the Gauss quadrature.

In one-dimension, the Gauss quadrature for approximately computing the integral in (4.73) is given by

$$\int_{-1}^{1} g(\xi)\, d\xi = \sum_{l=1}^{n_{int}} w_l\, g(\xi_l) + R \approx \sum_{l=1}^{n_{int}} w_l\, g(\xi_l), \tag{4.75}$$

where n_{int} is the number of integration points, ξ_l is the coordinate of the l th integration point, w_l is the weight of the l integration point, and R is the remainder. The two-point Gaussian quadrature is given by

$$\int_{-1}^{1} g(\xi)d\xi = g\left(-\frac{1}{\sqrt{3}}\right)+g\left(\frac{1}{\sqrt{3}}\right)+\frac{g^{(4)}(\bar{\xi})}{135} \approx g\left(-\frac{1}{\sqrt{3}}\right)+g\left(\frac{1}{\sqrt{3}}\right), \tag{4.76}$$

where $g^{(4)}(\bar{\xi})$ is the 4-th derivative of the function g at some point in the interval (-1,1). Thus the 2-point Gauss quadrature is 4th-order accurate.

Gauss quadrature in two-dimension to approximate the integral in (4.74) is given by

$$\int_{-1}^{1}\int_{-1}^{1} g(\xi,\eta)d\xi d\eta = \sum_{l=1}^{n_{int}} w_l\, g(\xi_l,\eta_l) + R \approx \sum_{l=1}^{n_{int}} w_l\, g(\xi_l,\eta_l), \tag{4.77}$$

where (ξ_l,η_l) is the l th integration point coordinates. The 4-point two-dimensional Gauss-quadrature is 4-th order accurate and is given by

$$\int_{-1}^{1}\int_{-1}^{1} g(\xi,\eta)d\xi d\eta \approx g\left(-\frac{1}{\sqrt{3}},-\frac{1}{\sqrt{3}}\right)+g\left(\frac{1}{\sqrt{3}},-\frac{1}{\sqrt{3}}\right)+g\left(\frac{1}{\sqrt{3}},\frac{1}{\sqrt{3}}\right)+g\left(-\frac{1}{\sqrt{3}},\frac{1}{\sqrt{3}}\right). \tag{4.78}$$

4.3.4 Computation of Integrals

4.3.4.1 Mass Matrix

The elements of the mass-matrix, given by (4.11), is computed on an element by element basis as

$$M_{AB} = \iint_{\Omega} \rho c_p N_A N_B r dr dz = \sum_{i=1}^{n_{elem}} \iint_{\Omega_{el}} \rho c_p N_A N_B r dr dz, \tag{4.79}$$

where n_{elem} is the number of elements. As stated earlier, the shape functions N_A 's are non-zero only when the node A is part of the element. Hence, in the 4-node case, each

element contributes to at most 16 members[11] of the mass matrix. In the actual implementation, all the 16 non-zero elements are computed as a 4 by 4 elemental mass matrix. This elemental mass matrix is added to the appropriate elements of the global mass-matrix through the assembling procedure to be described later.

The members of the elemental mass matrix for the *i* th element is given by

$$M_{ab}^{e_i} = \iint_{\Omega_{e_i}} \rho c_p N_a N_b r dr dz \quad , \tag{4.80}$$

where '*a*' and '*b*' are local node number (see Figure 4.5). The above integral is evaluated in local coordinates for easier computation. In local coordinates, the integral (4.80) is given by

$$M_{ab}^{e_i} = \int_{-1}^{1}\int_{-1}^{1} \rho c_p N_a(\xi,\eta) N_b(\xi,\eta) \left(\sum_{a=1}^{4} N_a(\xi,\eta) r_a \right) j(\xi,\eta) d\xi d\eta \quad , \tag{4.81}$$

where $j(\xi,\eta)$ is the Jacobian determinant given by

$$j(\xi,\eta) = \frac{\partial r}{\partial \xi}\frac{\partial z}{\partial \eta} - \frac{\partial r}{\partial \eta}\frac{\partial z}{\partial \xi} \quad . \tag{4.82}$$

The integral in (4.81) is in the same form as (4.77) and therefore the 4-point Gauss quadrature is used to evaluate (4.81) approximately.

4.3.4.2 Stiffness Matrix

The members of the stiffness matrix given in (4.13) are computed as

$$K_{AB} = \sum_{i=1}^{n_{elem}} \iint_{\Omega_{e_i}} k \left(\frac{\partial N_A}{\partial r}\frac{\partial N_B}{\partial r} + \frac{\partial N_A}{\partial z}\frac{\partial N_B}{\partial z} \right) r dr dz \quad . \tag{4.83}$$

---

[11] In the heat conduction problem, there is only one unknown per node which is the nodal temperature. It is possible to have more than one unknown per node, in which case, the element will contribute to more than 16 members of the mass matrix.

As in mass matrix case, the elemental stiffness matrix is computed and is added to the global stiffness matrix through the assembling procedure described in Section 4.3.5. The elemental stiffness matrix members for the i th element are given by

$$K_{ab}^{e_i} = \iint_{\Omega_{e_i}} k\left(\frac{\partial N_a}{\partial r}\frac{\partial N_b}{\partial r} + \frac{\partial N_a}{\partial z}\frac{\partial N_b}{\partial z}\right) r dr dz \tag{4.84}$$

The above integral can be computed in the local coordinates as

$$K_{ab}^{e_i} = \int_{-1}^{1}\int_{-1}^{1} k\left(\frac{\partial N_a}{\partial r}\frac{\partial N_b}{\partial r} + \frac{\partial N_a}{\partial z}\frac{\partial N_b}{\partial z}\right)\left(\sum_{a=1}^{4} N_a(\xi,\eta) r_a\right) j(\xi,\eta)\, d\xi d\eta \tag{4.85}$$

The derivatives of the shape function are evaluated using the chain rule and are given by the matrix equation

$$\begin{pmatrix} \frac{\partial N_a}{\partial r} & \frac{\partial N_a}{\partial z} \end{pmatrix} = \begin{pmatrix} \frac{\partial N_a}{\partial \xi} & \frac{\partial N_a}{\partial \eta} \end{pmatrix} \begin{pmatrix} \frac{\partial \xi}{\partial r} & \frac{\partial \xi}{\partial z} \\ \frac{\partial \eta}{\partial r} & \frac{\partial \eta}{\partial z} \end{pmatrix}, \tag{4.86}$$

with

$$\begin{pmatrix} \frac{\partial \xi}{\partial r} & \frac{\partial \xi}{\partial z} \\ \frac{\partial \eta}{\partial r} & \frac{\partial \eta}{\partial z} \end{pmatrix} = \begin{pmatrix} \frac{\partial r}{\partial \xi} & \frac{\partial r}{\partial \eta} \\ \frac{\partial z}{\partial \xi} & \frac{\partial z}{\partial \eta} \end{pmatrix}^{-1} = \frac{1}{j}\begin{pmatrix} \frac{\partial z}{\partial \eta} & -\frac{\partial r}{\partial \eta} \\ -\frac{\partial z}{\partial \xi} & \frac{\partial r}{\partial \xi} \end{pmatrix}. \tag{4.87}$$

Using (4.64), the derivatives of the shape function are given as

$$\begin{pmatrix} \frac{\partial N_a}{\partial r} & \frac{\partial N_a}{\partial z} \end{pmatrix} = \frac{1}{j}\begin{pmatrix} \frac{\partial N_a}{\partial \xi} & \frac{\partial N_a}{\partial \eta} \end{pmatrix} \begin{pmatrix} \sum_{c=1}^{4} \frac{\partial N_c}{\partial \eta} z_c^e & -\sum_{c=1}^{4} \frac{\partial N_c}{\partial \eta} r_c^e \\ -\sum_{c=1}^{4} \frac{\partial N_c}{\partial \xi} z_c^e & \sum_{c=1}^{4} \frac{\partial N_c}{\partial \xi} r_c^e \end{pmatrix}. \tag{4.88}$$

With the above relation, it is possible to compute the integrand in (4.85) at any coordinate. The integral (4.85) is found by using the 4-point Gauss quadrature. This yields the members of the element stiffness matrix.

4.3.4.3 Force Matrix

The computation of force matrix is quite different from that of the mass and stiffness matrix. This is mainly because of the BCs. Three different BCs have been considered in Section 4.2.2. The contribution of the insulation BC to the force matrix is zero as given in (4.21) and hence nothing needs to be done for this BC. In the case of Dirichlet BC, the number of equations is reduced as shown in Section 4.2.2.3. Therefore, only the convection BC contributes to the force matrix directly. The convection BC also has a stiffness component whose computation is also considered in this section. The force and stiffness contribution of the convection BC are given by (4.29) and (4.25) respectively. These are computed in terms of element boundaries as

$$B_{AD}^{f_i} = \int_{\Gamma_i} hN_A N_{b_D}^i r \, d\Gamma_i = \sum_{j=1}^{n_i^e} \int_{\Gamma_{e_j}^i} hN_A N_{b_D}^i r \, d\Gamma_{e_j}^i \quad , \tag{4.89}$$

$$K_{AB}^{f_i} = \int_{\Gamma_i} hN_A N_B r \, d\Gamma_i = \sum_{j=1}^{n_i^e} \int_{\Gamma_{e_j}^i} hN_A N_B r \, d\Gamma_{e_j}^i \quad . \tag{4.90}$$

The above matrices are found by computing the elemental bounding surface and then adding them to the corresponding global matrix through the assembling procedure described in Section 4.3.5. The elemental integrals in (4.89) and (4.90) in the local system of coordinates is given by[12]

$$B_{ad}^{f_i e_j} = \int_{\Gamma_{e_j}^i} hN_a N_{b_d}^i r \, d\Gamma_{e_j}^i = \int_{-1}^{1} hN_a N_{b_d}^i r \frac{l\left(\Gamma_{e_j}^i\right)}{2} d\xi \tag{4.91}$$

$$F_{ab}^{f_i e_j} = \int_{\Gamma_{e_j}^i} hN_a N_b r \, d\Gamma_{e_j}^i = \int_{-1}^{1} hN_a N_b r \frac{l\left(\Gamma_{e_j}^i\right)}{2} d\xi \quad , \tag{4.92}$$

[12]This transformation is valid only for piece-wise linear shape functions.

where $l\left(\Gamma_{e_j}^i\right)$ is the length of the element bounding surface $\Gamma_{e_j}^i$. Note that on any element bounding surface in the local coordinate, either ξ or η is changing. The above integrals are valid for bounding surface over which only ξ is changing. In the case of changing η, the elemental integrals in (4.91) and (4.92) are obtained by replacing all ξ by η. Now, the one-dimensional 2 point Gauss quadrature formula given by (4.76) can be used to compute the integral (4.91) and (4.92) numerically. This would yield the elemental force contribution due to convection BC.

4.3.5 Assembling of Elemental Matrices

Initially the global mass and stiffness matrices are made zero. The 4 by 4 elemental mass and stiffness matrices have to be added to the appropriate members of the corresponding global matrices. For any i th element, let the global node numbers corresponding to local node numbers (1,2,3,4) be given by $\left(a_1^i, a_2^i, a_3^i, a_4^i\right)$. For example in Figure 4.3, corresponding to local node numbers of element 12, the global numbers are (15,16,20,19). The contribution of the i th element to global matrices is given by

$$M_{a_j^i a_k^i} = M_{a_j^i a_k^i} + M_{jk}^{e_i}, \tag{4.93}$$

$$K_{a_j^i a_k^i} = K_{a_j^i a_k^i} + K_{jk}^{e_i}. \tag{4.94}$$

The global B^{f_i} and K^{f_i} matrices are computed by assembling the contributions from each elemental bounding surface. In the local coordinates, any elemental bounding surface j has a local node numbering (1,2) and the corresponding global node number $\left(a_1^j, a_2^j\right)$. Also, the outside temperature shape function number corresponding to the local nodes (1,2) is $\left(b_1^j, b_2^j\right)$. The contribution of the j th elemental bounding surface to the global B^{f_i} and K^{f_i} matrices is given by

$$B_{a_k^i b_m^j}^{f_i} = B_{a_k^i b_m^j}^{f_i} + B_{km}^{f_i e_j} \tag{4.95}$$

$$K^{f_i}_{a_k^i a_m^j} = K^{f_i}_{a_k^i a_m^j} + K^{f_i e_j}_{km} \quad (4.96)$$

Now all the global matrices are computed; i.e., we have all the known matrices in (4.35). A state-space model can be obtained by following the procedure in Section 4.2.3.

4.4 Summary

An approach to obtain a state-space model of an axi-symmetric heat conduction energy equation using FE approximation is presented. To simplify the development of FE model, the formulation is presented for a specific element, i.e., 4-node quadrilateral element. The general theoretical development and the actual implementation procedures are discussed in this chapter.

In the following chapter, the state-space model is used to design a controller that would establish a necessary temperature distribution inside the material.

CHAPTER V

CONTROLLER DESIGN ASPECTS OF HEAT CONDUCTION EQUATION

A lumped state-space model of the boundary controlled heat conduction system can be obtained using the procedure developed in the last chapter and is given as

$$\begin{aligned} \dot{T} &= \tilde{A}T + \tilde{B}^c u^c + \tilde{B}^e u^e \\ y &= \tilde{C}T + \tilde{D}^c u^c + \tilde{D}^e u^e \end{aligned}, \tag{5.1}$$

where $T \in \Re^n$ is the nodal temperature vector, $u^c \in \Re^{m_c}$ is the control input vector that can be varied as desired, $u^e \in \Re^{m_e}$ is the exogenous input vector that cannot be varied, and $y \in \Re^p$ is the measurement vector.

5.1 Open Loop System Properties

The lumped system in (5.1) is said to be open-loop stable if all the eigenvalues of $\tilde{A}$ have negative real parts, i.e.,

$$real\left(\lambda_i\left(\tilde{A}\right)\right) < 0 \quad \forall i, \tag{5.2}$$

where $\lambda_i(\cdot)$ is the i th eigenvalue. The system in (5.1) is assumed to be stabilizable and detectable[1]. If this is not the case, there is a need for more actuators or sensors to control the system. The number and locations of sensors and actuators may be such that some states (or some linear combination of states) are either uncontrollable or unobservable. These states, however, are stable due to the stabilizability and detectability assumptions.

[1]See Sections 2.5.2 and 2.5.3 for definitions and some discussions.

A minimum realization of the system (5.1), found by retaining the controllable and observable modes, can be used to design a controller as shown later.

In any lumped model of DPS, it is possible to have states (or a linear combination of states) that are either weakly controllable or weakly observable. Qualitatively, a state is said to be weakly controllable, if a small change in the state requires a very large input. Hence, if a controller tries to alter a weakly controllable state, it would request a large control input from the actuators, i.e., the controller gain is high. Similarly, a state is said to be weakly observable, if a small change in the output is created by a very large change in the state. This would make the observer[2] gain very high. A judgment on the number of weakly controllable and observable states can be made by computing the Hankel singular values of the system, which are given by

$$\sigma_i = \sqrt{\lambda_i\left(\tilde{W}_c\tilde{W}_o\right)}, \tag{5.3}$$

with $\sigma_1 \geq \sigma_2 \cdots \geq \sigma_n \geq 0$. $\tilde{W}_c$ and $\tilde{W}_o$ are controllability and observability Grammians of the system and is found by solving the following Lyapunov equations

$$\tilde{A}\tilde{W}_c + \tilde{W}_c\tilde{A}^T + \tilde{B}^c\left(\tilde{B}^c\right)^T = 0 \tag{5.4}$$

$$\tilde{A}^T\tilde{W}_o + \tilde{W}_o\tilde{A} + \tilde{C}^T\tilde{C} = 0. \tag{5.5}$$

A significant drop in σ_i after the k th singular value would be observed if there are $(n\text{-}k)$ weakly observable or controllable states.

5.2 Reduced Order Models for Controller Design

A practical controller that tries to alter the dynamics of weakly controllable or observable modes will either saturate the actuators due to high control gain or be too sensitive to sensor noise due to high observer gain. Both saturation of actuators, and

---

[2]Observer is a state-estimator that uses inputs and outputs of the system.

sensitivity to sensor noise are undesirable in any control system. Hence, the controller can be designed using a Reduced-Order Model (ROM), in which all the weakly controllable and observable modes are eliminated. The balanced truncation method can be used for obtaining the ROM and is described in the following section.

5.2.1 Balanced Truncation Method

In this method, an invertible transformation matrix P is used to transform the system into balanced system of coordinates [78] such that

$$T^l = P^{-1}T. \tag{5.6}$$

Here T^l is new state-vector containing a linear-combination of nodal temperatures. In the new coordinates all system matrices are transformed as

$$\left(\tilde{A},\tilde{B}^c,\tilde{B}^e,\tilde{C},\tilde{D}^c,\tilde{D}^e\right)\rightarrow\left(P^{-1}\tilde{A}P,P^{-1}\tilde{B}^c,P^{-1}\tilde{B}^e,\tilde{C}P,\tilde{D}^c,\tilde{D}^e\right)\equiv\left(A,B^c,B^e,C,D^c,D^e\right), \tag{5.7}$$

The controllability grammian W_c and the observability grammian W_o of the transformed system have the following form

$$\begin{aligned} W_c &= diag(\Sigma_1,\Sigma_2,0,0)\in\Re^{n\times n} \\ W_0 &= diag(\Sigma_1,0,\Sigma_3,0)\in\Re^{n\times n}, \end{aligned} \tag{5.8}$$

where Σ_1, Σ_2, Σ_3 are positive definite diagonal matrices with

$$\Sigma_1 = diag(\sigma_1,\sigma_2,\cdots,\sigma_l) \tag{5.9}$$

with

$$\sigma_1\geq\sigma_2\cdots\geq\sigma_l>\sigma_{l+1}=\cdots=\sigma_n=0.$$

The σ_i's are the Hankel singular values of the system. Since there are l non-zero σ_i's, the minimum realization has an order l. A significant drop in σ_i after the k th singular value would be observed if there are $(n\text{-}k)$ weakly observable or controllable states. The $k\leq l$

order ROM containing the modes associated with k largest Hankel singular values can be obtained by partitioning the transformed system as

$$T^l = \begin{bmatrix} T_1^l \\ T_2^l \end{bmatrix} A = \begin{bmatrix} A_{11} & A_{12} \\ A_{21} & A_{22} \end{bmatrix} \quad B^c = \begin{bmatrix} B_1^c \\ B_2^c \end{bmatrix} \quad B^e = \begin{bmatrix} B_1^e \\ B_2^e \end{bmatrix}$$
$$C = \begin{bmatrix} C_1 & C_2 \end{bmatrix} \quad P = \begin{bmatrix} P_1 & P_2 \end{bmatrix} \tag{5.10}$$

where $A_{11} \in \Re^{k \times k}$, $A_{22} \in \Re^{(n-k)\times(n-k)}$ and all other matrices are of appropriate dimension. The ROM after elimination (n-k) weakest controllable\observable modes is given by

$$\dot{T}_1^l = A_{11} T_1^l + B_1^c u^c + B_1^e u^e$$
$$y \approx y_r = C_1 T_1^l + D^c u^c + D^e u^e. \tag{5.11}$$

Several balancing methods have been developed to obtain the transformation matrix P and most of them require a minimum realization of the original Full Order Model (FOM). This is not always available, even when this condition is satisfied, the system may be weakly observable/controllable and hence for all practical purposes, the system is non-minimum. The numerically robust Schur method [79] has no minimality requirement and therefore can be used instead. Here a k th order ROM that retains the most controllable and observable states is directly obtained as follows

$$T_1^l = S_{L,big}^{'} T$$

$$A_{11} = S_{L,big}^T \tilde{A} S_{R,big}$$
$$B_1^c = S_{L,big}^{'} \tilde{B}^c \quad B_1^e = S_{L,big}^{'} \tilde{B}^e$$
$$C_1 = \tilde{C} S_{R,big} \quad D^c = \tilde{D}^c \quad D^e = \tilde{D}^e. \tag{5.12}$$

$S_{L,big}$, $S_{R,big}$ are matrices of dimension n by k and are computed using the orthonormal basis for the left and right eigenspaces associated with the k largest eigenvalues of the matrix $(W_c W_o)$. The matrices W_C and W_O are the controllability and the observability Grammians of the FOM.

5.2.2 On Other Model Reduction Techniques

There are other methods such as Routh approximation , Aggregation, Singular perturbation that may be used to generate ROM. These methods do not necessarily retain the most observable and controllable modes in the ROM; rather, they optimize other criteria such as matching low frequency response of the original system, approximating impulse response etc. These methods are not utilized in this work as the main purpose of a ROM is in the design of controllers that excite the most controllable and observable modes alone.

5.3 Controller Design

A feedback controller can stabilize the system, shape the transient response as desired, and establish a specified temperature distribution. The controller is designed using the ROM. The design is performed in two stages. In the first stage, an observer based state-feedback controller is designed to shape the transient dynamics as described in Section 5.3.1. In the second stage, the desired temperature distribution is established by adding an appropriate bias to the state-feedback control law as shown in Section 5.3.2.

5.3.1 Shaping Transient Dynamics

State-feedback is the most general linear control law and is given as

$$u^c = K_s T_1^l, \tag{5.13}$$

where K_s is the state-feedback constant gain matrix. With the above control law, the transient response of the lumped system can be shaped to satisfy reasonable design requirements. The state-feedback controller is designed as a Linear Quadratic Regulator (LQR). The LQR is found by minimizing the following quadratic performance

$$J_c = \int_0^\infty \left(\left(T_1^l\right)^T Q T_1^l + \left(u^c\right)^T R u^c \right) dt \tag{5.14}$$

where Q and R are weighting matrices of appropriate dimension. The state-feedback gain that minimizes the cost in (5.14) is given by

$$K_s = -R^{-1}\left(B_1^c\right)^T X \tag{5.15}$$

where $X \geq 0$ is the solution of the Riccati equation

$$A_{11}^T X + XA_{11} - XB_1^c R^{-1}\left(B_1^c\right)^T X + Q = 0. \tag{5.16}$$

The weighing matrices Q and R are the design parameters that can be selected to give a reasonable transient response. The closed-loop system is given by

$$\dot{T}^l = A_{cl}T^l + B^e u^e \tag{5.17}$$

with

$$A_{cl} = \begin{bmatrix} A_{11} + B_1^c K_s & A_{12} \\ A_{21} + B_2^c K_s & A_{22} \end{bmatrix} \tag{5.18}$$

The transient response of the closed-loop lumped system is determined by the matrix A_{cl}.

To implement the state-feedback controller, it is necessary to measure all the states of the ROM, i.e., T_1^l. The measurements of all states are very rarely available and hence the states are reconstructed from the available measurements using an observer. In this case, the control law in (5.13) is modified as

$$u_1^c = K_s \hat{T}_1^l, \tag{5.19}$$

where $\hat{T}_1^l$ is the estimate of T_1^l and is found by using an observer. The observer dynamics is governed by

$$\dot{\hat{T}}_1^l = A_{11}\hat{T}_1^l + B_1^c u^c + B_1^e u^e + L(y - C_1 T_1^l - D_1^c u^c - D_1^e u^e), \tag{5.20}$$

where L is the observer gain matrix that is selected to shape the estimated state transient response. The separation principle [80] allow us to design the controller and the observer separately. The observer is designed as a Linear Quadratic Estimator (LQE) using the

ROM. The LQE is a dual problem of the LQR and the observer gain is found by minimizing a performance index similar to (5.14) that includes the effect of state disturbance and measurement noise. For an optimal LQE, the weighting matrix Q_o is the covariance of state-disturbance and the weighting matrix R_o is the covariance of the measurement noise. In this section, we treat these weighting matrix as design matrix to shape the transients of the estimator. The observer gain L that minimize the LQE performance index is given by

$$L = -X_o C_r^T R_o^{-1}, \tag{5.21}$$

where $X_o \geq 0$ is the solution of the Riccati equation

$$A_{11} X_o + X_o A_{11}^T - X_o C_1^T R_o^{-1} C_1 X_o + Q_o = 0. \tag{5.22}$$

The closed-loop system is given by

$$\begin{pmatrix} \dot{T}_1^l \\ \dot{T}_2^l \\ \dot{\hat{T}}_1^l \end{pmatrix} = \underbrace{\begin{pmatrix} A_{11} & A_{12} & B_1^c K_s \\ A_{21} & A_{22} & B_2^c K_s \\ 0 & 0 & A_{11} + B_1^c K_s - LC_1 - LD_1^c K_s \end{pmatrix}}_{A_{cl}} \begin{pmatrix} T_1^l \\ T_2^l \\ \hat{T}_1^l \end{pmatrix} + \begin{pmatrix} B_1^e \\ B_2^e \\ B_1^e - LD_1^e \end{pmatrix} u^e + \begin{pmatrix} 0 \\ 0 \\ L \end{pmatrix} y \tag{5.23}$$

The transient response of the controlled lumped system is determined by the A_{cl} matrix. The transfer function of the dynamic controller in the Laplace domain is given by

$$u(s) = K_s \left(sI - A_{11} - B_1^c K_s + LC_1 + LD_1^c K_s \right)^{-1} \left(Ly(s) + \left(B_1^e - LD_1^e \right) u^e(s) \right). \tag{5.24}$$

5.3.2 Reference Tracking

In addition to shaping the transient response, the controller has to establish the desired temperature distribution inside the material. The required nodal temperatures, denoted by T_d, corresponding to any desired temperature distribution inside the material can be found by using the approximation in (4.8). Therefore, the reference tracking requirement is achieved if, in the steady state,

$$T = T_d. \tag{5.25}$$

In the balanced coordinates, achieving (5.25) is equivalent to satisfying

$$T^l = P^{-1}T_d\,. \tag{5.26}$$

To achieve this, a bias input u_b is added to the control law in (5.19) as

$$u_1^c = K_s\hat{T}_1^l + u^b \tag{5.27}$$

The states of the controlled balanced system in the steady state is given by the solution to the system of equations[3]

$$\begin{bmatrix} A_{11} + B_1^c K_s & A_{12} \\ A_{21} + B_2^c K_s & A_{22} \end{bmatrix} T^l(\infty) = -\left(B^c u^b + B^e u^e\right) \tag{5.28}$$

Hence, the bias input that would achieve (5.26) must satisfy the matrix equation

$$B^c u^b = -\begin{bmatrix} A_{11} + B_1^c K & A_{12} \\ A_{21} + B_2^c K & A_{22} \end{bmatrix} P^{-1}T_d - B^e u^e \equiv v\,. \tag{5.29}$$

A bias input u^b exist, if the vector v lies in the range space of B^c. A formal set of conditions for the existence of the bias input for an arbitrary reference is given in a later section. In Section 5.4, an example is presented to demonstrate the modeling and control design technique developed in Chapter IV and this chapter.

5.3.3 Robustness of closed-loop system

The LQR guarantees a minimum Gain Margin (GM) of $\left(\frac{1}{2}, \infty\right)$ and a minimum Phase Margin (PM) of $\pm 60^\circ$ in all the loops that may be formed at the input side of the plant [81]. An estimate of the actual GM and the PM can be obtained by computing the smallest singular value of the return difference *G(s)* at the input for all frequencies [82]. If one chooses a positive number α such that

---

[3]We assume that the observer has no steady-state bias, i.e., $\hat{T}_1^l(\infty) = T_1^l(\infty)$.

$$\underline{\sigma}[I+G(j\omega)] \geq \alpha \quad ,\forall\omega \tag{5.30}$$

where $\underline{\sigma}(\cdot)$ denote the smallest singular value, then there is a guaranteed gain margin of

$$GM = \frac{1}{1\pm\alpha} \tag{5.31}$$

and a guaranteed phase margin of

$$PM = \pm 2\sin^{-1}\left(\frac{\alpha}{2}\right). \tag{5.32}$$

For the observer-based controller, there is no guarantee on any minimum GM and PM [82]. The observer-based controller may be unstable even though the closed-loop system is stable. These defects can be overcome by a proper choice of the observer design matrices Q_O, R_O. The Loop Transfer Recovery (LTR) [83] procedure is one way to design a stable compensator[4] and recover the robustness properties that the state-feedback controller for the observer-based controllers by appropriately choosing the weightings. This approach can be found in [83] and will not be described in this Section.

5.4. Illustration of the Modeling and Control Techniques on a Simple Problem

The simple conduction problem illustrated in Figure 5.1 is modeled in this section. The material is inside an axi-symmetric cylinder. The top and the bottom of the cylinder are insulated. The cylindrical material is inside a furnace. The furnace is capable of establishing an axi-symmetrical temperature profile with varying temperatures along the length of the cylinder. Heat transfer from the furnace into the material occurs through convection. The BC's for this problem are given by the following set of equations

[4]Valid only for minimum phase systems

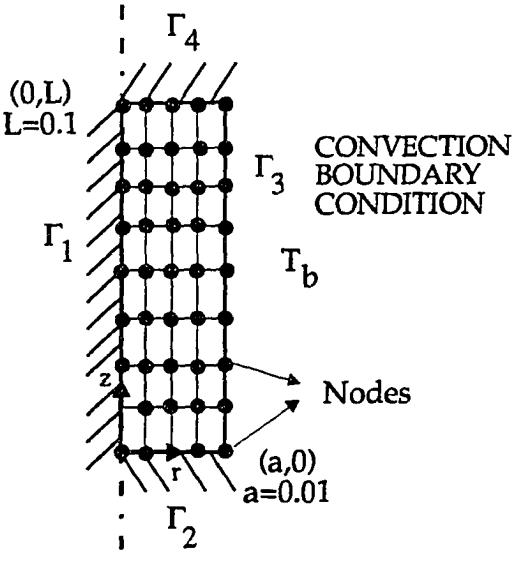

Figure 5.1. Discreitzation of the surface ϕ =0.

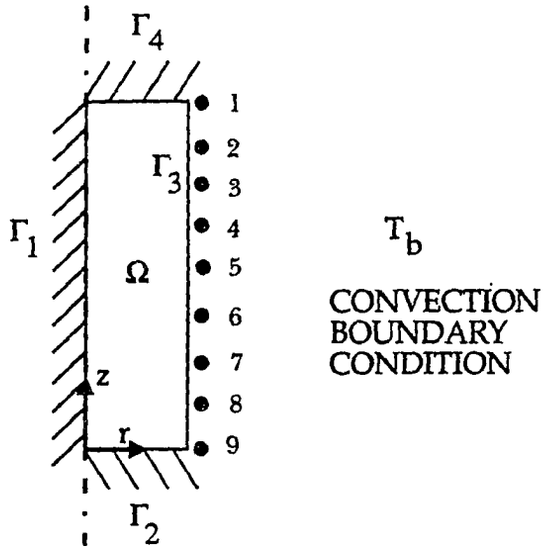

Figure 5.2. Parameterization of convection boundary condition.

$$\left.\frac{\partial T}{\partial z}\right|_{z=0} = 0$$
$$\left.\frac{\partial T}{\partial z}\right|_{z=L} = 0$$
$$k\frac{\partial T}{\partial r} + h(T - T_b)\big|_{r=a} = 0 \qquad (5.33)$$

The control problem is to determine the boundary temperature T_b so that a prescribed temperature distribution can be established inside the material. Later on, the desired interface shape is specified in terms of a desired temperature distribution. In order to obtain a FE model, the domain has to be discretized. The domain is discretized into a 5 by 9 grid resulting in 45 nodal points and 32 elements as shown in Figure 5.1. Since this problem has no Dirichlet BC, all the nodal temperatures are unknowns and hence the state space model has 45 states. The convection boundary surface temperature T_b is approximated by 9 basis functions Hence there are 9 control inputs and they correspond to the boundary surface temperatures at certain key points (see Figure 5.2). Also, there is no exogenous input u^e.

The outputs from the system are limited due to practical considerations. Four sets of output measurements are considered and they are

(a) All states are measurable, i.e. $\tilde{C} = I$.

(b) Only the nodal surface temperatures Γ_3 are measurable (see Fig 5.2). This set of measurements results in a set of collocated sensors and actuators.

(c) The nodal outside surface Γ_3 and the center surface Γ_1 temperatures are measurable.

(d) The nodal outside surface Γ_3 and the nodes at the radial direction on the surface z=0.5*L, with L being the length of the cylinder are measurable. This configuration may, for example correspond to crystal growth, if the interface shape can be observed using imaging techniques.

Of the four sets, (a) is not practical and (b) is the most practical set of measurements. Set (a) of measurements result in all states to be equally observable while with set (b), (c) and (d) some states may be weakly observable or completely unobservable. A Hankel singular values plot of all the three systems are given in Figure 5.3. From the figure, the set (a) corresponding to all states being measured has larger Hankel singular values than any other set. Also, we can see that there is a significant drop in Hankel singular values for systems (b) and (d) around the 36th singular value. This qualitatively implies that about 9 states in (b) and (d) are very weakly observable with respect to other states.

Initially, all boundary temperatures are made 1.0 and the nodal temperatures corresponding to this open loop control are shown in Figure 5.4. Due to the symmetry in the input, initial conditions and the geometry, all the nodes in the same vertical line have the same temperature. In the steady state, all the temperatures go to 1.0. The open loop lumped system is stable with very slow transient behavior and takes more than 8 hours to reach the steady state.

The regulator design is performed to improve the transient response. If all the states are measurable as in set (a) of measurements, the state-feedback controller given by (5.13) can be used for this purpose. Further, there are no states that are weakly controllable. Hence, the controller design is performed using the Full Order Model (FOM). The state-feedback gain is found using (5.15) by appropriately choosing the Q and R weighing matrices. For this problem $Q = 10\,I$ and $R = I$ yielded the reasonable transient response. In order to compare the response of closed-loop system to the open-loop system, an additional bias input is included as in (5.27). The bias input u_b is selected such that all the points in the cylinder are at temperature 1.0 as in the open-loop case and these are found using Equation (5.29). Note, since we did not change coordinates, $P = I$.

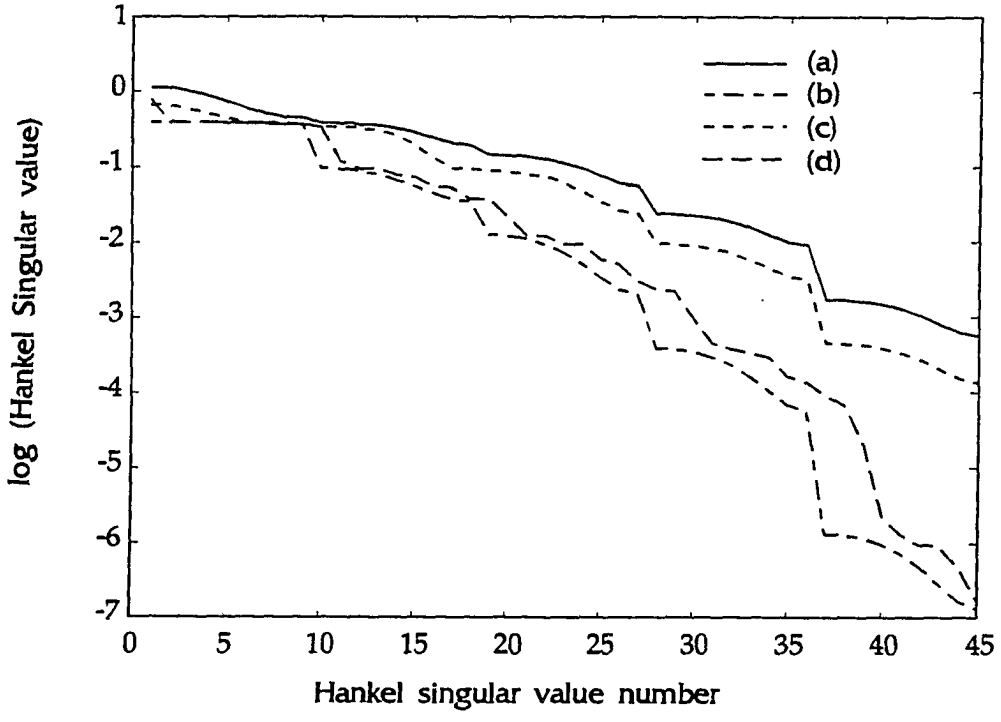

Figure 5.3. Hankel singular value plot for four set of measurements.

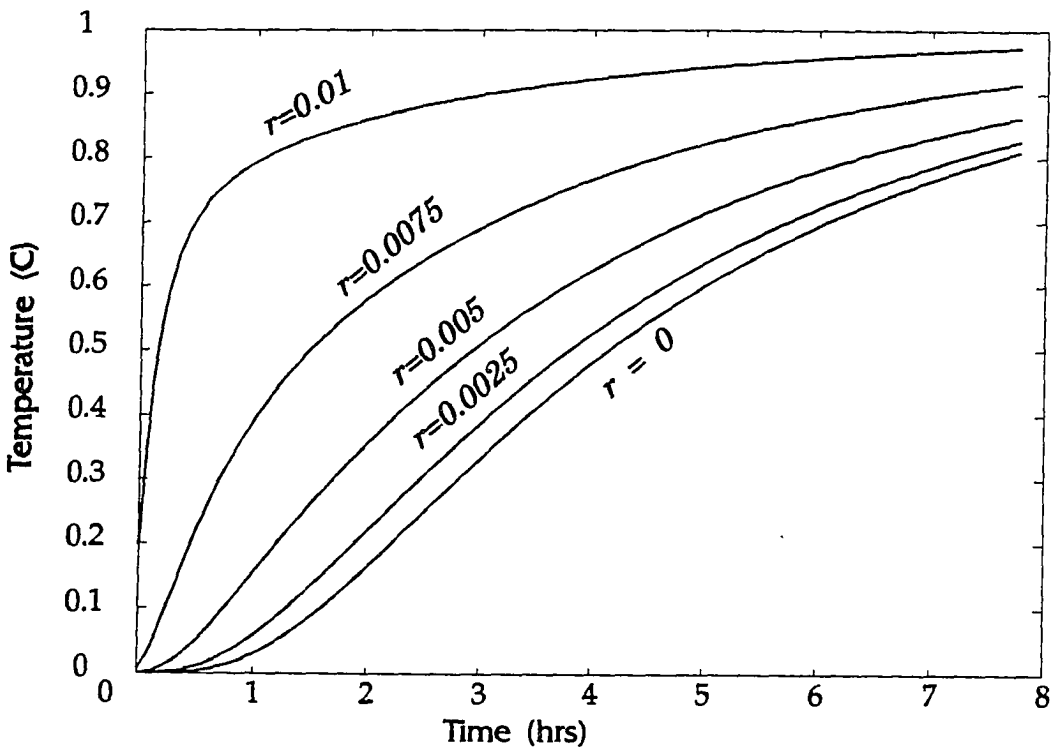

Figure 5.4 Open loop response of the system. The boundary nodal temperatures are at 1C for t >0.

The simulated nodal temperatures are shown in Figure 5.5a and the corresponding controller output are plotted in Figure 5.5b.

The state-feedback control cannot be implemented for systems (b), (c) and (d) as all the states are not available for feedback. To overcome this problem, an observer may be designed and this requires all the states to be observable through the measurements. All states are observable through measurement sets (b), (c) and (d) as is evident from the Hankel singular value plot. However, many modes are very weakly observable, especially for systems (b) and (d). Hence, the control design must be performed using a ROM. The ROM is found using the transformations in (5.12).

The separation principle [80] is exploited to design the controller and the observer separately. Both the observer and the controller gains are designed using the ROM. The state-feedback gain K is determined as before using Equation (5.15). In order to have the comparable cost as in the previous case, the Q_r and R_r matrices are selected as

$$\begin{aligned} Q_r &= S_{R,big}^{'} Q S_{R,big} \\ R_r &= R \end{aligned} \quad , \tag{5.34}$$

where Q and R are the weighing matrices for the system (a). The observer is designed as a Linear Quadratic Estimator (LQE). The LQE weighing matrices are selected as $Q_o = 10\, I$ and $R_o = I$. The observer gain L is determined using (5.21). The control law in (5.27) is used to impose a temperature of 1.0 everywhere inside the material. This is achieved by choosing bias input using (5.29).

In the present design, all observer based controllers have some unstable modes. All the unstable eigenvalues have very small real part. The closed-loop system is stable. The gain and phase margins are computed using the return difference at the input. All controllers have margins that are not too different as the state-feedback controller. Even with good robustness of the closed-loop system, the idea of using an unstable compensator for a stable plant is not logical. This observer must be re-designed using

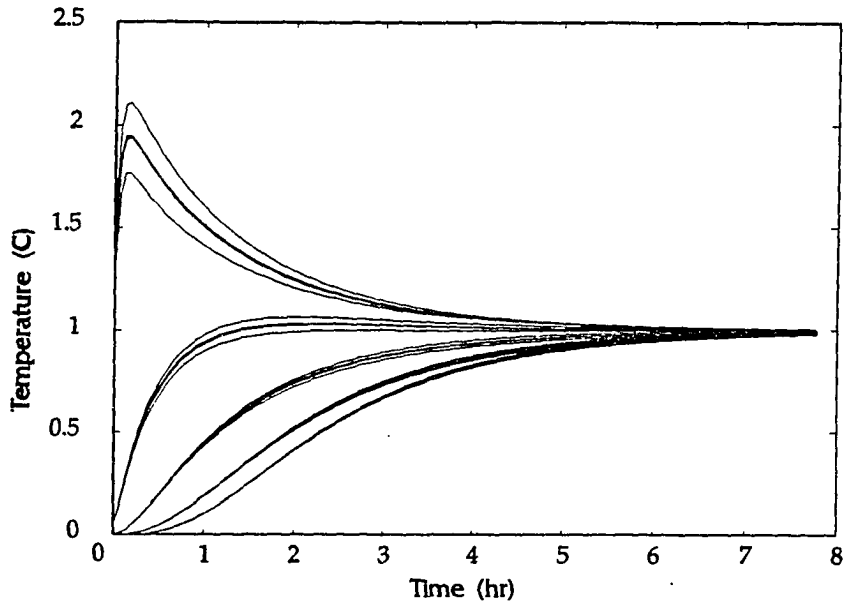

Figure 5.5(a) Transient response of system operating with the state feedback controller. The bias inputs are selected such that all nodes are at 1 C in the steady-state

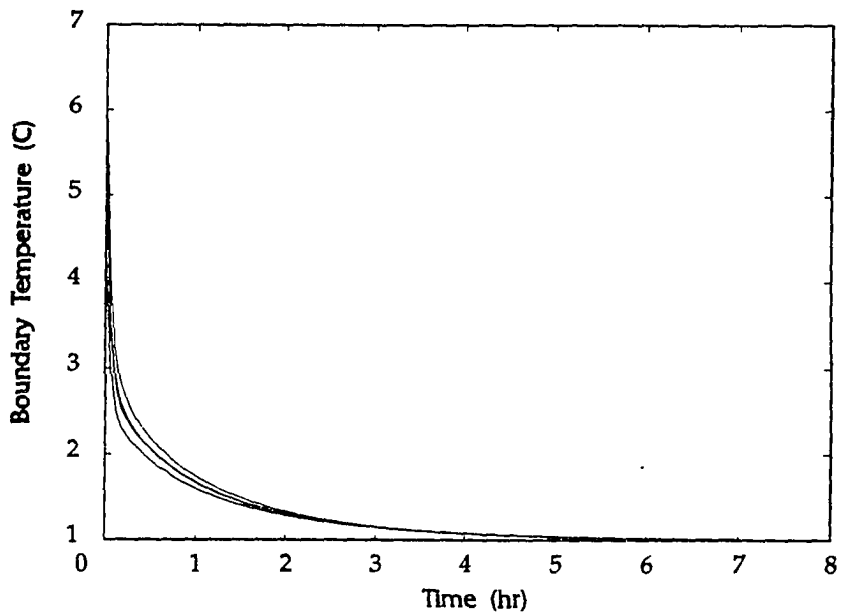

Figure 5.5(b) Boundary nodal temperatures requested by the controller.

LTR technique if applied on a real system. However, for the illustration of control methodology, the present controller is satisfactory.

This observer based controller with an appropriate bias is implemented on systems (b), (c) and (d). The reduced order model for system (b) has 27 states, as there is a significant drop in the Hankel singular value beyond 27. The nodal temperatures under the observer based control are given in Figure 5.6(a) and the corresponding controller output are given in Figure 5.6(b). For the same cost, the observer based controller is slower than the state-feedback controller. Similarly, for system (c), the reduced order model has 36 states and the simulated nodal temperatures and the controller output are given in Figures 5.7(a) and 5.7(b). In the case of system (d), 27 modes are retained in the reduced model. The simulated nodal temperatures for this system operating under closed-loop is plot in Figure 5.8(a). The boundary input that establishes this temperature is plotted in Figure 5.8(b).

In this example, the controller is designed to shape the transient response and the desired temperature distribution inside the material is obtained by suitably choosing the bias input. The bias input is found as a solution of an algebraic equation in (5.29). A solution to this equation may or may not exist. Hence, it is possible that there is no bias input that would establish a certain desired temperature distribution. In the next section, a set of necessary and sufficient conditions are derived for the existence of the bias input.

5.5 Necessary and Sufficient Conditions for Tracking Arbitrary Temperature Distribution

In many situations, it is necessary to establish a certain distribution inside the continuum. Depending on the location of the actuators and sensors, this desirable distribution may or may not be feasible. For example consider the problem of heat conduction in a bar shown in Figure 5.9, where the bar can be heated or cooled from one end. The other end of the bar is insulated. It is physically impossible to achieve a

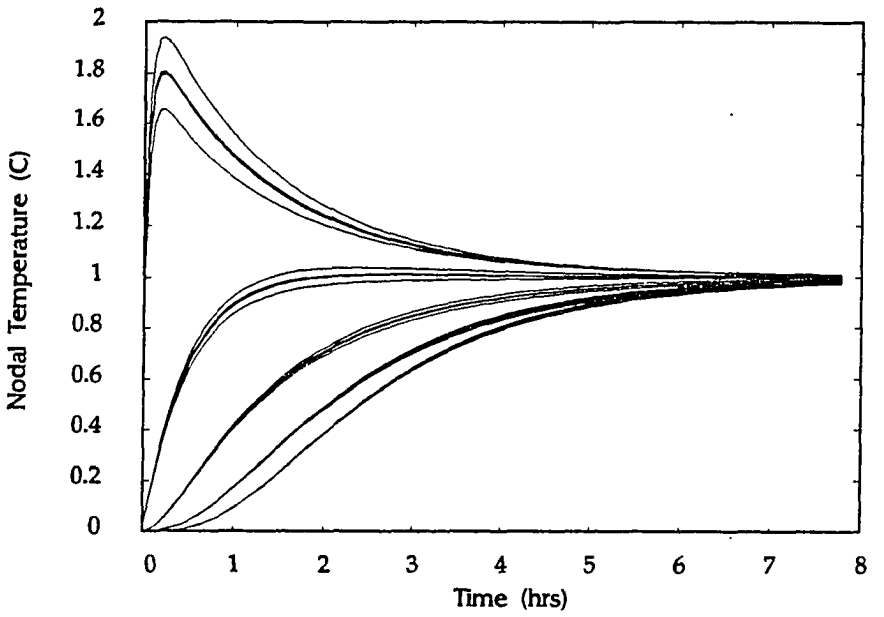

Figure 5.6(a) Transient response of the system (b) operating with the observer based controller. The bias inputs are selected such that all nodes are at 1 C in the steady-state.

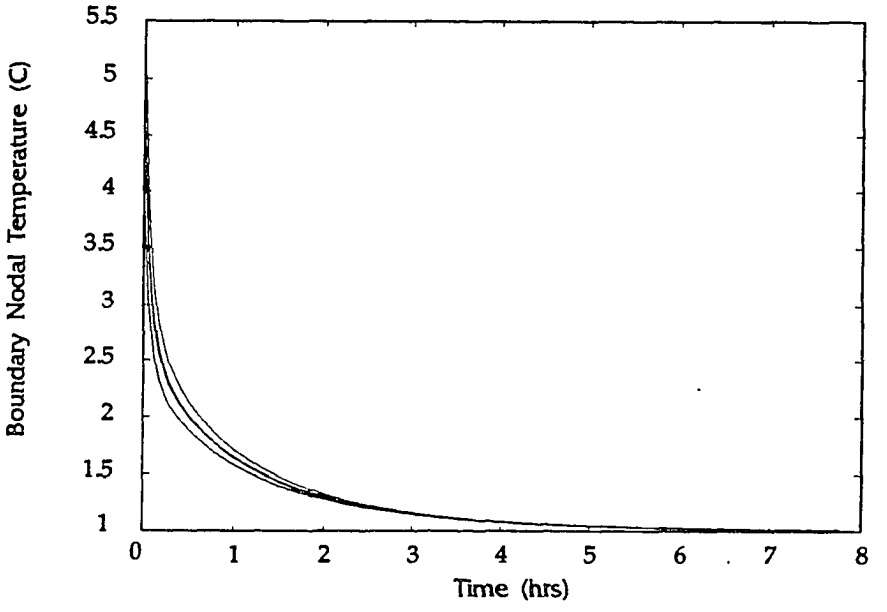

Figure 5.6(b) Requested boundary nodal temperature by the controller.

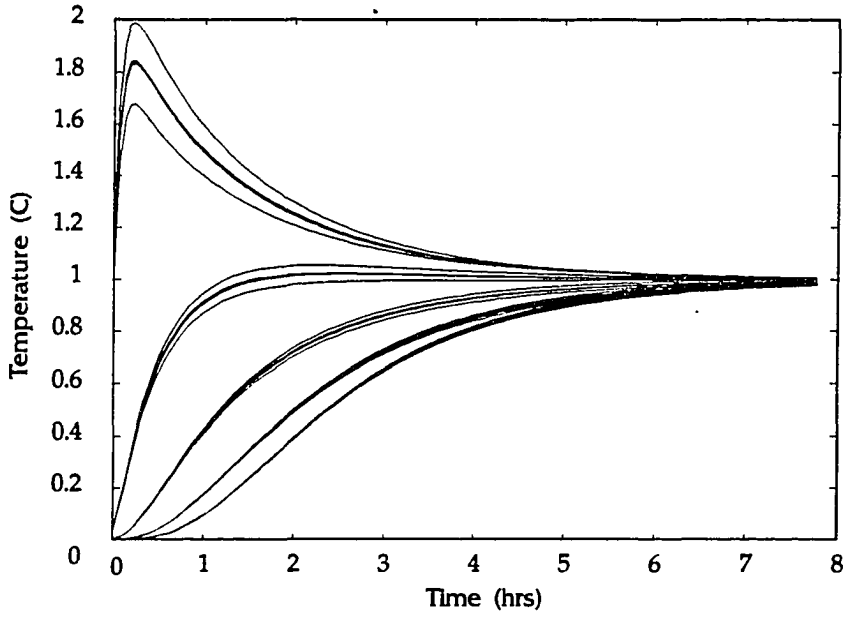

Figure 5.7(a) Transient response of the system (c) operating with the observer based controller. The bias inputs are selected such that all nodes are at 1 C in the steady-state.

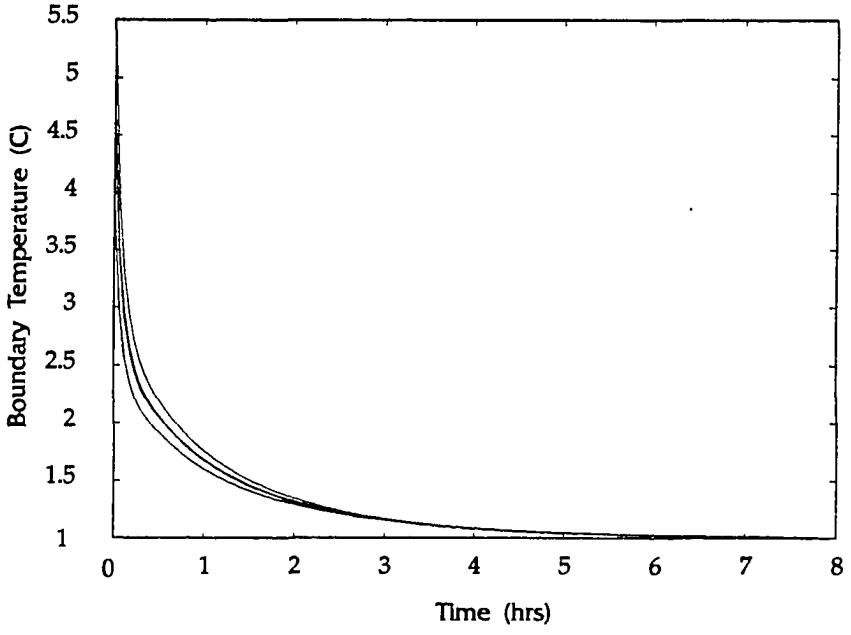

Figure 5.7(b) Requested boundary temperatures by the controller.

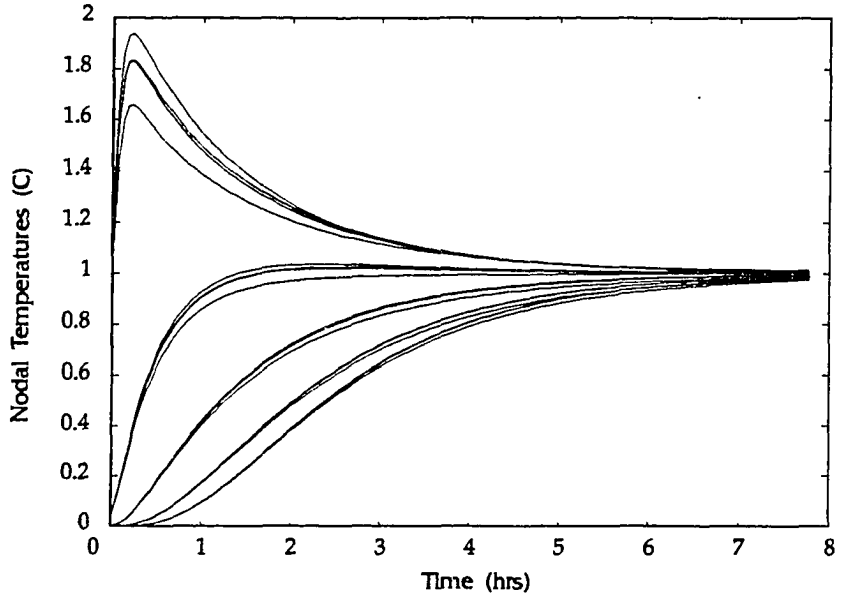

Figure 5.8(a) Transient response of the system (d) operating with the observer based controller. The bias inputs are selected such that all nodes are at 1 C in the steady-state.

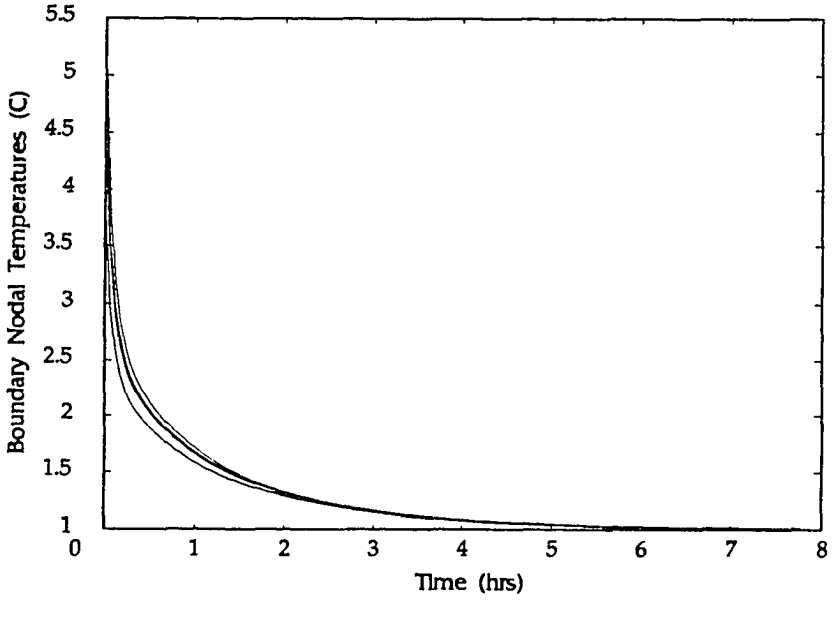

Figure 5.8(b) Requested boundary temperatures at the nodes by the observer based controller for system (d).

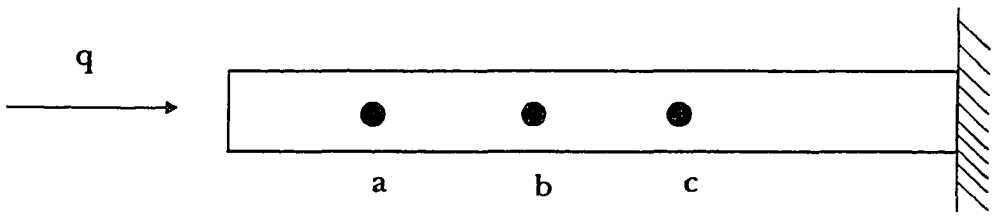

Figure 5.9 One-dimensional heat conduction problem. In the steady-state, it is not possible to have the temperatures at points 'a' and 'c' to be higher than the temperature at point 'b'.

temperature distribution that has higher temperatures at points '*a*' and '*c*' than point '*b*' in the steady state. Such informations are embedded in the state-space model. However, there are no general conditions that one may use to extract these informations. The main motivation of this section is to develop necessary and sufficient conditions for establishing a given distribution inside the continuum. Further, if a particular distribution is not achievable, a procedure is proposed to find the closest distribution that is achievable in the weighted least-square sense.

State-space realization of the lumped DPS is given by (5.1). The exogenous inputs u^e is assumed to be constant. It is possible to redefine the "zero" state and "zero" output of the system to the steady state established by u^e. With this definition, the state-space realization of the lumped heat conduction equation is given by

$$\begin{aligned} \dot{T} &= \tilde{A}T + \tilde{B}^c u^c \\ y &= \tilde{C}T + \tilde{D}^c u^c, \end{aligned} \tag{5.35}$$

where the pair $(\tilde{A}, \tilde{B}^c)$ is stabilizable and the pair $(\tilde{A}, \tilde{C})$ is detectable. A fictitious measurement vector $z \in \Re^n$ containing all state-variable is introduced as follows:

$$z = T \tag{5.36}$$

The matrices $\tilde{B}^c$ and $\tilde{C}$ are assumed to have full column and row ranks respectively. The problem of establishing a distribution can be transformed to the following requirement

$$z = T_d \tag{5.37}$$

where T_d is the desired nodal temperature.

The state-space system of DPS in (5.35) is not minimal most of the times due to practical difficulties in having enough sensors and actuators. Some states may not be controllable. The controllable subspace X_c of the system is defined as follows:

$$X_c = \{x_c \in \Re^n : \exists u(t), 0 \le t \le \tau < \infty \; such\, that\; x(\tau) = x_c \; \forall \; initial\, conditions\}$$

All states of (5.35) are observable through the fictitious measurement z in (5.36) as $(\tilde{A}, I)$ is completely observable. Hence, a minimum realization can be obtained by eliminating the uncontrollable states. This is done by using a non-singular matrix P to transform the coordinate system as

$$x = P^{-1}T = \begin{pmatrix} x_c \\ x_{nc} \end{pmatrix}, \tag{5.38}$$

where $x_c \in \Re^l$ and $x_{nc} \in \Re^{n-l}$. The state-space model in the new coordinates is given by

$$\begin{aligned} \dot{x} &= Ax + Bu \\ y &= Cx + Du \\ z &= Px \end{aligned} \tag{5.39}$$

The matrix P is selected so that the matrices A, B have special structures as given below:

$$\begin{aligned} A &= P^{-1}\tilde{A}P = \begin{pmatrix} A_{11} & A_{21} \\ 0 & A_{22} \end{pmatrix} \quad B = P^{-1}\tilde{B}^c = \begin{pmatrix} B_1 \\ 0 \end{pmatrix} \\ C &= P\tilde{C} = [C_1 \quad C_2] \\ P &= [P_1 \quad P_2] \end{aligned} \tag{5.40}$$

Here, the pair (A_{11}, B_1) is completely controllable. The controllable subsystem of (5.35) is given by

$$\begin{aligned} \dot{x}_c &= A_{11}x_c + B_1u \\ y &= C_1x_c + Du \\ z &= P_1x_c \end{aligned} \tag{5.41}$$

Since P is invertible, P_1 has full column rank . B_1 is assumed to have full column rank[5]. Also, because of the stabilizability assumption all uncontrollable modes are stable and

[5]If this is not true then the actuators are not linearly independent of each other and therefore can be represented by a reduced set of linearly independent actuators.

therefore $x_{nc} \rightarrow 0$ in the steady-state. Further the input u does not excite x_{nc} and therefore non-zero initial conditions are created by disturbances.

Proposition 1:- The controllable subspace X_c of $\Re^n$ for the system in (5.35) is the same as the range space of the matrix P_1.

Proof:- Let $v \in X_c$ such that v is not in the range space of P_1. Hence v can be written as

$$v = P_1 w_1 + P_2 w_2 = P\begin{bmatrix} w_1^T & w_2^T \end{bmatrix}^T, \quad w_2 \neq 0$$

This implies that the corresponding $P^{-1}v$ has the form $\begin{bmatrix} w_1^T & w_2^T \end{bmatrix}^T$ with $w_2 \neq 0$ and therefore is in the uncontrollable space of the system in (5.35). This is a contradiction. Therefore v is in the range space of P_1.

The above proposition provides enough justification for using the system in (5.41) to characterize the trackability of the system in (5.35).

Theorem 1: Consider the system given by (5.41) with the pair (A_{11}, B_1) being controllable. Any constant desired temperature distribution $T_d \in \Re^n$ can be reached by the system, i.e., $z(t) = T_d$ for some finite $t > 0$ from arbitrary initial conditions of z if and only if T_d is in the range space of P_1.

Proof:

Sufficiency: Suppose T_d is in the range space of P_1, then there exist a x_c such that $T_d = P_1 x_c$. Further, since P_1 has full column rank, x_c is unique and is given by $x_c = (P_1^T P_1)^{-1} P_1^T T_d$. Since the pair (A_{11}, B_1) is controllable, there exist a control sequence u that can take the state vector to a desired x_c for some finite $t > 0$ from arbitrary initial conditions. This implies that $z(t) = T_d$ for some finite $t > 0$.

Necessity: Trivial as $z = P_1 x_c = T_d$ implies T_d is the range space of P_1.

The above theorem does not provide any solution regarding the tracking of desired temperature in the steady state. Before deriving a new condition for steady-state trackability, the system is assumed to be controlled using the following control law

$$u = Kx_c + u_b, \tag{5.42}$$

where K is any stabilizing state-feedback gain and u_b is the bias input for achieving non-zero steady state. The control law in (5.42), implemented using observers, includes all controllers that have an order less or equal to the number of states l of the system in (5.41). The closed-loop system for the control law in (5.42) is given as

$$\begin{aligned} \dot{x}_c &= (A_{11} + B_1 K)x_c + B_1 u_b = Fx_c + B_1 u_b \\ y &= C_1 x_c + Du \\ z &= P_1 x_c \end{aligned} \tag{5.43}$$

Theorem 2: Consider the system in (5.41) with the pair (A_{11}, B_1) assumed to be controllable and the pair (A_{11}, C_1) to be detectable. The system is controlled using a stabilizing control gain K as in (5.42) and the resulting closed-loop system is given by (5.43). Any constant reference temperature distribution T_d can be tracked in the steady state if and only if the following conditions hold

(a) T_d is in the range space of P_1 and

(b) the quantity w, defined as $w = F(P_1^T P_1)^{-1} P_1^T T_d$, is in the range space of B_1.

Sufficiency: Since T_d is the range space of P_1, the quantity w can be defined as $w = F(P_1^T P_1)^{-1} P_1^T T_d$. Also w is in the range space of B_1. Hence there exist a v such that

$$B_1 v = -w = -F(P_1^T P_1)^{-1} P_1^T T_d.$$

Let the bias input $u_b = v$ for all t >0. Since the closed-loop system is stable, the steady state solution exists and the state-vector is given by

$$x_c(\infty) = (-F)^{-1} B_1 u_b = (P_1^T P_1)^{-1} P_1^T T_d$$

Hence in the steady-state z is given by

$$z(\infty) = P_1 (P_1^T P_1)^{-1} P_1^T T_d = T_d$$

Necessity: By Theorem 1, T_d must lie in the range space of P_1. Hence there exist a $\tilde{w}$ such that $T_d = P_1 \tilde{w}$. Further since P_1 has full column rank $\tilde{w}$ is unique and is given by

$\tilde{w} = \left(P_1^T P_1\right)^{-1} P_1^T T_d$. Now the state-vector in the steady state is given by $\tilde{w}$. This implies $w = F\tilde{w} = -B_1 u_b$. Hence w is in the range space of B_1.

Note the detectability condition on the pair (A_{11}, C_1) is not used by the proof. However, this is necessary for the implementation of a stabilizing gain K in the control law given by (5.42). The above theorem provide a condition for tracking in the steady state. This condition depends on the closed-loop matrix F and hence depends on the state-feedback gain. In the next theorem, it is shown that if the given reference r satisfies conditions in theorem 2 for one stabilizing controller then it satisfies the condition for every other stabilizing controller.

Proposition 2:For any two gain K_1 and K_2 for which $(A_{11} + B_1 K_1)$ and $(A_{11} + B_1 K_2)$ are Hurwitz, $Range\left((A_{11} + B_1 K_1)^{-1} B_1\right) = Range\left((A_{11} + B_1 K_2)^{-1} B_1\right)$.

Proof: Let $x \in Range\left((A_{11} + B_1 K_1)^{-1} B_1\right)$. Then there exist y such that

$$x = (A_{11} + B_1 K_1)^{-1} B_1 y.$$

This implies $(A_{11} + B_1 K_2)x = B_1\left(y - (K_1 - K_2)x\right)$

or $x = (A_{11} + B_1 K_2)^{-1} B_1\left(y - (K_1 - K_2)x\right)$.

Hence $x \in Range\left((A_{11} + B_1 K_2)^{-1} B_1\right)$.

Theorem 3: Let the system in (5.41) be stabilized using the control law in (5.42). The control gain is given by K_1 and the corresponding closed-loop system matrix is given by F_1. Any desired temperature distribution T_d that can be tracked in steady-state for this controller can be tracked by any other stabilizing controller K_2 with the closed-loop system being F_2.

Proof: By Theorem 2, the reference T_d is in the range space of P_1 and the quantity w_1 given by $w_1 = F_1\left(P_1^T P_1\right)^{-1} P_1^T T_d$ is in the range space of B_1. This implies there exist v such that

$$w_1 = B_1 v.$$

Further F_1 is Hurwitz and hence invertible. This implies $F_1^{-1}w_1 = F_1^{-1}B_1v$, i.e., $F_1^{-1}w_1$ is in the range space of $F_1^{-1}B_1$. By proposition 2, $F_1^{-1}w_1$ is also in the range space of $F_2^{-1}B_1$. Hence there exist a $\tilde{v}$ such that

$$F_1^{-1}w_1 = F_2^{-1}B_1\tilde{v},$$

or $F_2F_1^{-1}w_1$ is in the range space of B_1. Now, the quantity w_2 is given as

$$w_2 = F_2\left(P_1^TP_1\right)^{-1}P_1^TT_d = F_2F_1^{-1}F_1\left(P_1^TP_1\right)^{-1}P_1^TT_d = F_2F_1^{-1}w_1.$$

Thus from the above relationship w_2 is also in the range space of B_1.

Proposition 3: Any desired temperature T_d satisfies conditions (a) and (b) of theorem 2 if and only if T_d is in the range space of $\phi = P_1F^{-1}B_1$.

Proof:

Sufficiency: Let T_d be in the range space of ϕ. Hence there exists a v such that $T_d = \phi v = P_1\left(F^{-1}B_1v\right)$. Therefore, T_d is in the range space of P_1 satisfying condition (a) of theorem 2. Now, the quantity w as in defined in theorem 2 is given by

$$w = F\left(P_1^TP_1\right)^{-1}P_1^TT_d = F\left(P_1^TP_1\right)^{-1}P_1^TP_1\left(F^{-1}B_1v\right) = B_1v.$$

Therefore, w is in the range space of B_1 satisfying condition (b) of theorem 2.

Necessity: Let T_d satisfy conditions (a) and (b) of theorem 2. Since the quantity w is in the range space of B_1, there exist a v such that

$$w = F\left(P_1^TP_1\right)^{-1}P_1^TT_d = B_1v.$$

Since T_d is in the range space of P_1

$$T_d = P_1\left(P_1^TP_1\right)^{-1}P_1^TT_d = P_1F^{-1}B_1v = \phi v.$$

Therefore T_d is in the range space of ϕ.

Proposition 4 The ϕ matrix is invariant to similarity transformations M that transforms the system (5.41) as

$$\left(A_{11}, B_1, C_1, P_1\right) \rightarrow \left(M^{-1}A_{11}M, M^{-1}B_1, C_1M, P_1M\right) \equiv \left(\overline{A}_{11}, \overline{B}_1, \overline{C}_1, \overline{P}_1\right)$$

Proof: It is easy to show that the closed loop matrix F is transformed to $M^{-1}FM$.

The transformed ϕ matrix is given by

$$\overline{\phi} = \overline{P}_1 \overline{F}^{-1} \overline{B}_1 = P_1 M M^{-1} F M M^{-1} B_1 = P_1 F^{-1} B_1 = \phi.$$

In many instances, the desired temperature may not be achievable in the steady-state. In these situations, it may be necessary to track a temperature distribution that is close to the original requirement. The closeness may be defined by the following performance index

$$J = \left(T_d - \hat{T}_d\right)^T W \left(T_d - \hat{T}_d\right), \tag{5.42}$$

where $\hat{T}_d$ is the closest temperature distribution to the original reference T_d that can be achieved and W is a positive definite matrix and therefore the following decomposition can be done

$$W = S^T S.$$

The procedure to find this optimal $\hat{T}_d$ is given in the next proposition.

Proposition 5: For a given desired temperature distribution T_d, the optimal $\hat{T}_d$ that minimizes J subject to satisfying conditions (a) and (b) of theorem 2 is given by

$$\hat{T}_d = \phi \left[\phi^T W \phi\right]^{-1} \phi^T W T_d.$$

Proof: By proposition 3, $\hat{T}_d$ must be in range space of ϕ. This implies for every $\hat{T}_d$ there exist a corresponding $\theta \in \Re^m$ such that $\hat{T}_d = \phi\theta$. Therefore the performance index J is given by

$$J = (T_d - \phi\theta)^T W (T_d - \phi\theta).$$

The θ corresponding to optimal J can be found in [88, pg 308-309] and is given by

$$\theta = \left[\phi^T W \phi\right]^{-1} \phi^T W T_d.$$

and hence $\hat{T}_d$ is given by

$$\hat{T}_d = \phi \left[\phi^T W \phi\right]^{-1} \phi^T W T_d.$$

5.6 Note on Observability

All conditions derived in the previous section used the controllability of the pair of $(\tilde{A}, \tilde{B}^c)$ and the observability of the system through the fictitious output z. Some of the controllable modes may be unobservable through the actual measurements y, i.e., the pair (A_{11}, C_1) is unobservable. In this situation, we cannot verify if the desired temperature distribution is established by the bias input through the on-line measurements.

Proposition 6: Any trackable distribution T_d that is in the range space of ϕ is observable through the measurement y if and only if $w = (P_1^T P_1)^{-1} P_1^T T_d$ can be written as a sum of observable eigenvectors of A_{11}, i.e.,

$$w = \sum_{i=1}^{n_o} k_i v_i, \quad C_1 v_i \neq 0, \ i = 1, 2 \cdots, n_o$$

where v_i is the eigenvector of A_{11} and n_o is the number of observable eigenvectors.

Proof: Follows directly from the definition of observability.

5.7 Extension of Conditions to Systems with Weakly Controllable modes

In practice there are many states that are weakly controllable using the available actuators. In Section 5.2, a ROM is obtained by eliminating these weakly controllable states. In this section, the original system in (5.35) is assumed to be asymptotically stable and hence it is feasible to find the grammians of the system. The weakly controllable states of the original system in (5.35) are determined by finding a a non-singular matrix P to transform the coordinate system as

$$x = P^{-1} T = \begin{pmatrix} x_c \\ x_{wc} \end{pmatrix}, \tag{5.43}$$

where $x_c \in \Re^k$ and $x_{wc} \in \Re^{n-k}$. The state-space model in the new coordinates is given by

$$\begin{aligned} \dot{x} &= Ax + Bu \\ y &= Cx + Du \\ z &= Px \end{aligned} \tag{5.44}$$

The matrix P is selected so that the controllability grammian of the transformed system is diagonal. The controllability grammian of the original system can be found by solving the Lyapunov equation given by (5.4). The controllability grammian of the transformed system is given by

$$W_c = P^{-1}\tilde{W}_c P^{-T}. \tag{5.45}$$

As $\tilde{W}_c$ is positive semi-definite matrix, the following factorization can be done either through singular value decomposition or symmetric eigenvalue eigenvector decomposition

$$\tilde{W}_c = U\Sigma U^T, \quad UU^T = I,$$

where

$$\Sigma = diag(\sigma_1, \sigma_2, \cdots, \sigma_n)$$

$$\sigma_1 \geq \sigma_2 \cdots \geq \sigma_l > \sigma_{l+1} = \cdots = \sigma_n = 0$$

Hence, if we let $P=U$, the transformed controllability grammian is given by

$$W_c = P^{-1}\tilde{W}_c P^{-T} = U^T U\Sigma U^T U = \Sigma.$$

In the new system of the coordinates, the system can be partitioned as

$$A = P^{-1}\tilde{A}P = \begin{pmatrix} A_{11} & A_{12} \\ A_{21} & A_{22} \end{pmatrix} \quad B = P^{-1}\tilde{B}^c = \begin{pmatrix} B_1 \\ B_2 \end{pmatrix}$$
$$C = P\tilde{C} = [C_1 \quad C_2]$$
$$P = [P_1 \quad P_2] \tag{5.46}$$

The ROM after elimination (n-k) weakest controllable modes is given by,

$$\dot{x}_c = A_{11}x_c + B_1 u$$
$$y = C_1 x_c + Du$$
$$z = P_1 x_c, \tag{5.47}$$

where the controllability grammian of the ROM is given by

$$\Sigma_1 = diag(\sigma_1, \sigma_2, \cdots, \sigma_k). \tag{5.48}$$

Proposition 7 Any desired temperature distribution T_d can be approximately achieved in the steady state without exciting the (n-k) weakly controllable modes, if T_d is in the range space of $\phi = P_1 A_{11}^{-1} B_1$.

Proof: The ROM found by preserving the k most controllable modes is given by (5.46). Further, it can be shown that A_{11} is Hurwitz [84]. Hence, an extension of theorem 2 and proposition 3 would yield the desired result.

Further, if the desired temperature T_d is not in the range space of ϕ then the result in proposition 5 can be used to find $\hat{T}_d$ that minimizes the performance index in (5.42).

5.8 Integral Control

In the earlier section, non-zero steady-state temperature distribution are established by using a control law that has a constant bias input. The required bias input is obtained from the state-space model of the system. Due to the inevitable modeling errors, the actual temperature distribution is not the same as the desired temperature distribution. The tracking itself is as good as the model of the system.

On-line measurements of the system can be used to overcome the modeling errors. In the earlier section, we used these measurements for shaping the transient dynamics. The same measurements can be used to alter the bias input thereby compensating for modeling errors, plant disturbances. The general tracking requirement is given by

$$z = T_d.$$

Only a few state-variables of the z (or a linear combination of them) are actually measured and this is denoted by y. Integral control is one method by which the on-line measurements are utilized to determine the input to the system. However, this method can track only the measured outputs, i.e., can achieve only

$$y = r$$

where r is the desired outputs. The integral control strategy has been modified to accommodate state tracking and this technique is known as the pseudo-integral control approach [87]. At this time, we determine inputs in open-loop fashion and leave this type of implementation for the future.

5.9 Summary.

The lumped state-space model of the heat conduction equation is used to implement a desirable temperature distribution inside the material by manipulating the boundary conditions. When some states are weakly controllable or observable, a ROM is found by retaining the most controllable and observable modes. An observer based state-feedback controller is designed by using the ROM to shape the transient response of the system. Desired temperature distribution inside the material is established by computing the appropriate bias input. Some general conditions regarding the existence of the bias input for a certain desirable temperature distribution are developed in this section.

CHAPTER VI

STATE-SPACE MODEL OF HEAT CONDUCTION PROBLEM WITH PHASE CHANGE

This chapter deals with the modeling aspects of the heat conduction problem including phase change. The AHC formulation as described in Section 2.5.2.2 is employed to yield a non-linear, fixed boundary heat conduction type governing equation. The technique described in Chapter IV is applied to the governing equation obtained using the AHC formulation.

6.1 Apparent Heat Capacity Formulation

The heat conduction problem with phase change is described by (2.2). In the AHC formulation, the governing equation for solid, liquid and interface regions are given by one equation as given below

$$c^A(T)\frac{\partial T}{\partial t} = \nabla \cdot (k \nabla T) \tag{6.1}$$

with c^A being the apparent heat capacity defined by

$$c^A(T) \equiv \frac{\partial H}{\partial T} = \rho c + \rho L \delta(T - T_m) \tag{6.2}$$

where H is the total enthalpy defined by (2.3). Equation (6.1) is similar to the regular heat conduction problem without phase change. The only difference is that the AHC is a function of temperature. Therefore, we can extend the finite element formulation in Chapter IV and obtain a state-space model as

$$\dot{T} = \tilde{A}(T)T + \tilde{B}(T)u \tag{6.3}$$

As before, the vector T contains the nodal temperatures. To compute $\tilde{A}, \tilde{B}$ matrices, it is necessary to know c^A and k at all temperatures. These are available except at the melting temperature T_m. The AHC function has an integral singularity at the melting temperature. One way to handle this singularity is to approximate the singularity by a finite function. Two schemes have been proposed in the literature to handle this singularity. They are the linear approximation [27] and the homographic approximation [28]. The linear piece-wise approximation of AHC is given by

$$c^A = \begin{cases} \rho_s c_s & T < T_m - \varepsilon \\ \dfrac{\rho_l c_l + \rho_s c_s}{2} + \dfrac{\rho_s L}{2\varepsilon} & T_m - \varepsilon \le T \le T_m + \varepsilon \\ \rho_l c_l & T > T_m + \varepsilon \end{cases} \tag{6.4}$$

where ε is a parameter that is selected by user. This approximation tends to actual singularity as $\varepsilon \to 0$ (see Figure 6.1). The homographic approximation is given by

$$c^A = \begin{cases} \rho_s c_s + \dfrac{\rho_s L}{2\eta}\left(\dfrac{1}{\left(1+|T-T_m|/\eta\right)^2}\right) & T < T_m \\ \rho_l c_l + \dfrac{\rho_l L}{2\eta}\left(\dfrac{1}{\left(1+|T-T_m|/\eta\right)^2}\right) & T > T_m \end{cases} \tag{6.5}$$

This approximation is illustrated in Figure 6.2 for various η.

Both techniques provide approximate solution to the phase change heat conduction problem. In this dissertation, the linear approximation is adapted, for no particular reason. In [28], the benefits of the homographic approximation over the linear approximation are summarized. The main advantage of the homographic approximation is the C^1 continuity of the approximated c^A.

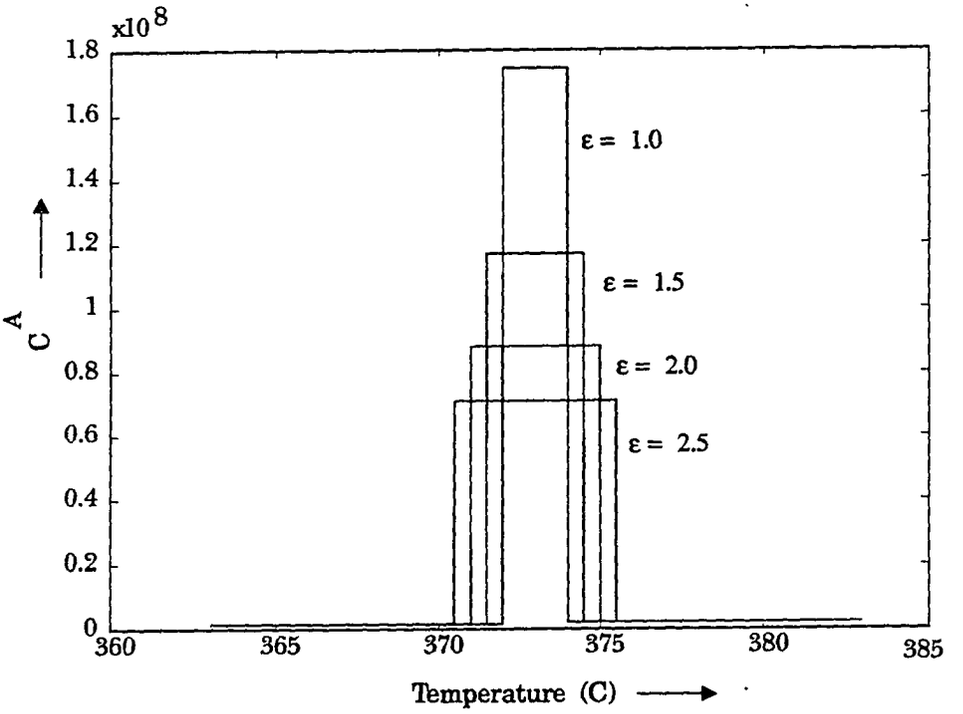

Figure 6.1 Linear approximation of AHC singularity.

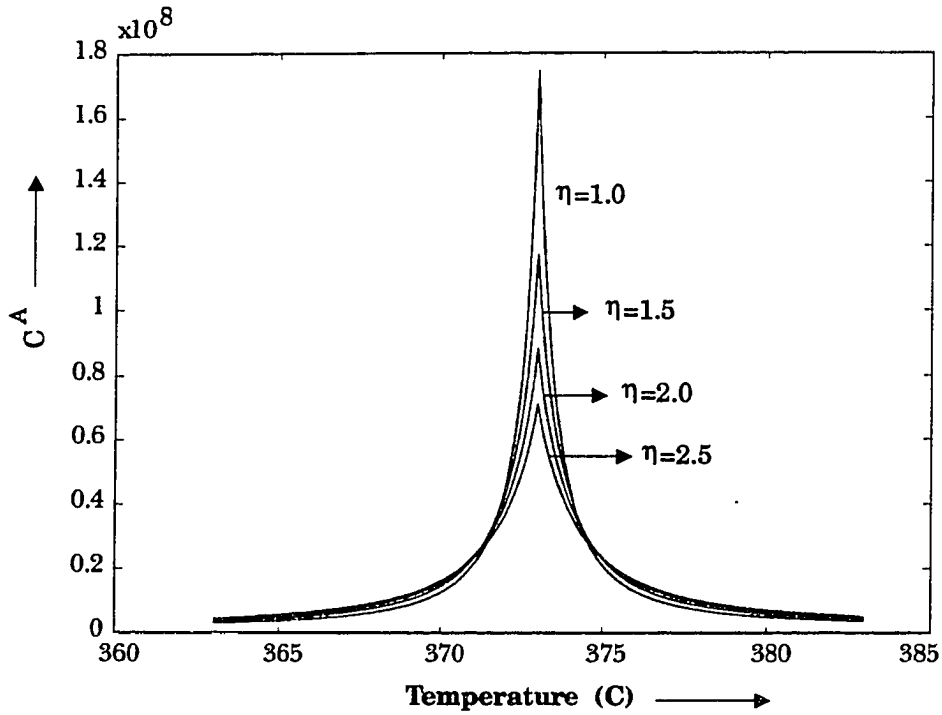

Figure 6.2. Homographic approximation of AHC singularity.

6.2 Finite Element Implementation

The computation of the elemental integrals are made using 4-point Gauss quadrature as in Section 4.3. The element stiffness matrix, mass matrix and force matrix all have the same forms as in the case of general heat conduction problem. The main difference is that the material properties are temperature dependent. Further, around the interface regions the material properties may vary within an element.

Consider any element depicted in Figure 6.3 and the four Gauss integration points. The region around the quadrature point is considered solid or liquid depending on the temperature of the quadrature point. The material property in the region is evaluated using the temperature of the quadrature points. This would yield approximate element matrices. A better approximation can be obtained by using higher order quadratures for performing integration.

6.3 Simulation of Phase Change Problem

The phase change problem has to be simulated to validate the model and verify the control algorithms. There are several methods to simulate (6.3). One of the simplest technique is the Euler method that works well for small time step Δt.

$$T(t+\Delta t) = T(t) + \Delta t\left(\tilde{A}(T(t))T(t) + \tilde{B}(T(t))u(t)\right) \tag{6.6}$$

The complete simulation procedure can be summarized in the following steps

(a) From the given initial temperature distribution *T(t)*, find the temperatures at all nodal points.

(b) Find the matrices $\tilde{A}, \tilde{B}$ using the finite element formulation and the boundary condition u.

(c) Find $T(t+\Delta t)$ using (6.6).

(d) Locate the new interface location.

(e) Repeat from step (a).

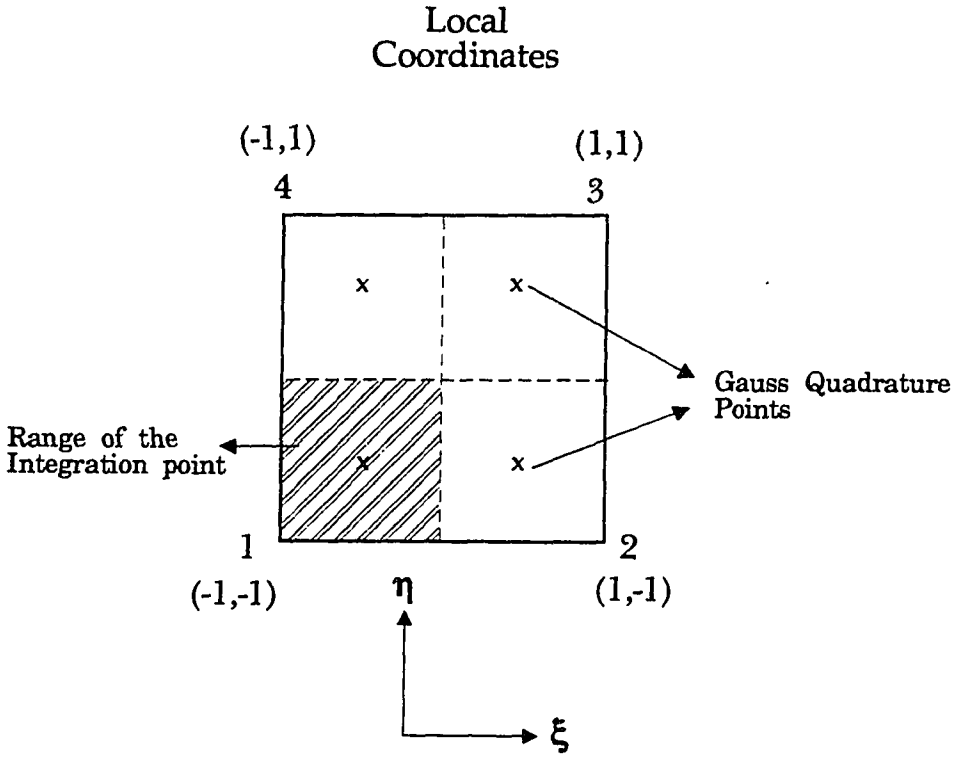

Figure 6.3. Role of integration points to determine the state of the material. The solid or liquid state of shaded region is determined by the temperature of the integration point.

6.3.1 User-Defined Parameters

There are many choices that the modeler has to make before simulating the crystal growth process. Some of them are:

(a) Mesh type, mesh size, type of interpolation function for temperature and BC

(b) Quadrature scheme, consistent or lumped matrix choice

(c) Singularity approximation method and the corresponding parameters

(d) Time integration method, time step Δt

The choices are usually a trade-off between accuracy and complexity of the model or the computational cost. In this dissertation, choices are made to keep the model simple. Consequently, the model is constructed using a coarse mesh, simple interpolation functions constructed using 4-node quadrilateral elements. Gauss 4-point quadrature scheme is employed to compute the element integrals.

The choice of integration time step is dependent on several factors. With large time steps the simulations may become unstable, inaccurate and in the case of phase change problems, some nodal points may solidify without releasing the latent heat as AHC does not take the peak value. This problem is termed as 'jumping of the latent heat peak' [29]. The choice of time integration scheme also affects the choice of time step. In general, the time step has to be smaller for explicit schemes than implicit schemes for similar accuracy. However, the number of computations in one time step is more with the implicit schemes.

6.4 Open Loop Simulation

The solidification of Lead Bromide inside a cylindrical ampoule shown in Figure 4.1 is modeled in this section. The spatial discretization of the surface ϕ=0 is done as before as seen in Figure 5.1. Linear approximation as given in (6.4) is used to represent the AHC c^A. The parameter ε must be chosen small so as to have a realistic

approximation. However, choosing ε small would require a small time step, a finer mesh and higher order Gaussian quadrature. With this in mind, ε is selected as 1.0 C. The choice of time step Δt is inter-dependent on other user-selected parameters such as the boundary and initial conditions. If the BC and the initial conditions are such that the temperatures are changing fast, then a smaller time step is necessary to have reasonable accuracy.

6.5 Validation of Finite Element Code

The finite element code developed for simulating the heat conduction with phase change problem is verified by the following methods:

(a) Symmetry of temperature distribution:

The code is simulated with all initial nodal temperature at constant temperature below the melting point. A constant outside temperature $T_b(z) = T_{constant}\ with\ T_{constant} > T_m$ is applied and the transient heat transfer problem is simulated. Due to symmetry all temperatures in a vertical line must be the same and hence the interface shape must be vertical during the melting process. The finite element solution satisfied this symmetry condition. Similar symmetrical boundary conditions are applied and the code satisfied the appropriate symmetry conditions.

(b) Qualitative comparison with commercial code, FIDAP.

The simple problem in Figure 4.1 is modeled using a commercial code FIDAP and the currently developed code The results matched qualitatively, i.e., the transient responses are similar and the steady-state solution are the same. It is difficult to compare the transient solutions quantitatively, as the FIDAP code uses different simulation scheme, many local approximations to reduce computation time. However, since the solution produced the same steady-state solution and similar transient response, we conclude that the code is working correctly.

(c) Comparison with steady-state analytical solution of heat-conduction equation

The steady-state solution of the heat conduction equation with no phase change can be found analytically for simple outside temperatures. These are verified with the steady-state solution provided with the present finite element code.

6.6 Summary

This chapter deals with the modeling of heat conduction problem with phase change. The AHC formulation is used to obtain a governing equation similar to the heat conduction problem. The AHC function has an integrable singularity at the melting temperature. The linear approximation is used to handle this singularity. A non-linear state-space model is obtained using the finite element procedure. This model is simulated using the Euler method.

CHAPTER VII

INTERFACE SHAPE CONTROL

As seen in the earlier chapters, the crystal growth process is governed by a non-linear state-space equation. One of the main objectives of this dissertation is to control the shape of the interface during crystal growth. The crystal growth dynamics is described in terms of a non-linear state-space model. The task of designing a controller (linear or non-liner) for a general non-linear system is a very difficult proposition. A standard approach is to linearize the non-linear system and utilize the linear control design procedures. This would result in finding a linear controller. Chapters IV and V contain a general method to model and control the linear heat-conduction problem. This chapter utilizes similar techniques to control the interface shape after linearizing the non-linear crystal growth model.

7.1 Linearization

Non-linearity of the crystal growth model is due to the movement of the interface surface. The interface movement rate for a typical crystal growth process is rather low and is usually in the range of 5 to 10 cm/day. Therefore, a linearized model is adequate for control design purposes.

Suppose the interface is required to move from an initial position "*a*" to position "*b*". This corresponds to the transition of temperature distribution from $T_a(r,z)$ to $T_b(r,z)$. For this temperature distribution transition, the linearization of the system can be performed in one of the following ways:

(a) Find the state-space model corresponding to the initial state T_a and fix it as the model representing the system. Design a single linear controller using this model.

(b) Use the final state T_b to find the state-space matrices and design a linear controller using the corresponding matrices.

(c) State-space model evaluated at any intermediate temperature, $T_a < T < T_b$ may be used to design the controller.

This dissertation utilizes (a) for control design purposes. The main justification is that in a practical situation, only T_a is known. Even though the required T_b is known, it is possible that this temperature distribution cannot be achieved using the existing actuators (heaters). The same is true for any intermediate temperature. Therefore, rather than using an unachievable model for control purposes, it is practical to use the technique proposed in (a). If the jump from one T_a to T_b is large so that one single model may not adequately represent the system, two controllers can be designed, or as many controllers as may be needed.

7.2 Control Objective and Design Framework

The control objective can be stated as follows : "Find the boundary condition, i.e., the temperature distribution outside the ampoule surface, such that the desired interface shape is established during crystal growth." As seen in Chapter V, the set of achievable interface shapes or temperature distributions in the steady-state is limited by the position and the number of actuators. This physical restriction would require a kind of pre-filter that would transform all unachievable requests of interface shape or temperature distribution to something that is achievable. This will be explained in a later section.

As in the linear heat conduction control, the measurements would affect the design and implementation of control algorithms. Also, in addition to setting a desired interface shape, it is necessary to grow crystal at a required rate which amounts to changing the

location of the desired interface shape. The control design procedure for each situation is different. To facilitate a good understanding, the control design problem is broken up into divisions based on the measurements and control objective as follows:

i. All states are measurable which amounts to the availability of all nodal temperatures.

(a) Control design is to establish a desired interface shape at a desired location.

(b) Control design is to establish and move a desired interface shape at a given rate.

ii. Only a few states are measured

(a) Control design is to establish a desired interface shape at a desired location.

(b) Control design is to establish and move a desired interface shape at a given rate.

7.3 Control Design Procedures

7.3.1 State-Feedback Shape Control of Interface at a Desired Location

7.3.1.1 Controller Design

In order to be able to design a state feedback controller as Linear Quadratic Regulator (LQR), it is necessary that all states are controllable. However, as seen in the linear heat conduction problem, many of the states may be weakly or totally uncontrollable. In this situation, one may have to obtain at least a minimum state-space realization of the linearized system. To avoid numerical problems, it may also be necessary to obtain a reduced-order model by eliminating weakly controllable states. For the crystal growth system considered in this dissertation, the original system is minimum and no numerical difficulties have been encountered while designing the controller. Therefore, in this section we design the controller using the linearized state-space model directly. However, if this is not feasible, the design techniques proposed in Section 7.4 can be used to determine the controller.

A linearized state-space model is found by performing open-loop simulation experiments. The boundary condition during the open-loop simulation is picked so that

steady-state interface is approximately in the neighborhood of the desired interface location. Note, it is not necessary for the steady-state interface to have the desired shape. This choice would ensure that the model used for designing the controller is "close" to the actual model in the steady state. One choice for the boundary condition is to use a constant temperature gradient as in Figure 7.1, with the boundary condition temperature at the desired interface location being equal to the melting temperature T_m. The gradient is chosen to be the same as the desired gradient in the material. This would ensure, that the steady-state interface location obtained through open-loop simulation is in the same location as the desired interface location. The model corresponding to the steady-state is used as the linearized model of the crystal growth process and is given as

$$\dot{T} = \tilde{A}T + \tilde{B}_1 u_1 + \tilde{B}_2 u_2 \tag{7.1}$$

As before, the control law to establish a non-zero steady state is given as

$$u_1 = K_s T + u_b \tag{7.2}$$

The state-feedback gain K_S is used to shape the transient dynamics and the bias input u_b is used to establish non-zero references. The state-feedback gain is found as a LQR and is found using a formula similar to (5.15).

To determine the bias input, it is necessary to the know the desired nodal temperatures. However, the control objective is to establish a desired solid-liquid interface shape in the steady-state. One can find several temperature distribution that would setup the desired steady-state interface shape. The control designer selects the initial desired temperature distribution and through Finite Element Approximation, the appropriate desired nodal temperatures can be found as in Figure 7.2.

A shortcoming of this technique is that the success of the control is at the hands of the designer. Almost always, the desired temperatures picked by the designer

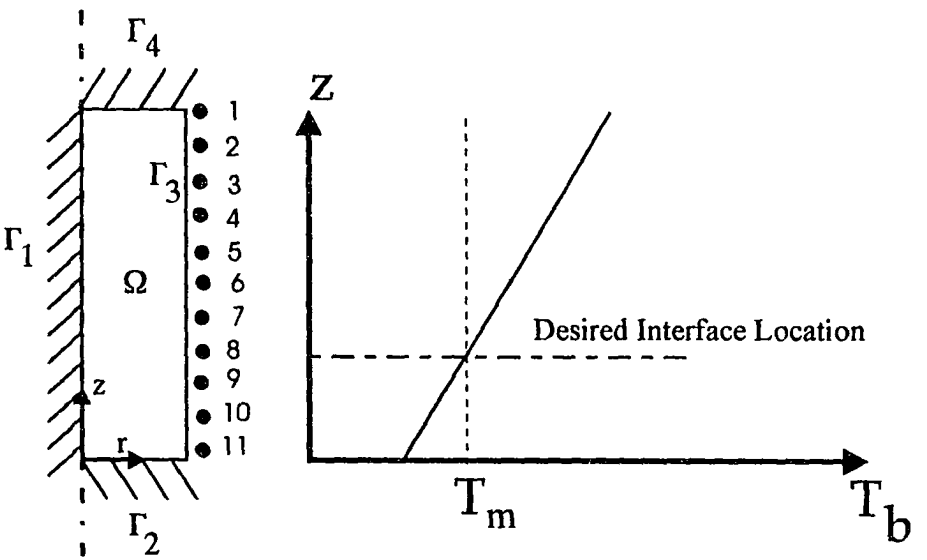

Figure 7.1. Choice of boundary condition to obtain a linearized model.

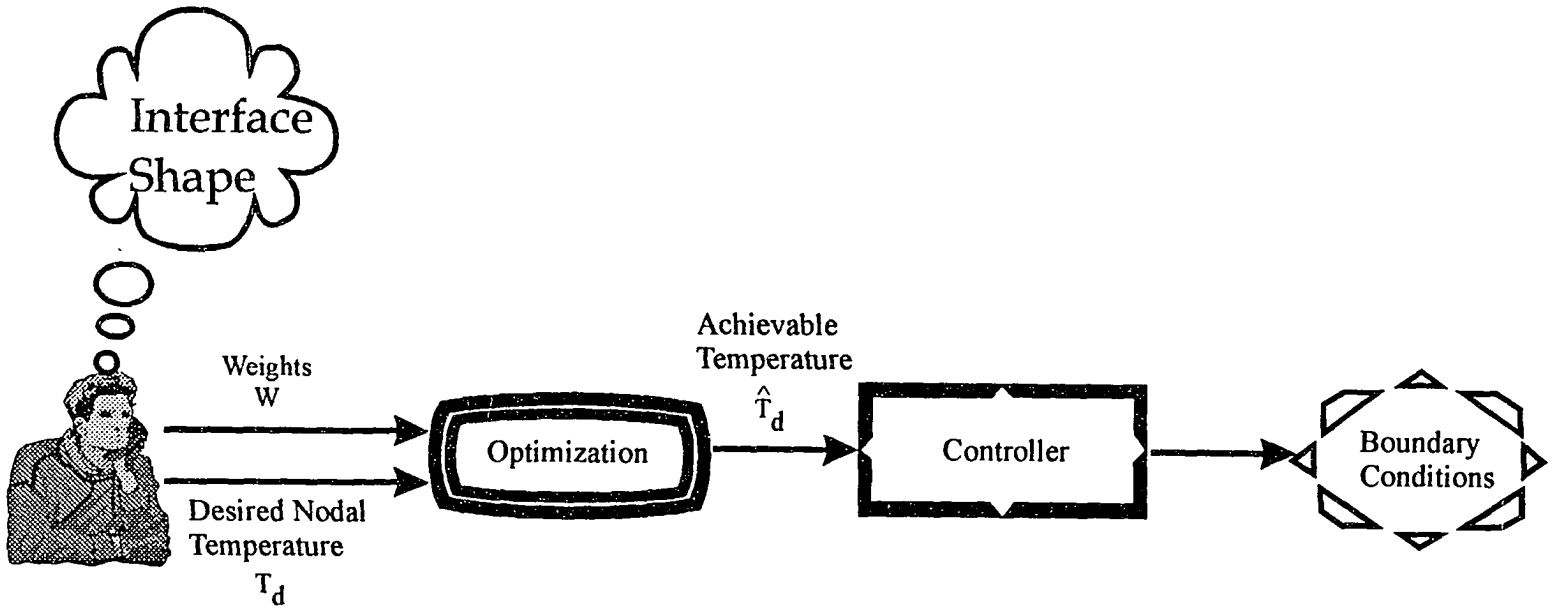

Figure 7.2. Designer requests to the controller.

cannot be achieved by any bias input. The condition for existence of a bias input in the case of the linear heat conduction problem has been stated and proved in Chapter V. Since, we are using a linearized model, the same theorem can be "loosely" applied to the crystal growth problem with the understanding that the results are only approximate. Therefore, we can use the designer selected nodal temperatures and minimize an objective function in (5.42) (stated below for clarity)

$$J = \left(T_d - \hat{T}_d\right)^T W \left(T_d - \hat{T}_d\right), \tag{7.3}$$

where $\hat{T}_d$ is the closest temperature distribution to the original designer-selected reference T_d that can be achieved and W is a positive definite weighting matrix. The minimization procedure can be seen in Proposition 5 of Section 5.5. The approach now is to request $\hat{T}_d$ as the reference temperature from the control system as shown in Figure 7.2.

7.3.1.2 Simulation Result

In this section, a controller is designed to establish a flat, and a convex interface shape at z=0.02 m. The material properties used for simulation are those of Lead Bromide and are given as

Liquid : $\rho = 6675.0$ kg / m^3 , $C_p = 230.0$ J / kg C , K= 0.26 W / m C

Solid : $\rho = 6675.0$ kg / m^3 , $C_p = 326.0$ J / kg C , K= 0.26W / m C

Latent Heat, L = 51650.0 J/kg Melting Point, T_m = 373.15 C

Convection Heat Transfer Coefficient, h = 100 W / m^2 C

The material is in a cylindrical ampoule (not considered in the model) as shown in Figure 4.1. The enthalpy formulation is employed as in Chapter VI and a non-linear state-space model is obtained after discretizing the domain as in Figure 7.3. The model has 66 states with 11 inputs. We assume all the 11 inputs can be manipulated as desired. In the event this is not feasible, some of the 11 inputs become exogenous inputs that cannot be altered

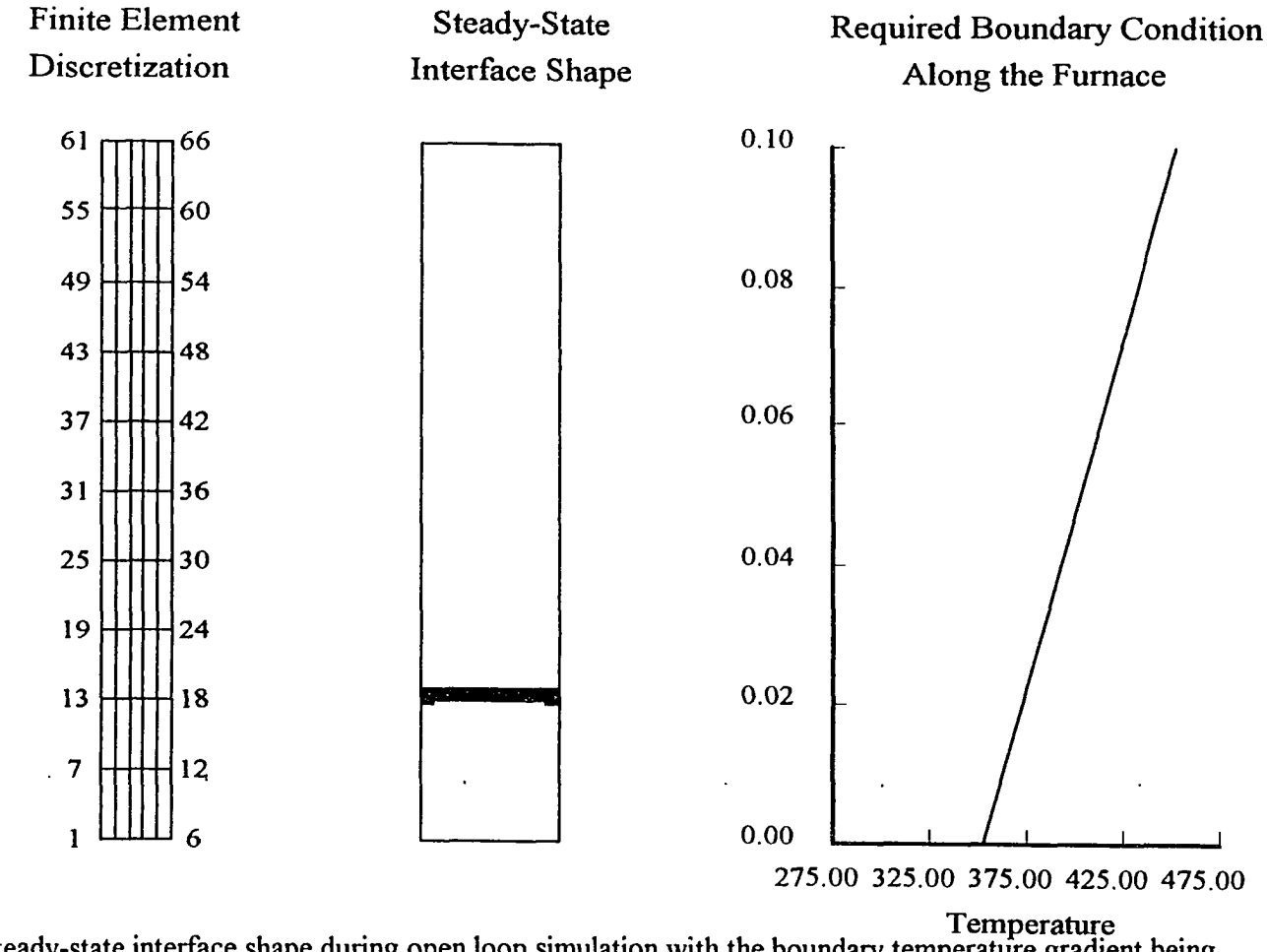

Figure 7.3 Steady-state interface shape during open loop simulation with the boundary temperature gradient being 10 C/cm gradient . The model used for the control design corresponds to this steady-state condition.

independently. This would affect the controllability of the system. We also assume that all the states can be measured in this section.

To get a linearized model with the interface around z=0.02m, a gradient is applied as in Figure 7.1 with the temperature at z=0.02 being 373.15, the melting point of Lead Bromide. The system is simulated until a steady-state is reached. The interface shape in the steady-state can be seen in Figure 7.3. The system matrices corresponding to this system is used as the "Linearized Model" of the crystal growth system. An insight into the dynamics of the linearized model can be obtained by computing the eigenvalues, which are given in Table 7.1.

Before designing a state-feedback controller, we have to ensure if the system is controllable. A judgment on the controllability can be obtained by computing the Hankel Singular Values as in Chapter V. From the Hankel singular value plots, we conclude that the system is completely controllable and therefore a state-feedback controller can be computed. The state-feedback control gain K_S is computed as linear quadratic gain with the cost $Q = 5\, I_{66}$, where I_n is n th order Identity matrix and $R = I_{11}$. The cost is chosen in such a way so as to have a reasonable transient response as in Chapter V. The eigenvalues of the closed-loop system are given in Table 7.2. Note, none of the eigenvalues are complex; therefore; at least the linearized closed-system will have no overshoot if the system is minimum-phase.

The importance of feedback can be seen by comparing the singular values of the open-loop and the closed-loop system. The singular values for the open-loop and the closed-loop system at various frequencies are plotted in Figure 7.4. It can be observed that closed-loop system has a higher band-width than the open-loop system. This is one of the advantages of feedback. Under a different design scheme, feedback can be used to achieve stability and performance in presence of uncertainties. This approach is not taken in this dissertation and will be considered as a part of the future work.

Table 7.1 Open Loop System Eigenvalues

-0.0060	-0.0061	-0.0064	-0.0068	-0.0073	-0.0078	-0.0084	-0.0089	-0.0093	-0.0095	-0.0096
-0.0185	-0.0189	-0.0199	-0.0216	-0.0237	-0.0260	-0.0283	-0.0304	-0.0320	-0.0331	-0.0331
-0.0334	-0.0342	-0.0376	-0.0427	-0.0490	-0.0492	-0.0510	-0.0564	-0.0569	-0.0636	-0.0646
-0.0660	-0.0663	-0.0674	-0.0693	-0.0701	-0.0752	-0.0752	-0.0774	-0.0782	-0.0785	-0.0796
-0.0871	-0.0900	-0.0923	-0.1020	-0.1026	-0.1103	-0.1139	-0.1186	-0.1229	-0.1287	-0.1303
-0.1307	-0.1352	-0.1503	-0.1503	-0.1622	-0.1683	-0.1698	-0.1725	-0.1826	-0.1918	-0.1950

Table 7.2. Closed Loop System Eigenvalues

-0.0114	-0.0115	-0.0116	-0.0120	-0.0125	-0.0134	-0.0145	-0.0156	-0.0166	-0.0173	-0.0175
-0.0217	-0.0222	-0.0238	-0.0263	-0.0295	-0.0329	-0.0362	-0.0362	-0.0374	-0.0394	-0.0414
-0.0416	-0.0434	-0.0438	-0.0471	-0.0510	-0.0531	-0.0546	-0.0593	-0.0629	-0.0657	-0.0682
-0.0688	-0.0712	-0.0758	-0.0788	-0.0798	-0.0808	-0.0834	-0.0846	-0.0876	-0.0883	-0.0897
-0.0941	-0.0946	-0.1026	-0.1073	-0.1126	-0.1192	-0.1193	-0.1288	-0.1348	-0.1351	-0.1361
-0.1368	-0.1512	-0.1600	-0.1632	-0.1710	-0.1736	-0.1850	-0.2076	-0.2255	-0.2370	-0.2405

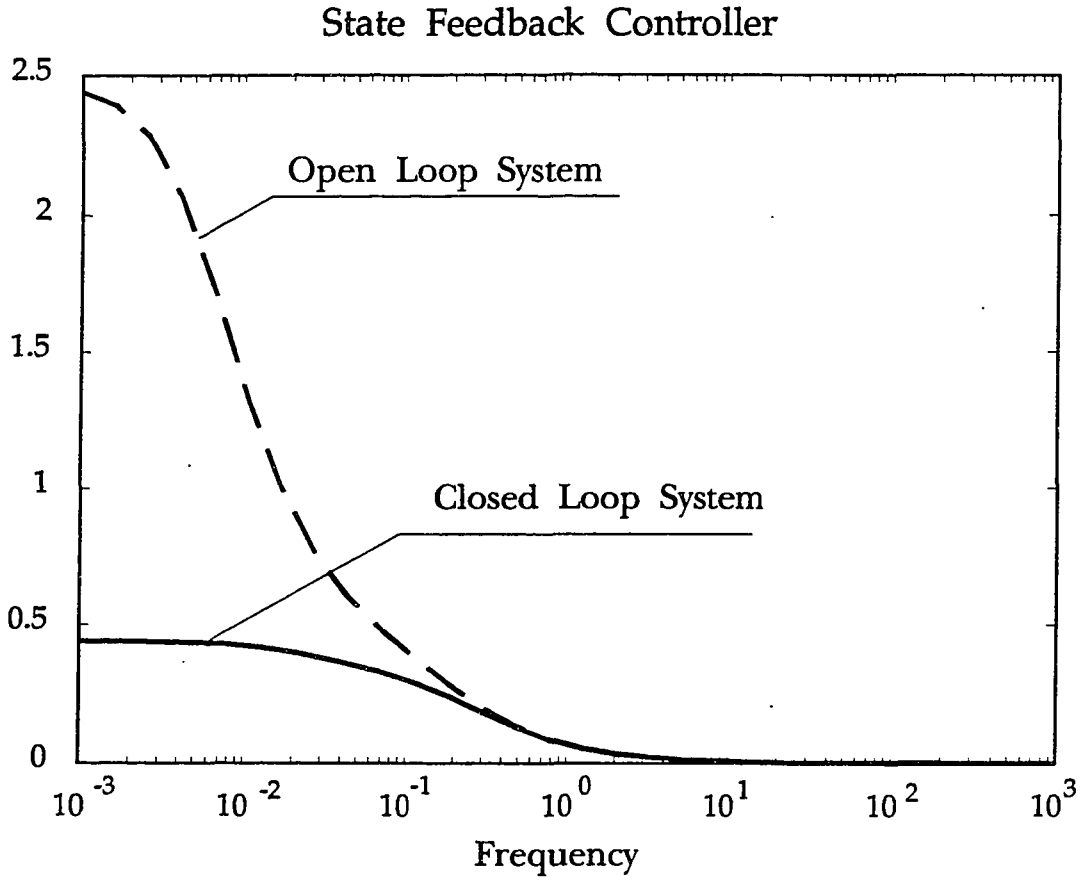

Figure 7.4 Singular value plot for open-loop and closed-loop systems.

The linearized model and the state-feedback gain are not dependent on the desired interface shape but on the interface location. However, the bias input will be dependent on the desired shape. At first, a flat interface is desired at z=0.02. As in Figure 7.2, the designer has to select the equivalent temperature distribution and in this case this distribution is chosen as

$$T(r,z) = T_m + \left(z - z_{interface}\right)T_{gradient} = 373 + (z - 0.02)\cdot 10.0 \tag{7.4}$$

where T_m is the melting point of Lead Bromide (373.15 C), $z_{interface}$ is the location of the desired interface (0.02 m), and $T_{gradient}$ is desired temperature gradient (10 C/cm). Note, the desired temperature distribution is not a function of r for flat interface. The corresponding desired nodal temperatures for the temperature distribution in (7.4) are found using the finite element approximation. Now, the task is to find a bias input so that the performance index in (7.3) is minimized. The weighting matrix W has to be selected and as a first shot, $W = I_{66}$ is attempted. Theoretically, we would like to apply more emphasis on the nodes near the interface, as we will see in the convex interface shape case. The achievable nodal temperature corresponding to this choice is calculated as

$$\hat{T}_d = -\left(F^{-1}\tilde{B}_1\right)\theta, \tag{7.5}$$

where the parameter θ is given by

$$\theta = -\left[\left(F^{-1}\tilde{B}_1\right)^T W\left(F^{-1}\tilde{B}_1\right)\right]^{-1}\left(F^{-1}\tilde{B}_1\right)^T W T_d. \tag{7.6}$$

The matrix F in the above equation is the linearized closed loop system given by

$$F = \tilde{A} + \tilde{B}_1 K_s. \tag{7.7}$$

Based on the linearized model, the steady-temperature distribution and steady-state outside temperate are shown in Figures 7.5 and 7.6.

Nodes numbered 16 to 24 in Figure 7.3 are the nodes around the interface region. Based on visual inspection, there is a good match between the desired and the actual

temperatures. The crystal growth system is simulated with this controller as shown in Figure 7.7. The initial conditions are such that all nodes are at 370 (entire material is solid). Even though our linearized model does not exactly represent the model in the initial state, the controller designed using this model is able to establish the desired temperature distribution. The desired and the actual nodal temperatures are plotted in Figure 7.8 and the requested outside temperature profiles are plotted in Figure 7.9. The steady-state interface shape is plotted in Figure 7.10 and the contour plot of the steady-state temperature distribution is given in Figure 7.11. The 2-norm of the error defined as

$$e = T - \hat{T}_d$$
$$\|e\|_2 = \sqrt{e^T e}, \qquad (7.8)\text{-}(7.9)$$

where T and $\hat{T}_d$ are the nodal temperatures and the desired nodal temperatures. The 2-norm of the error is plotted for various times and is shown in Figure 7.12. Note that the norm goes down to zero showing the effectiveness of the controller. To verify if there are no overshoots, we plot the interface location for one particular r=0 (along the axi-symmetric axis) with respect to time as in Figure 7.13. From the figure, we can conclude that there are no overshoots at least at for this r.

Having established a flat interface shape, we attempt to establish a convex interface with the base of the convex interface at z=0.02. The convex shape is described in terms of a sine function as

$$I(r) = I(R) + h\sin\left(\frac{\pi}{2}\left(1-\frac{r}{R}\right)\right) = 0.02 + 0.01\sin\left(\frac{\pi}{2}\left(1-\frac{r}{R}\right)\right), \qquad (7.10)$$

where $I(r)$ is the interface z-position at radial position r, R is the radius of the cylinder and h is the convexity parameter. The linearized model and the state-feedback gain K_s are the kept the same as the flat interface case as there are no obvious better choices. The desired temperature distribution that would achieve a convex interface shape is selected as

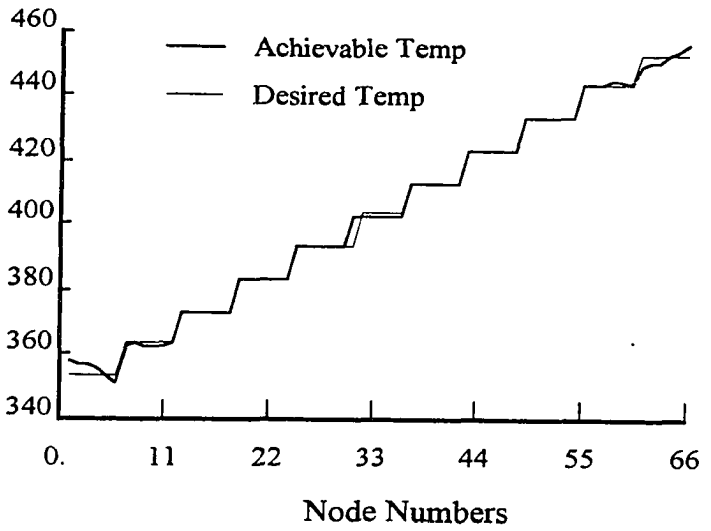

Figure 7.5. Desired nodal temperatures T_d and achievable nodal temperatures $\hat{T}_d$ based on the linearized state-space model.

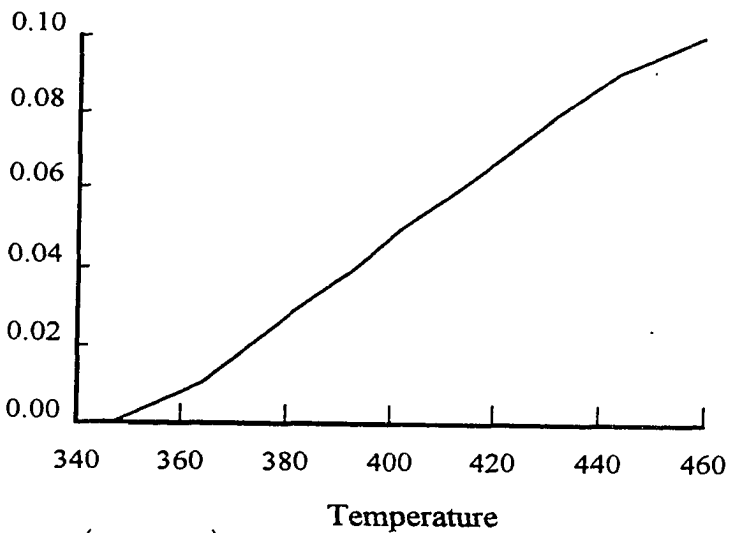

Steady-state inputs $(u_b - K_s T_\infty)$ at different z-locations.

z=0.00	z=0.01	z=0.02	z=0.03	z=0.04	z=0.05	z=0.06	z=0.07	z=0.08	z=0.09	z=0.1
345.93	362.31	373. 50	383.05	392.75	401.32	412.79	423.19	432.36	443.53	459.86

Figure 7.6. Steady-state inputs for establishing a flat interface at z=0.02.

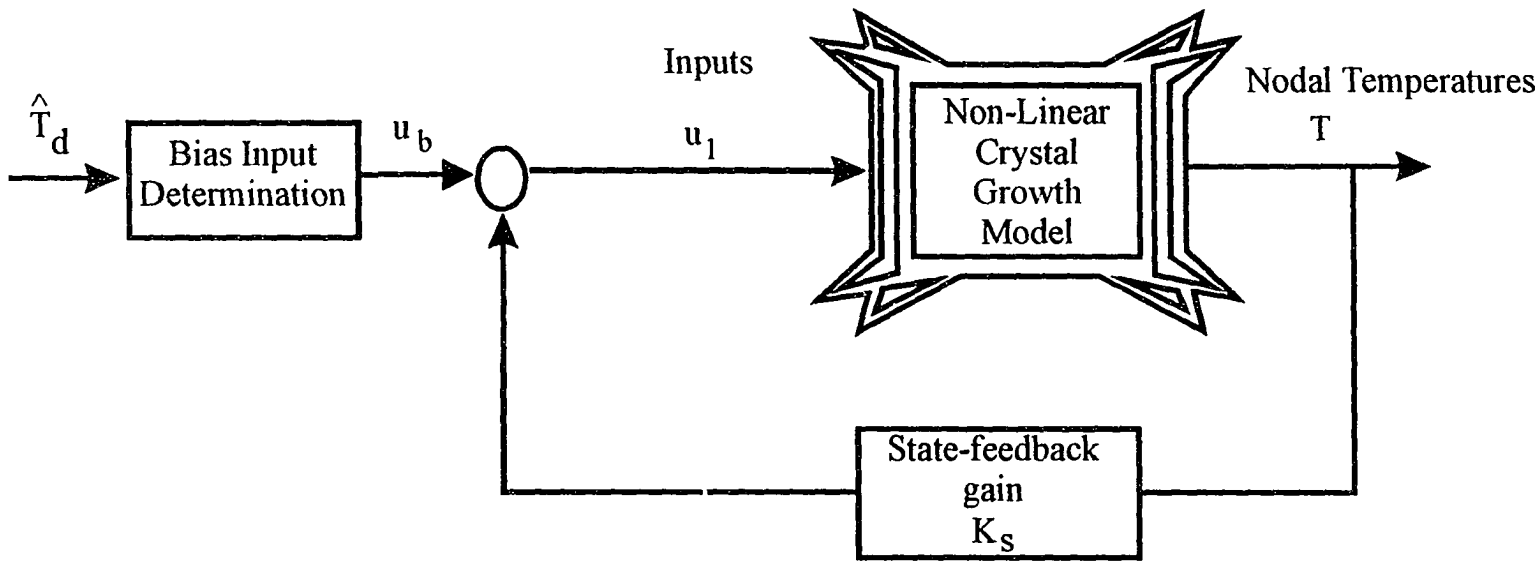

Figure 7.6. Implementation of state-feedback control with bias input.

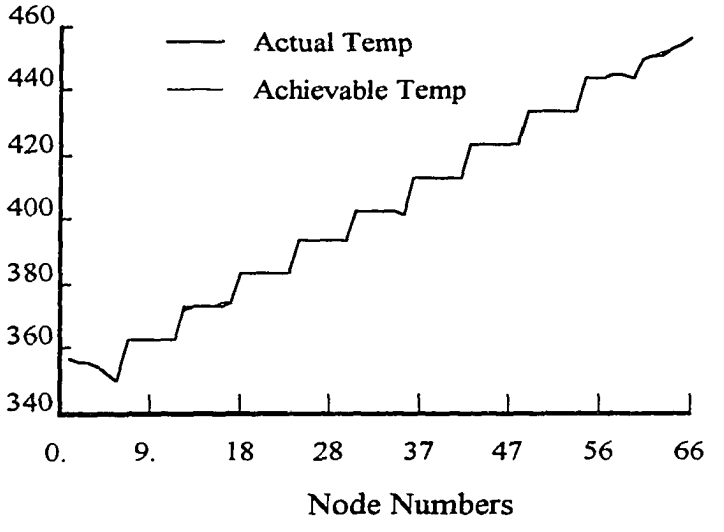

Figure 7.8. Achievable nodal temperatures $\hat{T}_d$ and actual steady-state nodal temperatures T based on the non-linear state-space model.

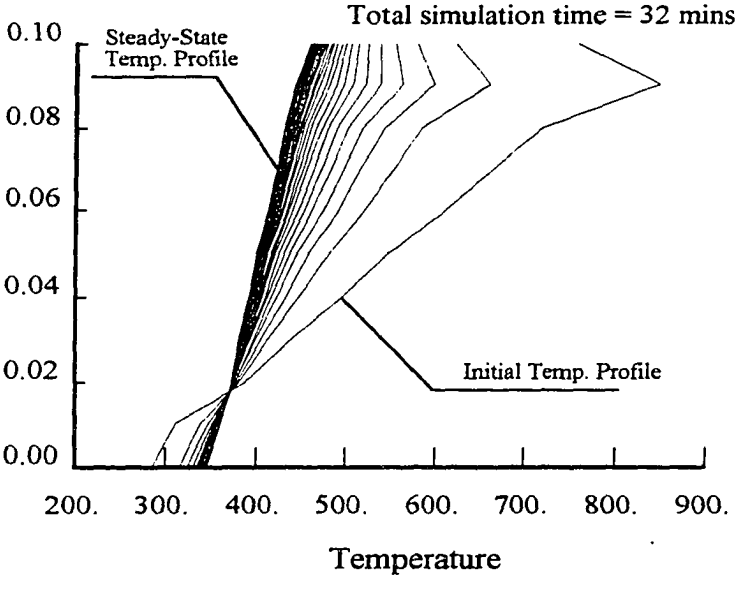

Steady-state inputs $(u_b - K_s T_\infty)$ at different z-locations.

z=0.00	z=0.01	z=0.02	z=0.03	z=0.04	z=0.05	z=0.06	z=0.07	z=0.08	z=0.09	z=0.1
345.96	362.41	374.23	383.14	392.78	401.35	412.83	423.24	432.42	443.60	459.94

Figure 7.9. Temperature profiles requested by the controller as a function of time.

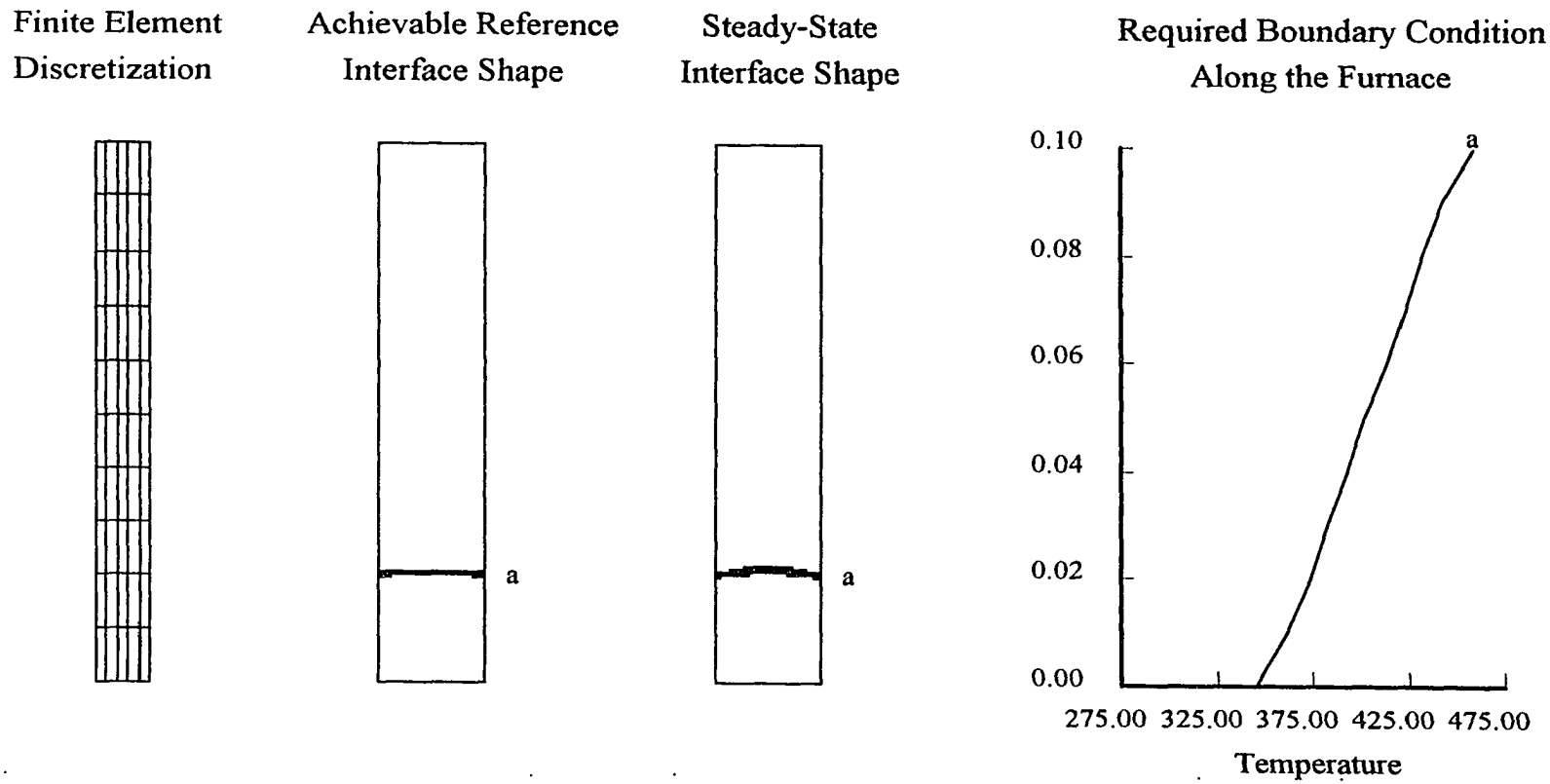

Figure 7.10 Steady-state interface shape and the corresponding steady-state boundary temperature for achieving a flat interface at z=0.02. Note, in this simulation, it is assumed that the temperature at all nodes are measured.

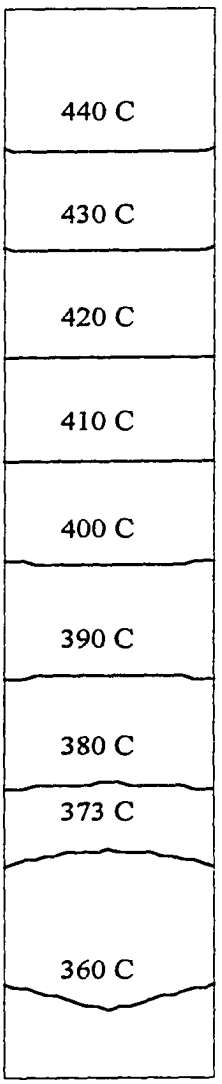

Figure 7.11 Contour plot of temperature distribution in the steady-state while establishing a flat interface at z=0.02.

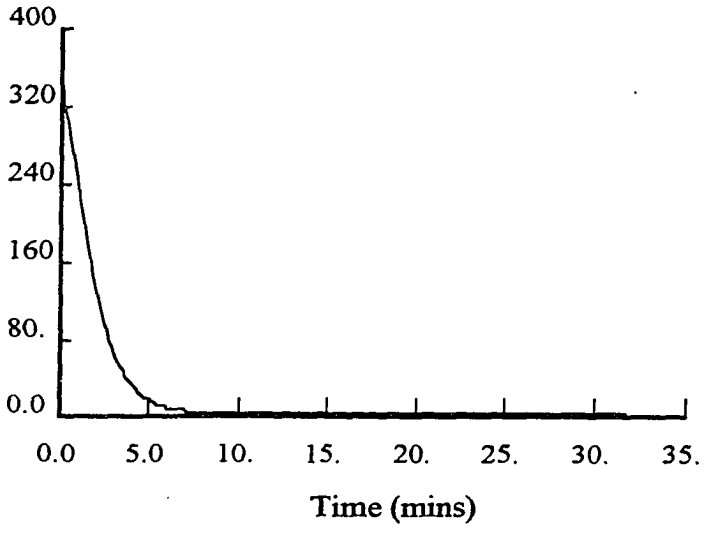

Figure 7.12 Plot of 2-norm of tracking error as a function of time.

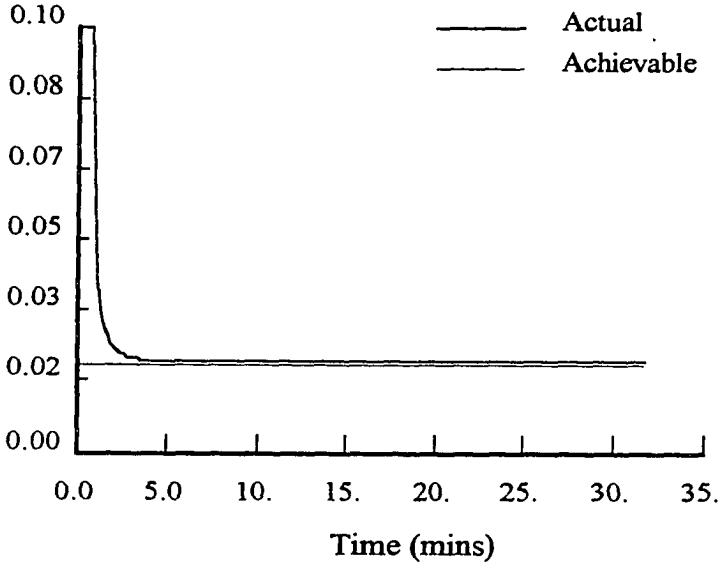

Figure 7.13 Interface height at the surface r=0.0 as a function of time. Note that there is no overshoot in the interface position at least for this particular plane, i.e., $r=0$.

$$T(r,z) = T_m + (z - I(r))T_{gradient}. \tag{7.11}$$

The bias input is calculated as before by minimizing the cost in (7.3) with the initial choice of W being I_{66}. The steady-temperature distribution and steady-state outside temperature based on the linearized model are shown in Figures 7.14 and 7.15. Note, that the resulting interface shape is not close to what we desired. This is mainly due to poor choice of weights. The minimization only provides us a least-square solution and the weight $W=I_{66}$ does not represent our objective to have the desired shape. Therefore, we need to place more importance around the interface region. Initially, only the nodes 16-24 are weighted more heavily than others. The optimized solution did not produce a crisp interface. Actually there were two interfaces (at least based on the model). After some iteration, the weights W as given below produced reasonable interface shape based on the linearized model.

$$W = \begin{bmatrix} I_6 & 0 & 0 & 0 & 0 \\ 0 & 20I_6 & 0 & 0 & 0 \\ 0 & 0 & 2000I_{12} & 0 & 0 \\ 0 & 0 & 0 & 200I_6 & 0 \\ 0 & 0 & 0 & 0 & I_{36} \end{bmatrix} \tag{7.12}$$

The steady state distribution and outside temperature based on this set of weights are shown in Figures 7.16 and 7.17.

The crystal growth system for this choice of bias input is simulated with the initial nodal temperatures being 370 C (same as before). Again, this controller is able to establish the desired temperature distribution. The actual and desired nodal temperatures are plotted in Figure 7.18 and the corresponding outside temperatures requested by the controller are plotted as function of time in Figure 7.19. The steady-state interface shape is plotted in Figure 7.20 and the contour plot at this steady-state is shown in Figure 7.21.

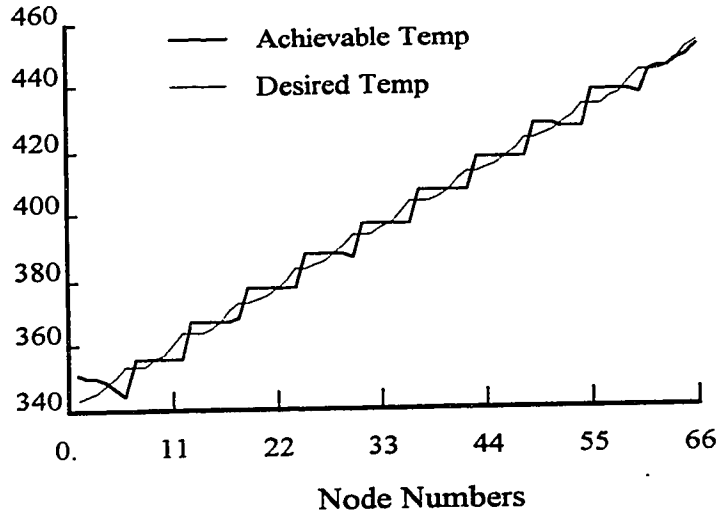

Figure 7.14. Desired nodal temperatures T_d and achievable nodal temperatures $\hat{T}_d$ based on the linearized state-space model with the weight $W=I_{66}$.

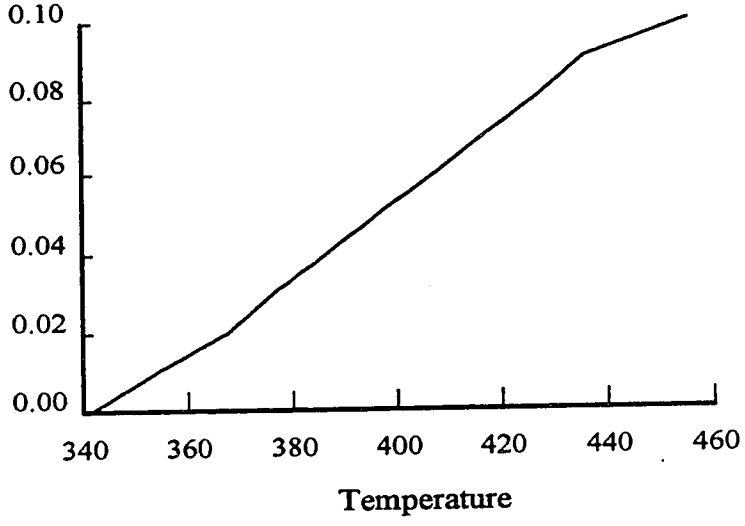

Steady-state inputs $(u_b - K_s T_\infty)$ at different z-locations.

z=0.00	z=0.01	z=0.02	z=0.03	z=0.04	z=0.05	z=0.06	z=0.07	z=0.08	z=0.09	z=0.1
347.17	358.44	370.45	380.08	390.04	400.07	410.07	420.05	429.98	439.93	454.95

Figure 7.15. Steady-state inputs for establishing a convex interface at z=0.02 based on $W=I_{66}$.

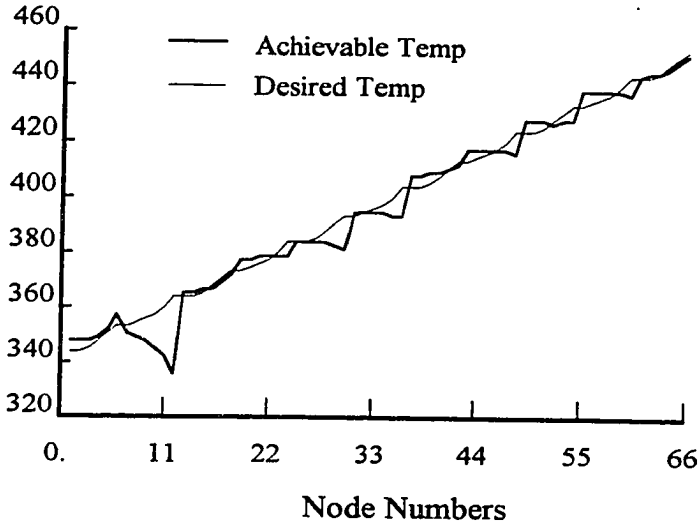

Figure 7.16. Desired nodal temperatures T_d and achievable nodal temperatures $\hat{T}_d$ based on the linearized state-space model for the weight W in Equation (7.12).

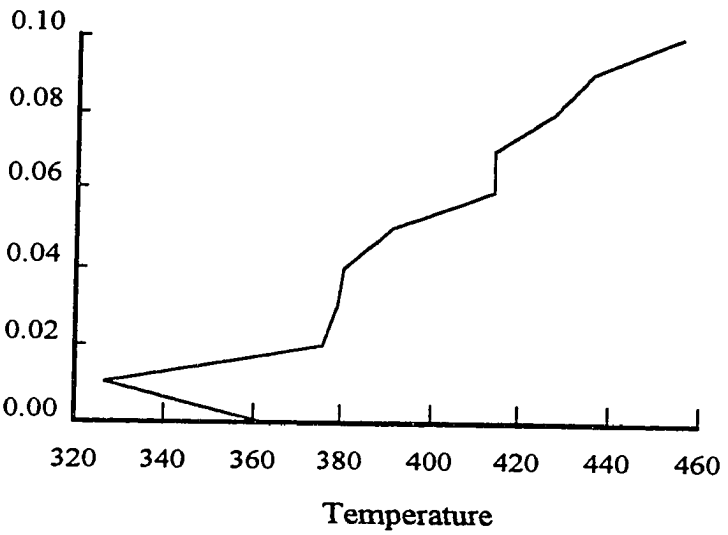

Steady-state inputs $(u_b - K_s T_\infty)$ at different z-locations.

z=0.00	z=0.01	z=0.02	z=0.03	z=0.04	z=0.05	z=0.06	z=0.07	z=0.08	z=0.09	z=0.1
362.69	326.74	375.59	378.95	380.16	390.84	414.13	414.03	427.30	435.90	455.52

Figure 7.17. Steady-state inputs for establishing a convex interface at z=0.02 based on W in Equation (7.12).

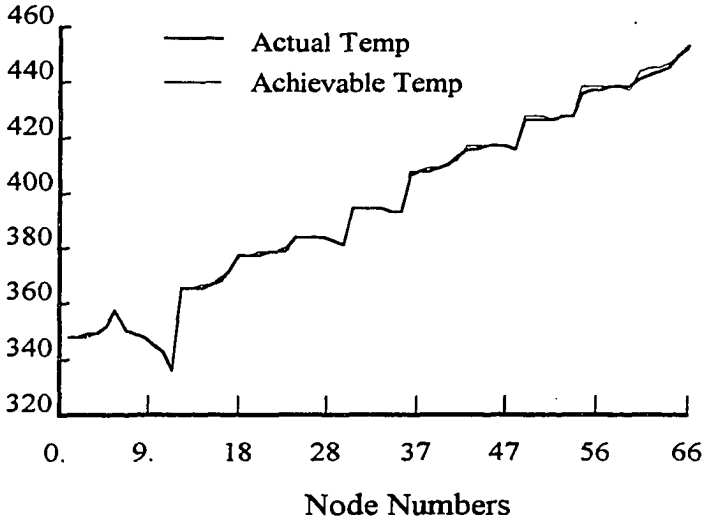

Figure 7.18. Achievable nodal temperatures $\hat{T}_d$ and actual steady-state nodal temperatures T based on the non-linear state-space model.

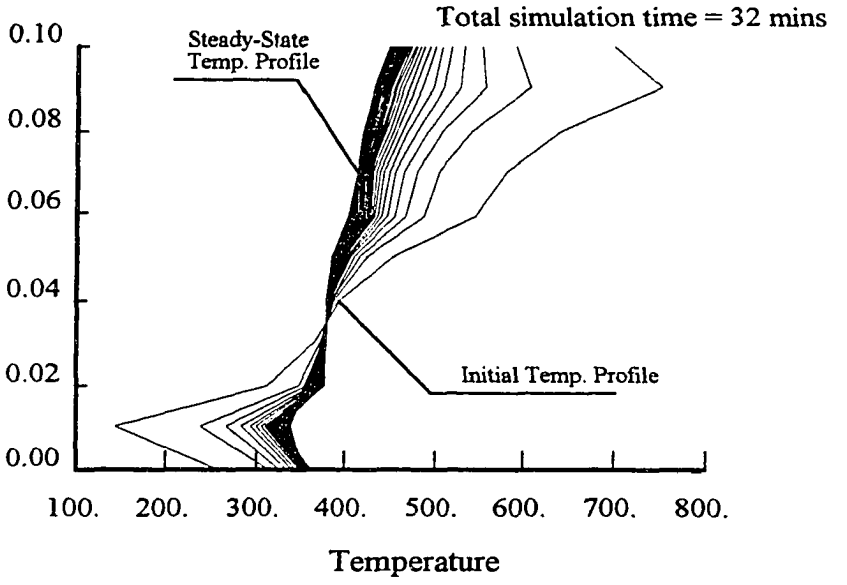

Steady-state inputs $(u_b - K_s T_\infty)$ at different z-locations.

z=0.00	z=0.01	z=0.02	z=0.03	z=0.04	z=0.05	z=0.06	z=0.07	z=0.08	z=0.09	z=0.1
362.77	326.71	376.68	379.37	380.22	390.86	414.16	414.09	427.36	435.97	455.60

Figure 7.19. Temperature profiles requested by the controller as a function of time.

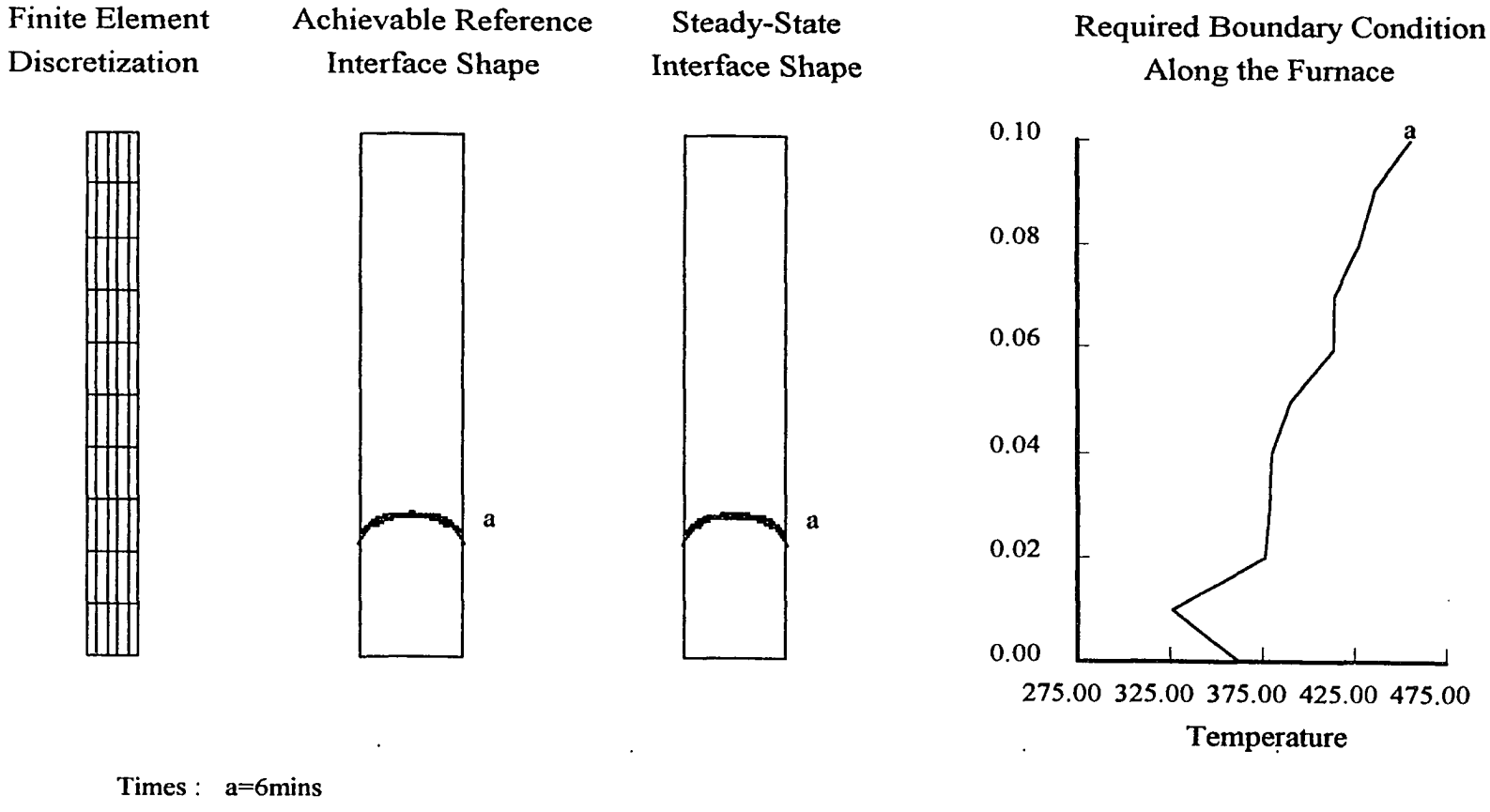

Figure 7.20 Steady-state interface shape and the corresponding steady-state boundary temperature for achieving a convex interface at z=0.02. Note, in this simulation, it is assumed that the temperature at all nodes are measured.

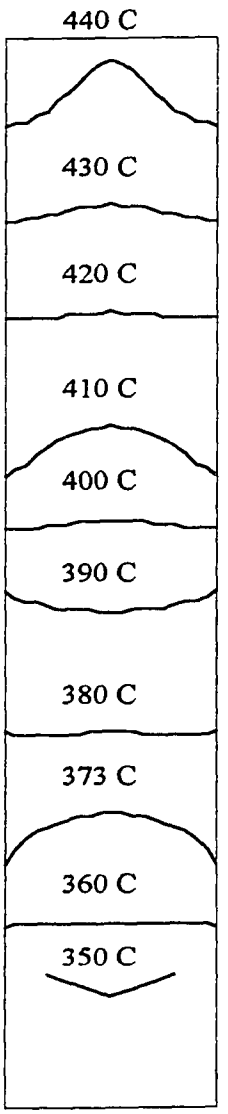

Figure 7.21 Contour plot of temperature distribution in the steady-state while establishing a convex interface at z=0.02.

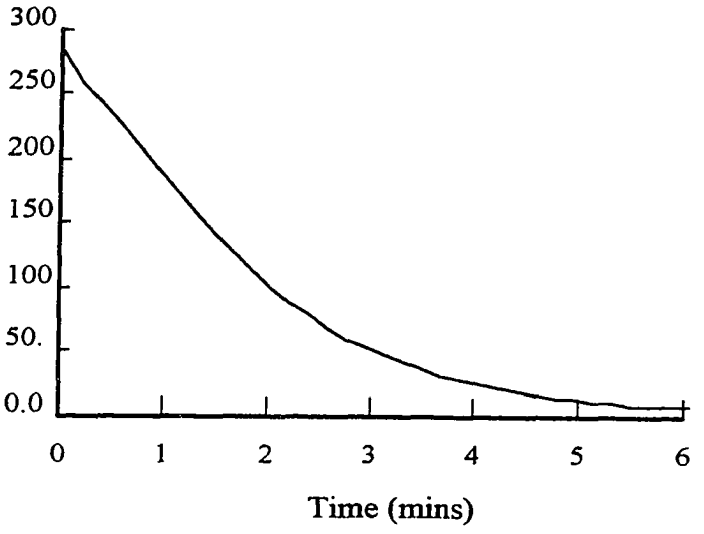

Figure 7.22 Plot of 2-norm of tracking error as a function of time.

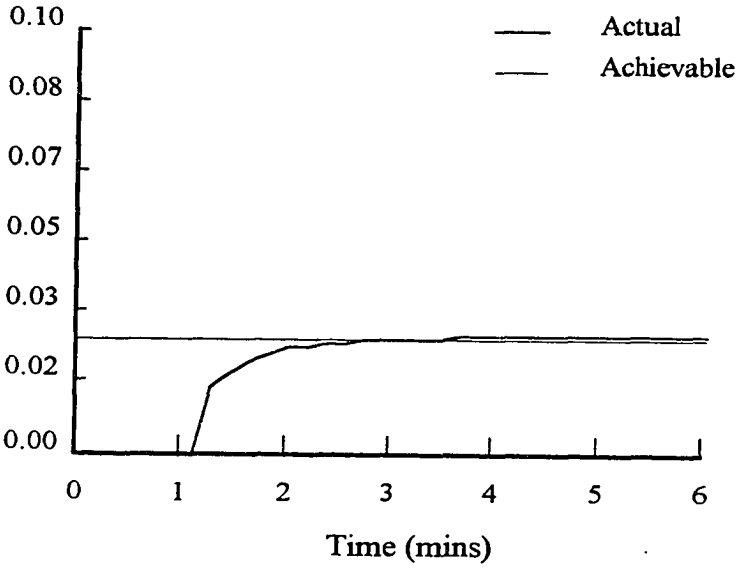

Figure 7.23 Interface height at the surface r=0.0 as a function of time.

The 2-norm of the error is shown in Figure 7.22 and the interface position at the plane r=0 for various time is shown in Figure 7.23.

Through a different approach Young [89] has predicted the rather complicated outside temperature to be one of the outside temperature that would establish a convex interface shape. The details behind this approach is beyond the scope of this dissertation.

7.3.2 State-Feedback Control to Grow Crystal at a Desired Rate

7.3.2.1 Controller Design

In the last section, a state-feedback controller is designed to establish a desired interface shape at a desired location. Here in this section, we would like to design a controller that would move the interface at a desired rate preserving the desired shape of the interface. Some basic ideas are derived on designing this controller by observing how crystals are grown currently. The crystals are grown by moving the ampoule; this can also be accomplished by moving the gradient at a constant rate. Theoretically, we can design the steady-state outside temperature and translate it across the material. However, we are not using the model to determine the boundary conditions and this can be argued to be an open-loop solution to the problem contrary to the main objective of this dissertation.

The main idea to the design of the controller is to move the desired temperature distribution instead of moving the temperature gradient. If the controller can find a bias input that would achieve the moving desired temperature at all times, then we achieve our objective of this section. Intuitively, we expect the translated temperature gradient to be achieved by a translated bias input and therefore, we are justified in adapting this strategy. Mathematically, the desired temperature requested from the controller can be formally stated as

$$\hat{T}_d(r,z,t)=\begin{cases}\hat{T}_d(r,z-vt,0) & \forall\,(z-vt)\geq 0\\ \hat{T}_d(r,0,0)-vtT_g & otherwise\end{cases}, \tag{7.13}$$

where v is the rate of crystal growth, t is the time, and T_g is the desired gradient in the solid region. Although, at any time $t=\tau$, the desired temperature gradient requested from the controller $\hat{T}_d(r,z,\tau)$ is not feasible. However, the manner in which we find the bias input would automatically provide a least-square solution with $W=I$.

7.3.2.2 Simulation

As in Section 7.3.1.2, we try to establish a flat and a convex interface at z=0.02m and then move it a rate of 1 cm/hr. We used the same linearized model, the state-feedback gain and the bias input as in Section 7.3.1.2, where a flat interface is established at z=0.02. This would establish a flat interface at z=0.02 as before. Once a steady-state is reached, we would like to grow the crystal at a rate of 1 cm/hr. Changing the desired temperature as in (7.13) would not change the linearized model or the state-feedback gain, rather would change only the bias input. The bias input is computed using $\hat{T}_d$ as before and is given by

$$u_b = \underbrace{-\left[\tilde{B}_1^T\tilde{B}_1\right]^{-1}\tilde{B}_1^T F}_{\phi}\hat{T}_d = \phi\hat{T}_d \tag{7.14}$$

In the actual implementation, the ϕ matrix is computed only once at the beginning as ϕ does not change with time. Now, the bias input at any time t is calculated as a function of the achievable temperature as

$$u_b(t) = \phi\hat{T}_d(t) \tag{7.15}$$

with $\hat{T}_d(t)$ being the desired nodal temperature at time t calculated by approximating the desired distribution in (7.13). Simulation results are provided in Figures 7.24 for the flat interface case. The 2-norm of the tracking error is plotted in Figure 7.25. It can be observed that as soon as the interface moves from the initial position z=0.02, the norm of tracking error increases. This is due to the fact that the bias inputs are determined from the model that corresponded to z=0.02. If the 2-norm error is too big, the bias input has

to be re-designed around the new z. The actual and the desired interface height is plotted as a function of time in Figure 7.26 and from this figure it can be seen that the controller is able to track the desired interface height with no overshoot.

Similar results are shown for the convex interface case are shown in Figure 7.27, 7.28 and 7.29. In general for this material, the controller based on a single linearized model is able to perform reasonably. Also, note from the Figure 7.27 that the behavior of the requested outside temperature is very close to the case where one would simply translate the outside temperature distribution.

7.3.3 Observer Based State-Feedback Control of Interface at a Desired Location

In the entire previous section, we assumed that all states are measurable. In almost any practical situation, only a few of the states can be actually measured. This section is devoted to the implementation of the state-feedback controller in the presence of partial measurements.

7.3.3.1 Controller and State-Estimator Design

A linearized state-space model is found as in the previous section and the resulting state-space equation is given in (7.1). Any set of measurements y can be found as a linear combination of the states as given by

$$y = \tilde{C}T \tag{7.16}$$

Note that in the presence of Dirichlet boundary condition there is an additional input dependence. The methods developed in this section can be readily extended to this situation. The control strategy for establishing the desired interface shape is given as

$$u_1 = K_s\hat{T} + u_b, \tag{7.17}$$

where $\hat{T}$ is an estimate of the nodal temperatures T. Note that the control strategy is similar to the state-feedback case as in (7.2) with the exception that the estimated states are used instead of the actual states.

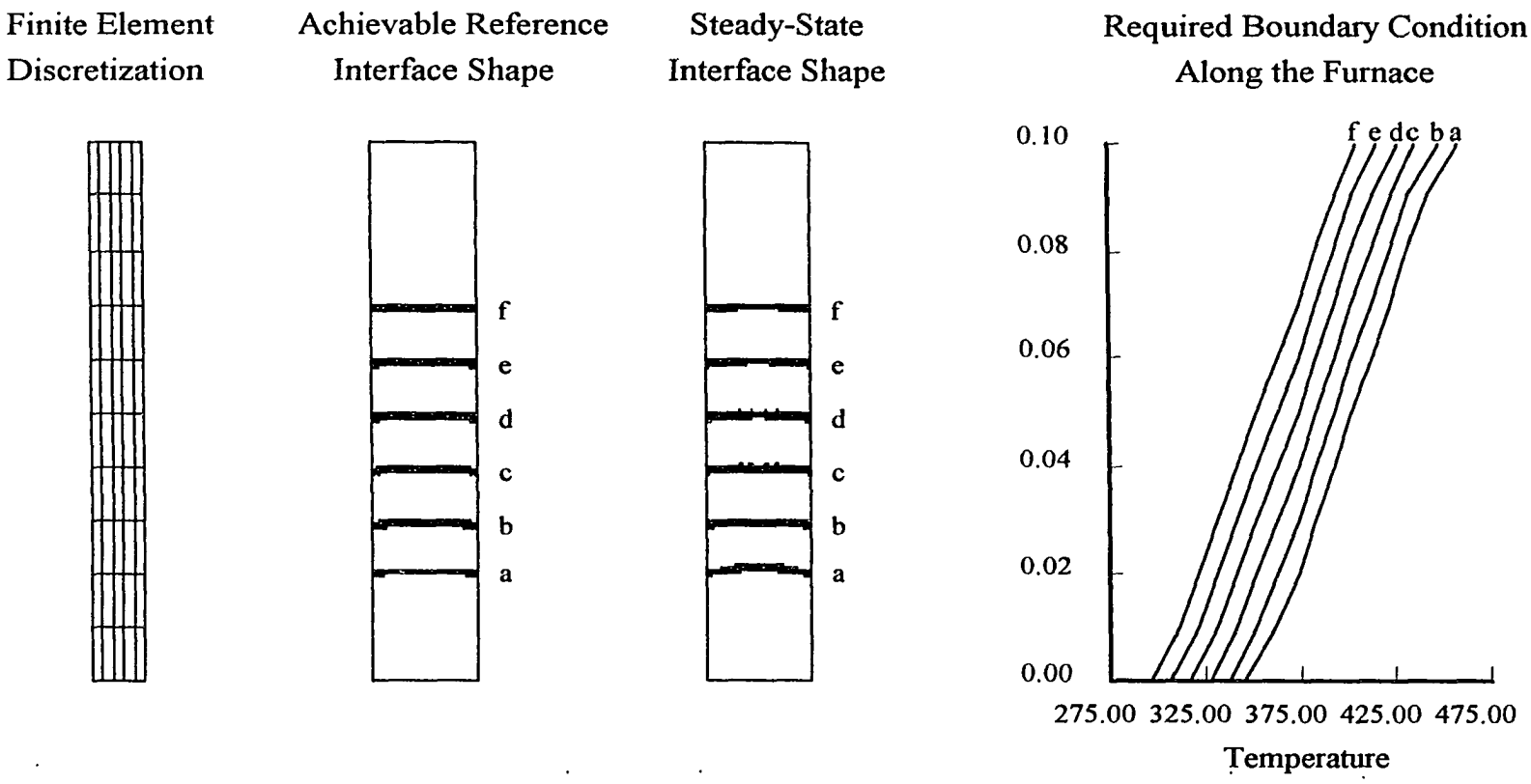

Times : a=32mins b=92mins c=152mins d=212mins e=272mins f=332mins

Figure 7.24 Steady-state interface shape and the corresponding steady-state boundary temperature for achieving a flat interface and moving it at a rate of 1 cm /hr.

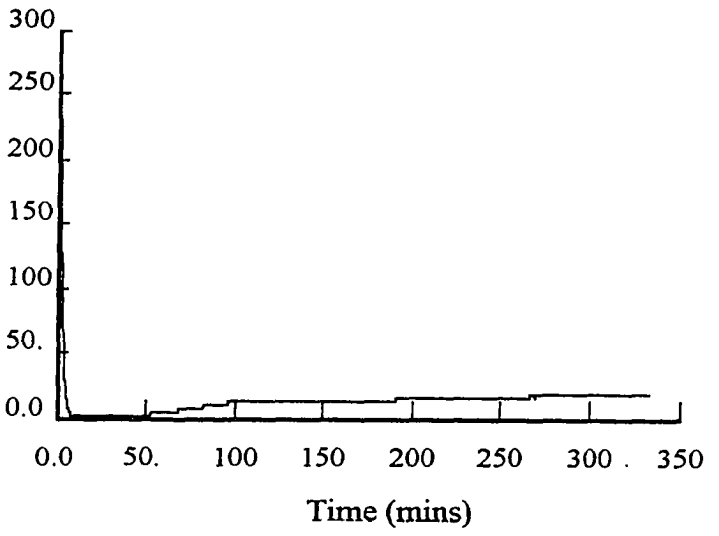

Figure 7.25 Plot of 2-norm of tracking error as a function of time. Note the tracking error begins to increase with the translation of interface.

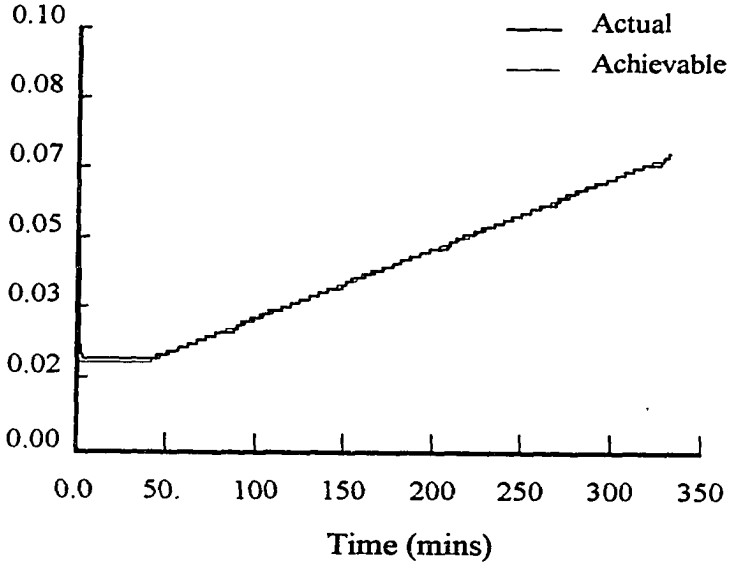

Figure 7.26 Interface height at the surface r=0.0 as a function of time. Note that there is no overshoot in the interface position at least for this particular plane, i.e., r=0.

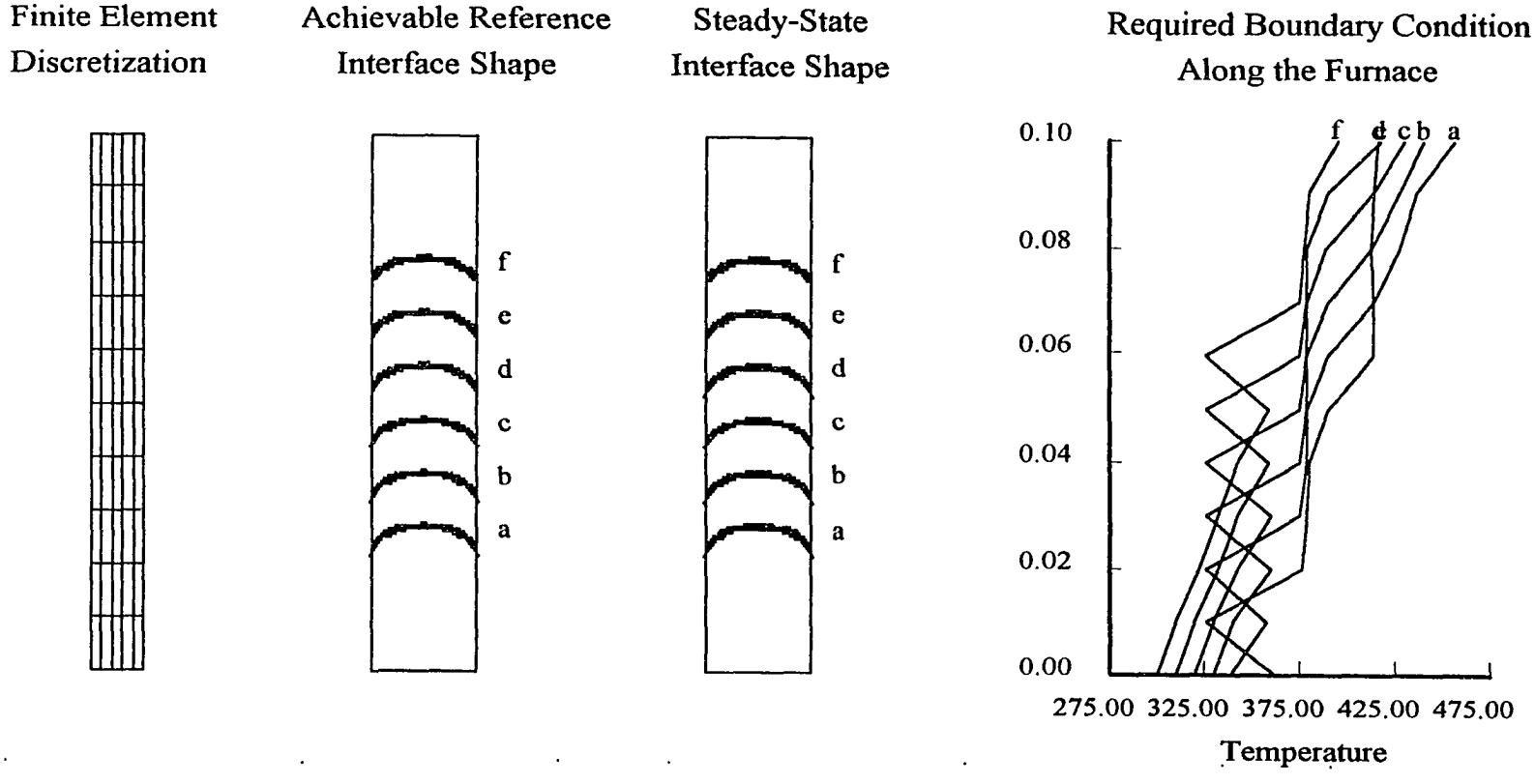

Times : a=6mins b=66mins c=126mins d=186mins e=246mins f=307mins

Figure 7.27 Steady-state interface shape and the corresponding steady-state boundary temperature for achieving a convex interface and moving it at a rate of 1 cm /hr.

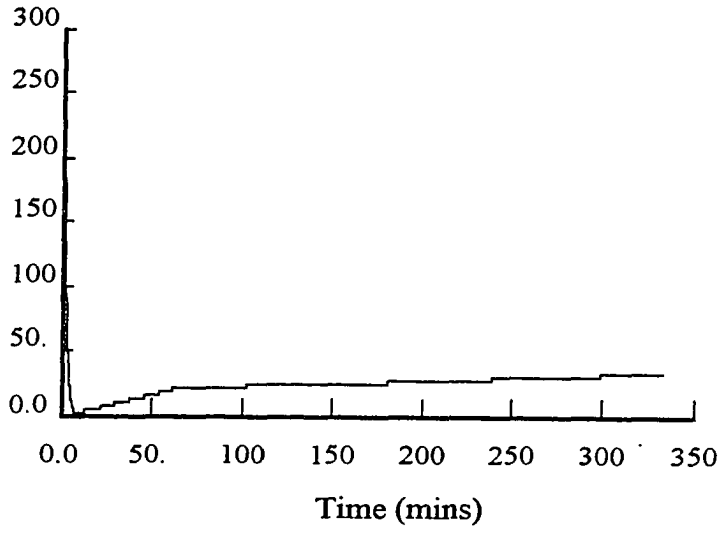

Figure 7.28 Plot of 2-norm of tracking error as a function of time for the convex interface shape case.

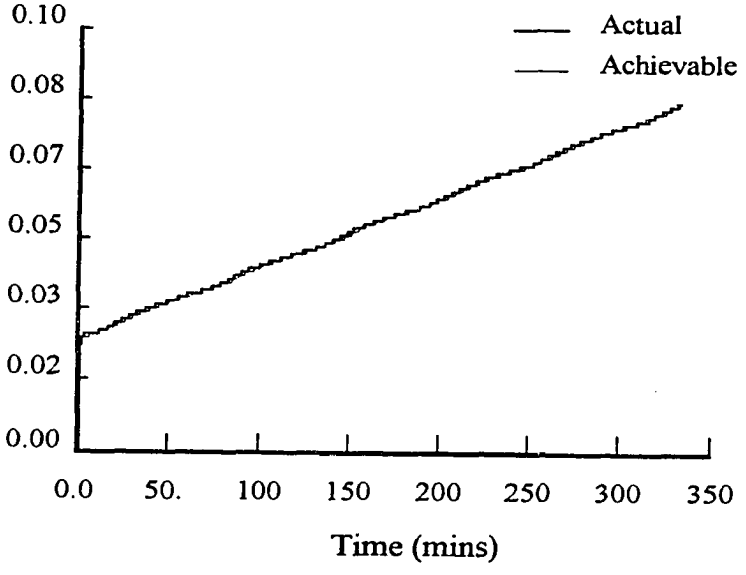

Figure 7.29 Interface height at the surface r=0.0 as a function of time

The pair $(\tilde{A}, \tilde{C})$ in (7.1) and (7.16) must be observable to compute an estimate of the nodal temperatures and the $(\tilde{A}, \tilde{B}_1)$ must be controllable for the existence of a state-feedback control. In the previous section, we assumed the system is controllable and if this is not so, we can use the techniques in this section to design a controller. The basic idea is to compute a reduced-order model that is completely controllable and observable by eliminating all uncontrollable and unobservable modes. As in Chapter V, the balanced truncation method [78] is used to determine the reduced order model. The order of the reduced order model can be found by plotting the Hankel singular values of the system. The *k*th reduced order after eliminating *(n-k)* weakest controllable\observable modes is given by

$$\begin{aligned} \dot{T}^r &= A^r T^r + B_1^r u_1 + B_2^r u_2 \\ y \approx y_r &= C^r T^r \end{aligned} \quad , \tag{7.18}$$

where $T^r \in \Re^k$, $A^r \in \Re^{k \times k}$, and all other matrices are of appropriate dimension. Note that the appropriate matrices can be found from the formulas in Section 5.2.1 and are stated here for convenience

$$T^r = S_{L,big}^T T \tag{7.19}$$

$$\begin{aligned} A^r &= S_{L,big}^T \tilde{A} S_{R,big} \\ B_1^r &= S_{L,big}^T \tilde{B}_1 \quad B_2^r = S_{L,big}^T \tilde{B}_2 \\ C^r &= \tilde{C} S_{R,big} \end{aligned} \quad , \tag{7.20}$$

where $S_{L,big}$, $S_{R,big}$ are matrices of dimension *n* by *k* and are computed using the orthonormal basis of the left and right eigenspaces associated with the *k* largest eigenvalues of the matrix $(W_c W_o)$. The matrices W_C and W_O are the controllability and the observability Grammians of the full order model.

The control strategy in (7.17) needs to be modified as all states are not controllable and observable. This is done by feeding back the estimated states of the reduced-order model as

$$u_1 = K_s \hat{T}^r + u_b \tag{7.21}$$

The reduced order state-feedback gain is found as a LQR and the state-estimate of T_r is found by using an observer. The observer dynamics is governed by an equation similar to (5.20) and is given by

$$\dot{\hat{T}}^r = A^r \hat{T}^r + B_1^r u_1 + B_2^r u_2 + L(y - C^r \hat{T}^r), \tag{7.22}$$

where L is the observer gain and is found as an LQE by a formula similar to (5.21).

As before, the designer selects the nodal temperature that would set up the desired interface shape. The objective function in (7.3) can be minimized to find the achievable nodal temperatures. There are basically two different ways to find the bias input. In this dissertation, we find the bias input based on the model and use no feedback to adjust for modeling error in the bias input. Therefore, we can directly use the bias inputs found in the state-feedback section. This would essentially set up the same steady-state interface shape as the state-feedback case. Although, this approach solves the reduced-measurement problem, it provides no new results. Another problem with this approach is that it restricts the bias input to be determined in an open-loop fashion only. Closed-loop bias input determination through techniques such as pseudo integral control approach [87] cannot be implemented with this choice. However, if we determine the bias-input using the "reduced-order model", pseudo integral control approach can be implemented. In the rest of this section, we attempt to design bias input using reduced-order model only.

Figure 7.30 shows the general method to find the bias input using the reduced-order model. The desired nodal temperature T_d specified by the designer is transformed to desired reduced order state through the following transformation

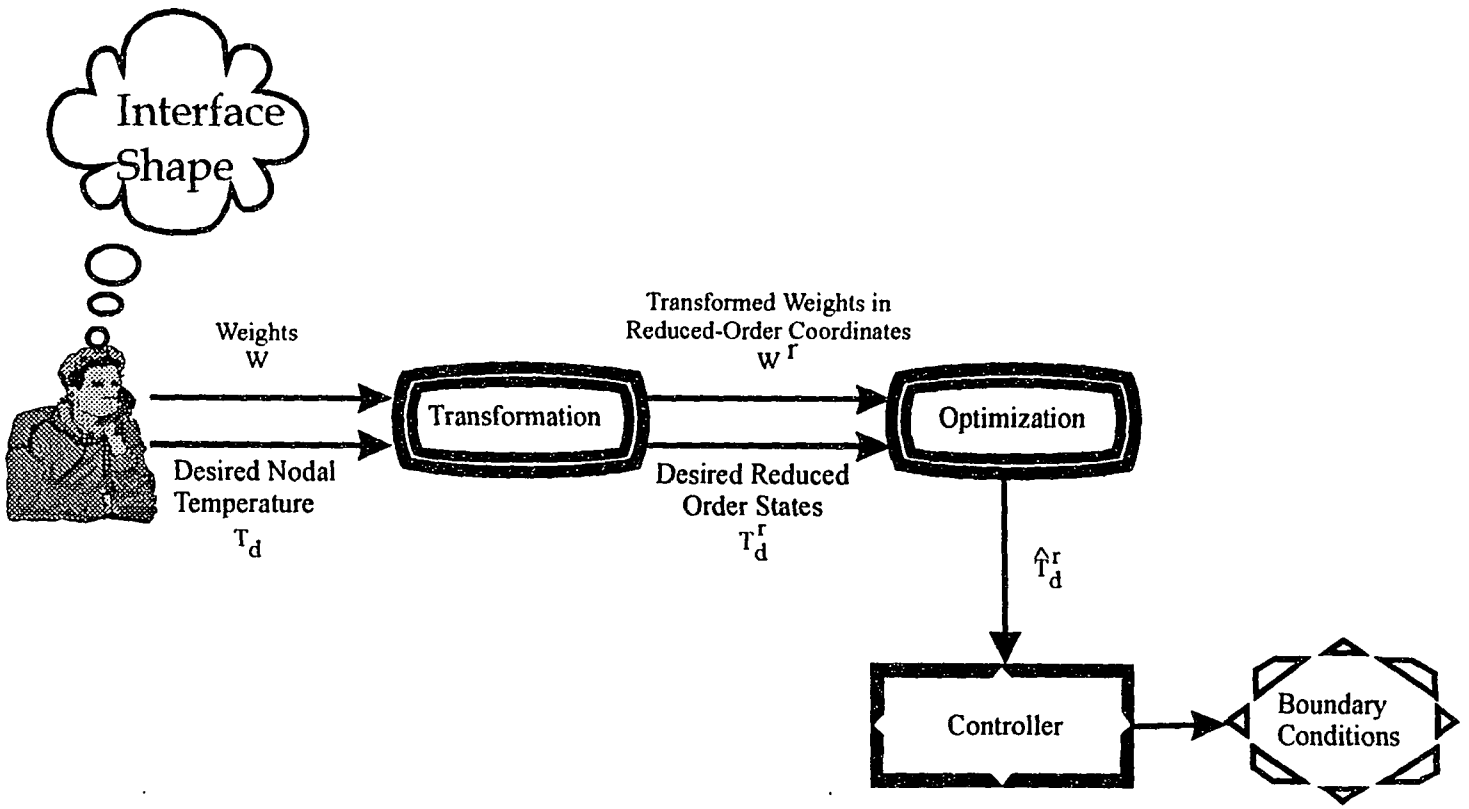

Figure 7.30. Basic method to determine the bias input in the presence of partial measurements.

$$T_d^r = S_{L,big}^T T_d \tag{7.23}$$

Just as in the state-feedback case, it is possible that the reduced state requested by the user cannot be achieved by any bias input u_b. Therefore, as before we cast an optimization framework and minimize an objective function similar to the one in (7.3)

$$J = \left(T_d^r - \hat{T}_d^r\right)^T W^r \left(T_d^r - \hat{T}_d^r\right), \tag{7.24}$$

where W^r is a user selected weight matrix. The states of the reduced-order state-space model have no physical meaning (rather a linear combination of nodal temperatures) and therefore, it is difficult to pick W. We propose a transformation that would transform weights used in the full order state-feedback case (Section 7.3.1.1) as

$$W^r = S_{R,big}^T W S_{R,big}. \tag{7.25}$$

The approach now is to request the $\hat{T}_d^r$ corresponding to the minimum J as the desired temperature distribution as in Figure 7.30.

7.3.3.2 Simulation Results

A state-feedback implemented using observer is designed establishing a flat and a convex interface. The linearized state-space model is the same as used in Section 7.3.1.2. This model has 66 states with 11 inputs. Here, we assume only the ampoule surface is measured. Therefore, the system has 11 outputs measured at the 11 nodal points on the ampoule surface. The Hankel singular values are computed for this system and 11 states are found to be weakly observable\controllable. Therefore, a 55th order reduced-order model is obtained using the balanced truncation technique. A state-feedback control gain is computed as linear quadratic regulator with the weighting matrices Q and R chosen as

$$Q = 5S_{R,big}^T S_{R,big}, \quad R = I_{11}. \tag{7.26}$$

This choice is made in an effort to minimize a similar cost as the full order state-feedback. This approach is expected to yield a similar transient response as the full order case. The

observer gain L is selected as a linear quadratic estimator and is computed with a cost chosen as

$$Q_o = 10\, I_{55},\ R_O = I_{11}. \tag{7.27}$$

The cost is chosen in such a way that the estimator dynamics is much faster than that of the actual system. Again, as before, the closed-loop and open-loop system are compared by plotting the corresponding singular values as shown in Figure 7.31. As before, feedback increased the band-width of the system.

The bias input is dependent on the desired interface shape. As before, we try to implement a flat interface at $z=0.02$ except that in this case, only a few measurements are available for feedback. The equivalent temperature distribution for establishing the flat interface is chosen as in (7.4). The weighting matrix W is selected to be same as before, i.e., $W = I_{66}$. The corresponding W^r is computed using the transformation in (7.25). The achievable reduced-order state-vector $\hat{T}_d^r$ for this weight choice is calculated using a relation similar to (7.5) and for this case is given as

$$\hat{T}_d^r = -\left(\left(F^r\right)^{-1} \tilde{B}_1^r\right)\theta^r \tag{7.28}$$

where

$$\theta^r = -\left[\left(\left(F^r\right)^{-1} \tilde{B}_1^r\right)^T W^r \left(\left(F^r\right)^{-1} \tilde{B}_1^r\right)\right]^{-1} \left(\left(F^r\right)^{-1} \tilde{B}_1^r\right)^T W^r T_d^r \tag{7.29}$$

with F^r is the linearized reduced order closed-loop system given by

$$F^r = \tilde{A}^r + \tilde{B}_1^r K_s \tag{7.30}$$

The steady-state temperature distribution and steady-state outside temperature based on the reduced-order linearized model are shown in Figures 7.32 and 7.33.

The implementation of the observer-based state-feedback controller is shown in Figure 7.34. There are some difficulties with choosing a single time-step for both the non-

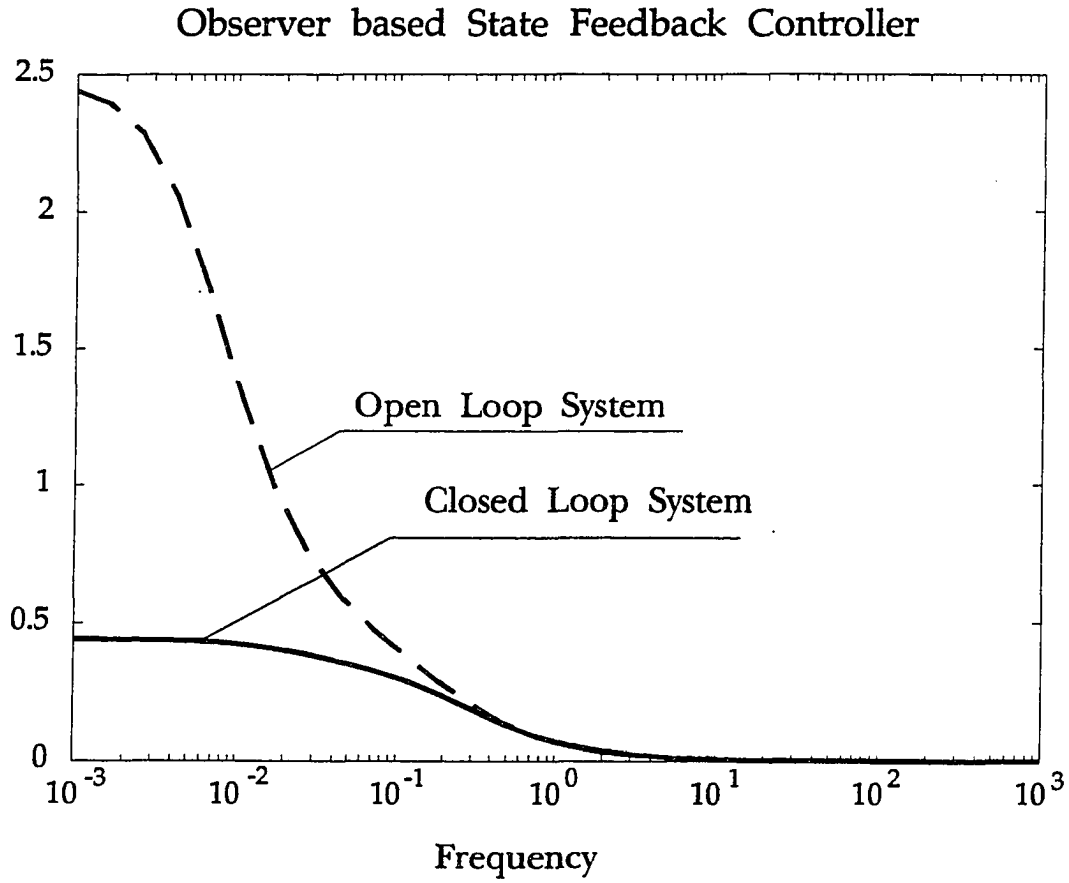

Figure 7.31 Singular value plot for open-loop and closed-loop systems.

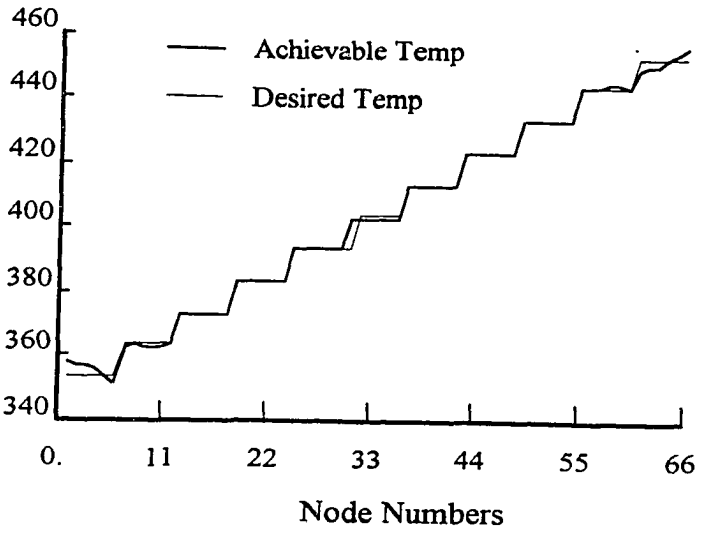

Figure 7.32. Desired nodal temperatures T_d and achievable nodal temperatures $\hat{T}_d$ based on the linearized reduced order state-space model.

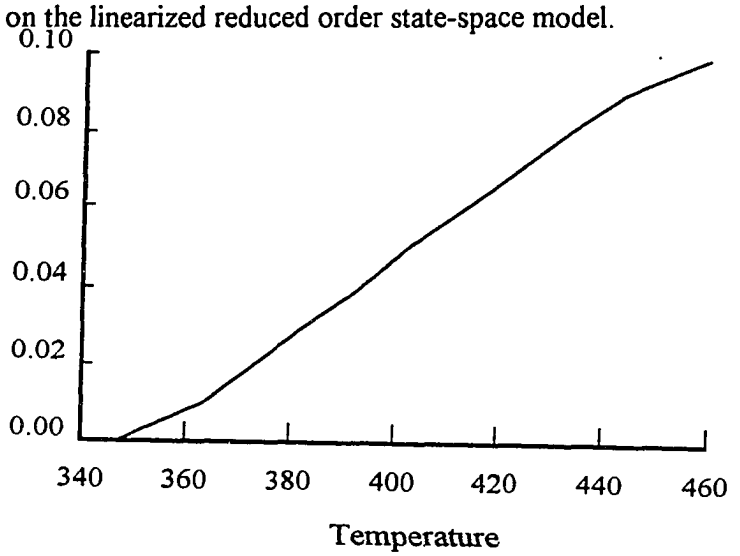

Steady-state inputs $\left(u_b - K_s T_\infty^r\right)$ at different z-locations.

z=0.00	z=0.01	z=0.02	z=0.03	z=0.04	z=0.05	z=0.06	z=0.07	z=0.08	z=0.09	z=0.1
346.96	363.66	372. 85	382.98	393.10	402.21	412.52	423.27	432.34	443.53	459.83

Figure 7.33. Steady-state inputs for establishing a flat interface at z=0.02.

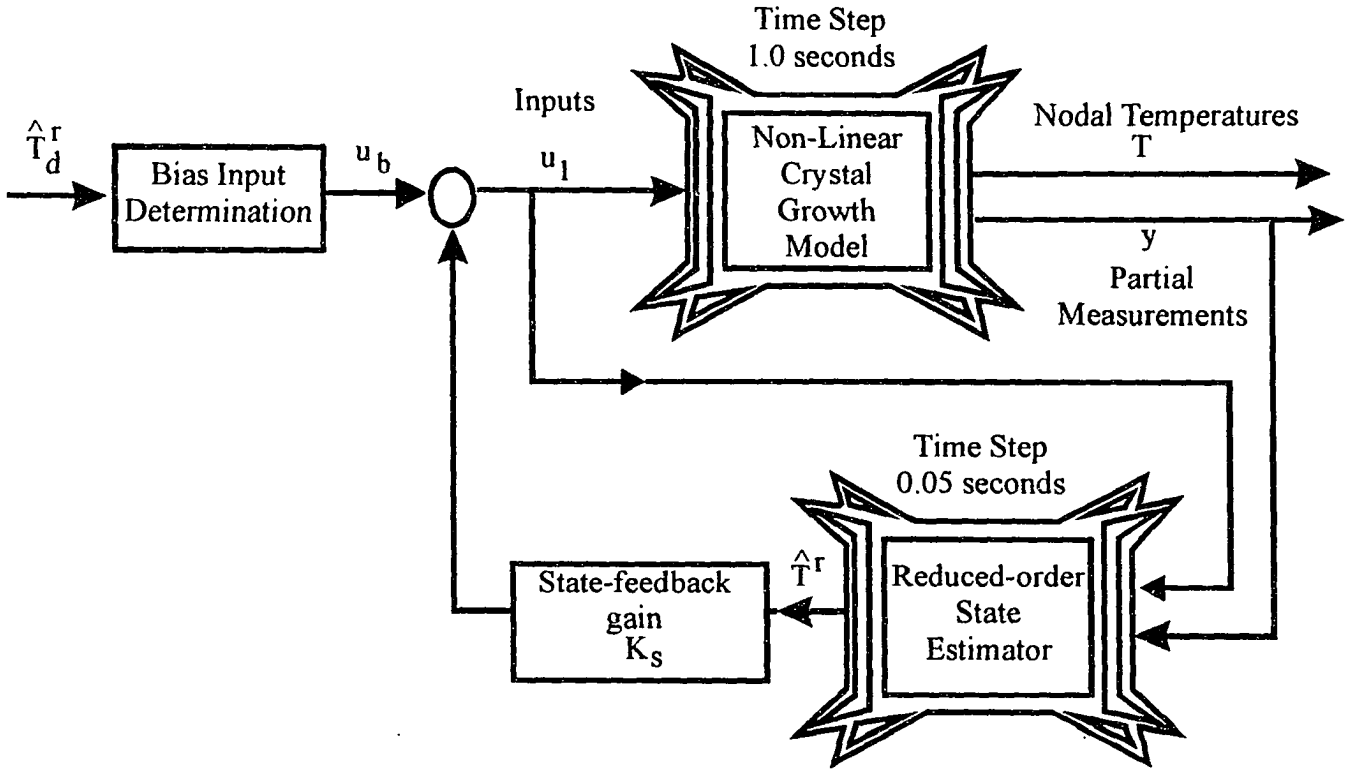

Figure 7.34. Implementation of observer based state-feedback control.

linear crystal growth system and the observer. The observer has a faster dynamics due to the design and therefore, needs a smaller time step. One way to handle this difficulty is to keep the time-step of the non-linear system to be an integer multiple of the estimator. This way, the estimator can go through a set of time step before the non-linear system can go through a single time step. In the simulations presented in this Section, the time-step for the estimator is selected as 0.05 seconds and that of the non-linear system to be 1.0 sec (a factor of 20).

The crystal growth system is simulated with this observer based state-feedback controller. All the initial nodal temperatures are assumed to be at 370 C. The actual and the achievable temperature distributions are plotted in Figure 7.35 and the requested temperature profiles are plotted in Figure 7.36. Note, the input request during start-up is very high during start-up. This is because of the initial choice for the states in the state-estimator. Ideally, the feedback controller must be started after the state-estimator converges. This is very essential in a practical implementation. The steady-state interface shape is plotted in Figures 7.37. The 2-norm of the error in the nodal temperature as given by (7.8) and (7.9) are plotted in Figure 7.38. To see, if there is any overshoot in the establishment of the interface, we plot the interface height at $r=0$ as a function of time as in Figure 7.39. Again due to poor initial condition for the state estimator, the control overshoots in the very beginning. However, this can be avoided by switching to closed-loop control after the estimator converges. The 2-norm of the estimator error defined as

$$\varepsilon = T^r - \hat{T}^r$$
$$\|\varepsilon\|_2 = \sqrt{\varepsilon^T \varepsilon} \tag{7.31}$$

is plotted in Figure 7.40. Note that the estimator error 2-norm goes down to zero.

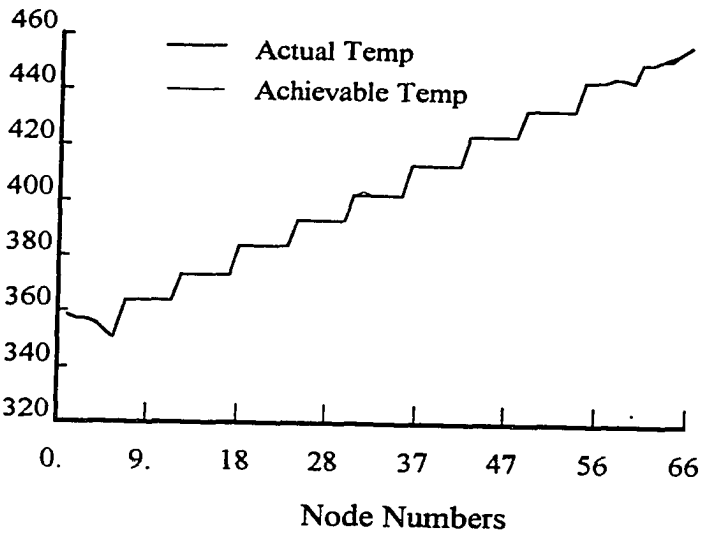

Figure 7.35. Achievable nodal temperatures $\hat{T}_d$ and actual steady-state nodal temperatures T based on the non-linear state-space model.

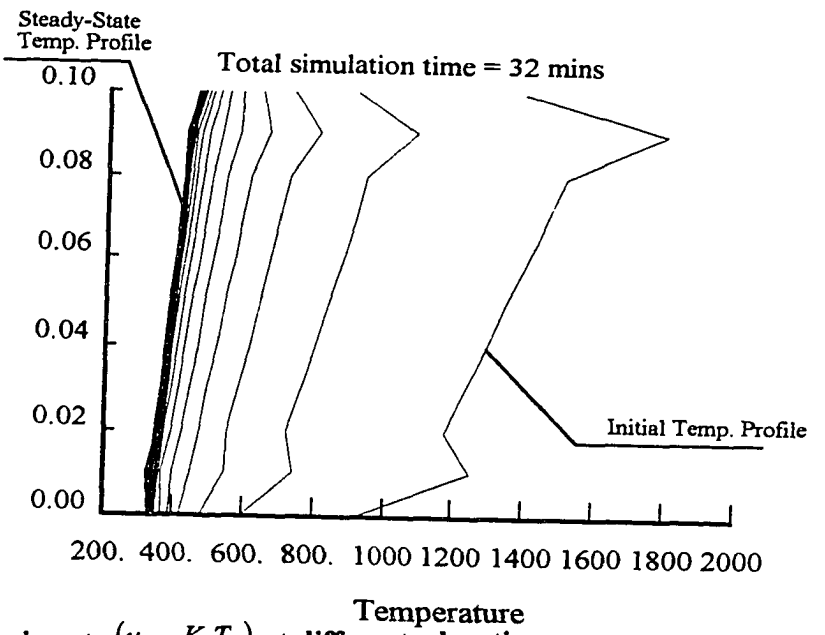

Steady-state inputs $(u_b - K_s T_\infty)$ at different z-locations.

z=0.00	z=0.01	z=0.02	z=0.03	z=0.04	z=0.05	z=0.06	z=0.07	z=0.08	z=0.09	z=0.1
346.99	363.75	373.32	383.06	393.14	402.23	412.55	423.31	432.39	443.59	459.88

Figure 7.36. Temperature profiles requested by the controller as a function of time.

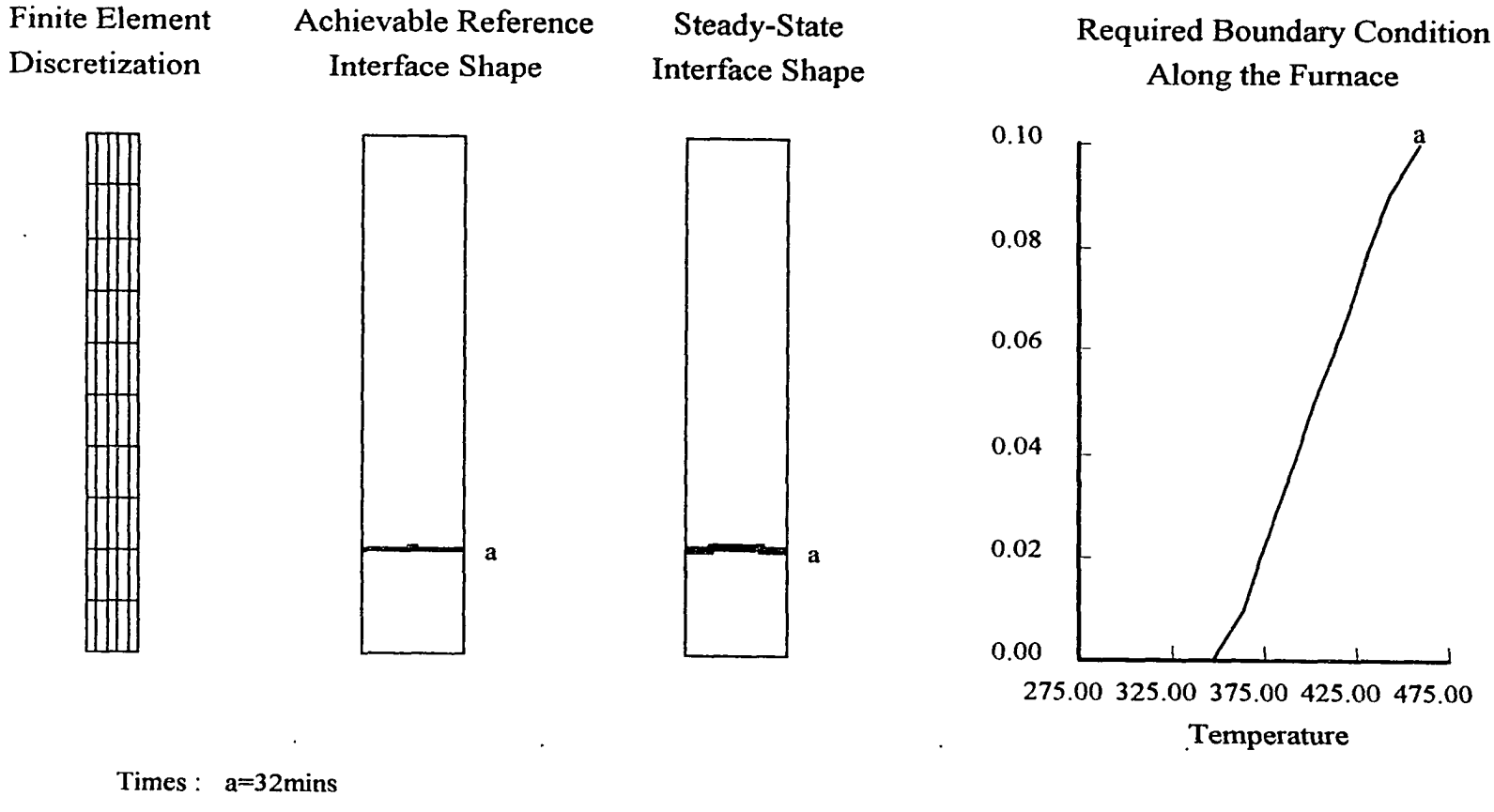

Figure 7.33 Steady-state interface shape for achieving a flat interface at z=0.02. In this simulation, the temperature on the nodes of the outer surface of the material are measured.

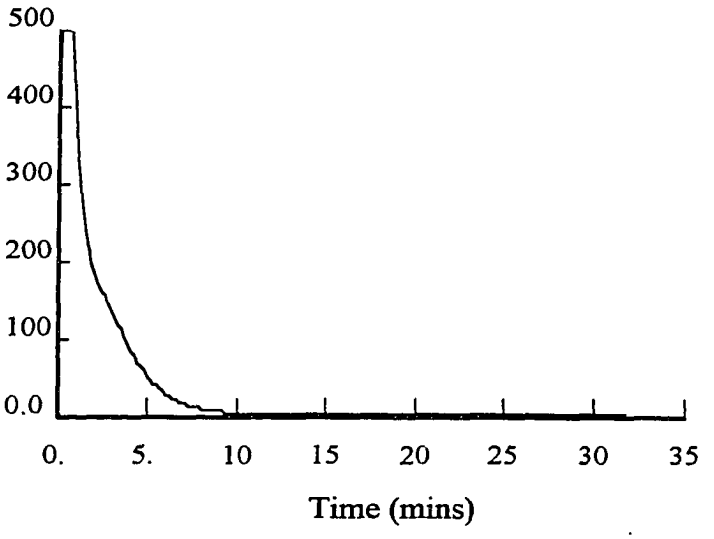

Figure 7.38 Plot of 2-norm of tracking error as a function of time.

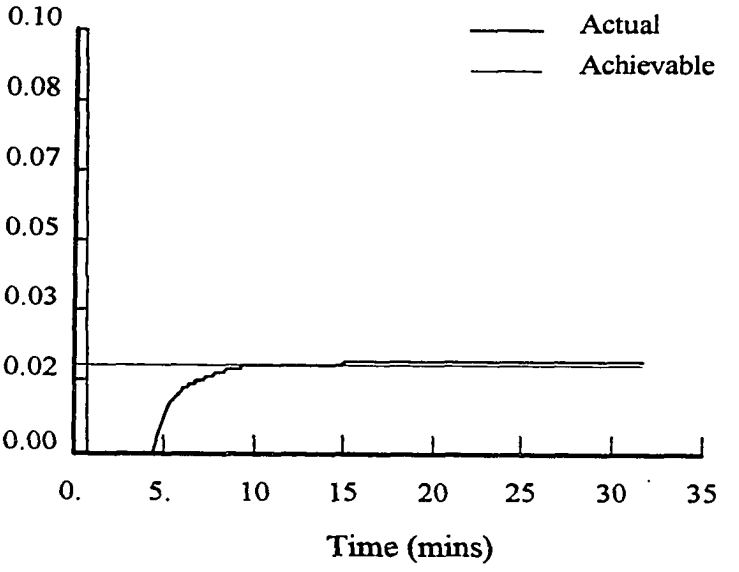

Figure 7.39 Interface height at the surface r=0.0 as a function of time. Note that there is undershoot/overshoot during startup. Over-shoot does not occur once the estimator converges.

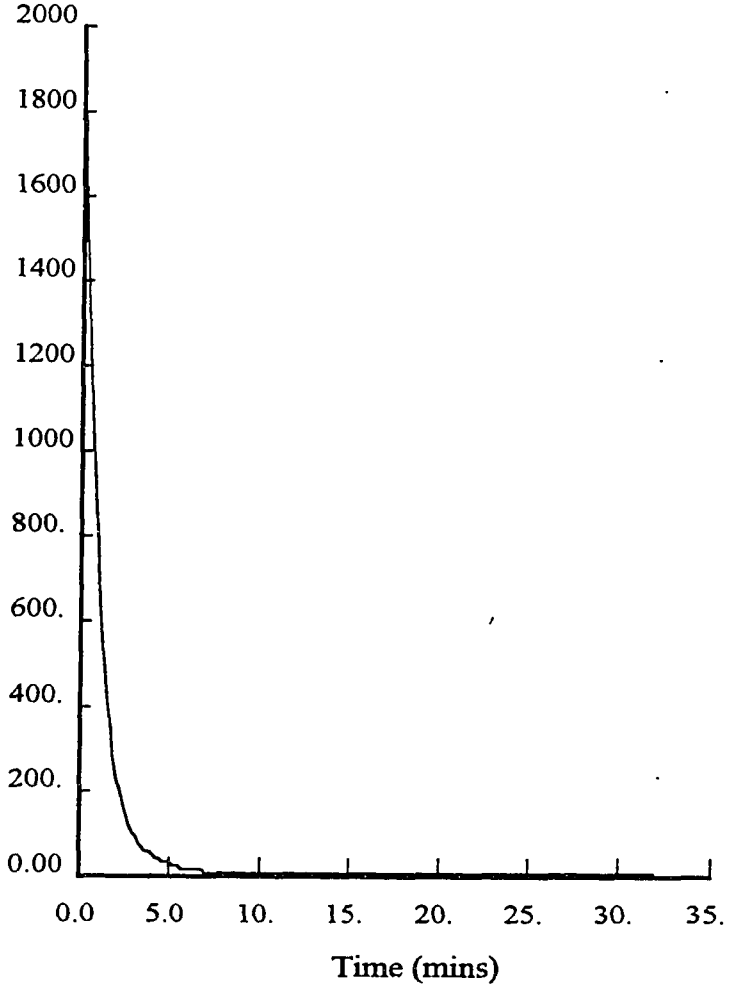

Figure 7.40. Plot of estimator error 2-norm as a function of time.

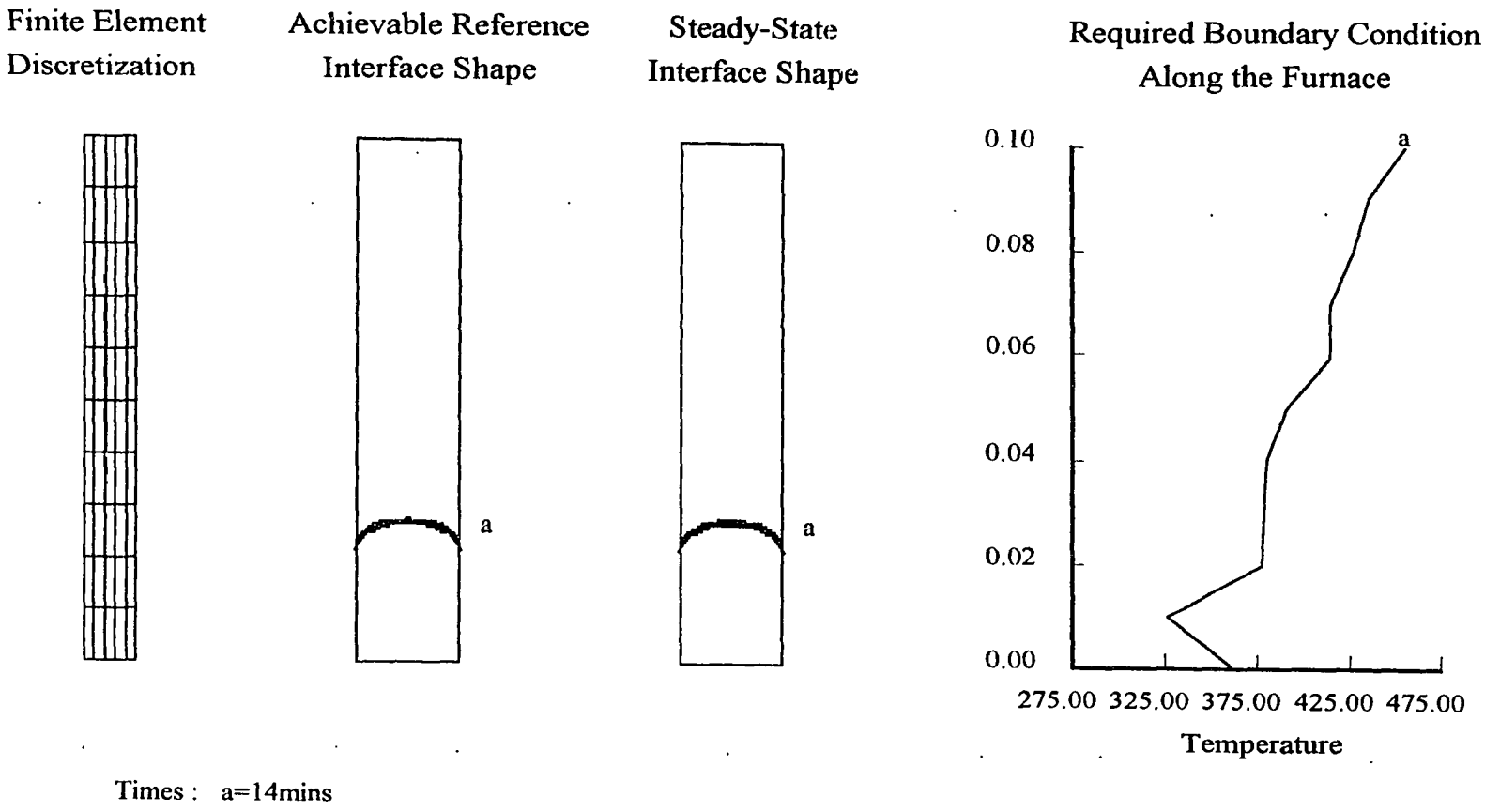

Figure 7.41 Steady-state interface shape for achieving a convex interface at z=0.02. In this simulation, the temperature on the nodes of the outer surface of the material are measured.

A similar control design procedure is followed to establish a convex interface shape. The desired nodal temperature T_d, and the weight W are selected as in equation (7.11) and (7.12). In order to make the presentation concise only the steady state interface shape and the requested boundary condition are plotted in Figure 7.41.

7.3.4 Observer Based State-Feedback Control to Grow Crystal at a Desired Rate

7.3.4.1 Controller Design

The strategy developed in Section 7.3.2 is used to translate the interface. As before, we translate the achievable nodal temperatures. To get the achievable nodal temperature from the reduced-order achievable states, we use the following transformation

$$\hat{T}_d = S_{R,big}\hat{T}_d^r \tag{7.32}$$

From the achievable nodal temperature $\hat{T}_d$, we can find the achievable temperature distribution $\hat{T}_d(r,z,t)$ using finite element approximation. Now the translated achievable temperature distribution is found using Equation (7.13) and the corresponding achievable reduced states are computed using the following equation

$$\hat{T}_d^r(t) = S_{L,big}^T\hat{T}_d(t) \tag{7.33}$$

As before, the bias input to establish this achievable reduced-order state is determined using Equation (7.28).

7.3.4.2 Simulation

This section contains simulation of crystal growth system operating with the observer-based controller. In the first case, we would like to grow crystal at a rate of 1cm/hr with the interface being flat during the growth period. In the second case, we attempt to establish a convex interface and grow it at the same rate 1 cm/hr. For both

cases, we use the same linearized model, same reduced-order state-feedback controller and observer as in the Section 7.3.2.2.

Initially, we apply the bias input used in Section 7.3.2.2 to establish a flat interface at z=0.02. This would establish the same interface as in Figure 7.37 in the steady-state. Once the steady-state is reached, the interface is translated by changing the achievable temperature distribution. The bias input is calculated as

$$u_b = \underbrace{-\left[\left(\tilde{B}_1^r\right)^T \tilde{B}_1^r\right]^{-1}\left(\tilde{B}_1^r\right)^T F^r}_{\phi} \hat{T}_d^r = \phi \hat{T}_d^r \tag{7.34}$$

The translated $\hat{T}_d^r$ can be found using (7.33) and therefore the bias input at any time t can be calculated as

$$u_b(t) = \phi \hat{T}_d^r(t) \tag{7.35}$$

The achievable, actual interface shape and the corresponding temperature profiles at some specific times are plotted in Figure 7.42. The 2-norm of tracking error, the interface height at r=0 surface and estimator error are plotted in Figures 7.43, 7.44, 7.45.

The procedure is applied for the convex interface shape case and the achievable, actual and the requested temperature profiles are plotted for specific times in 7.46.

7.4 Comments and Conclusions

This chapter provided simulation results to demonstrate the ability to control the solid-liquid interface shape during crystal growth by manipulating the boundary temperature. The boundary temperature is essentially found using a linearized model of the furnace. Depending on the number of on-line measurements, either the state-feedback or the observer based controller can be used. The designer translates the requirement of a desired interface shape into a requirement of a desired temperature distribution. Using some of the theorems developed in Chapter V, we find an achievable distribution that is "close" to the desired temperature distribution. The designer can also provide a weight

matrix to lay more emphasis on certain regions than others. The actual interface shape is very much dependent on the choice of the weight matrix. Translation of interface is achieved by translating the desired temperature distribution. From the simulation results, it is evident that this approach yielded the desired interface shape during crystal growth.

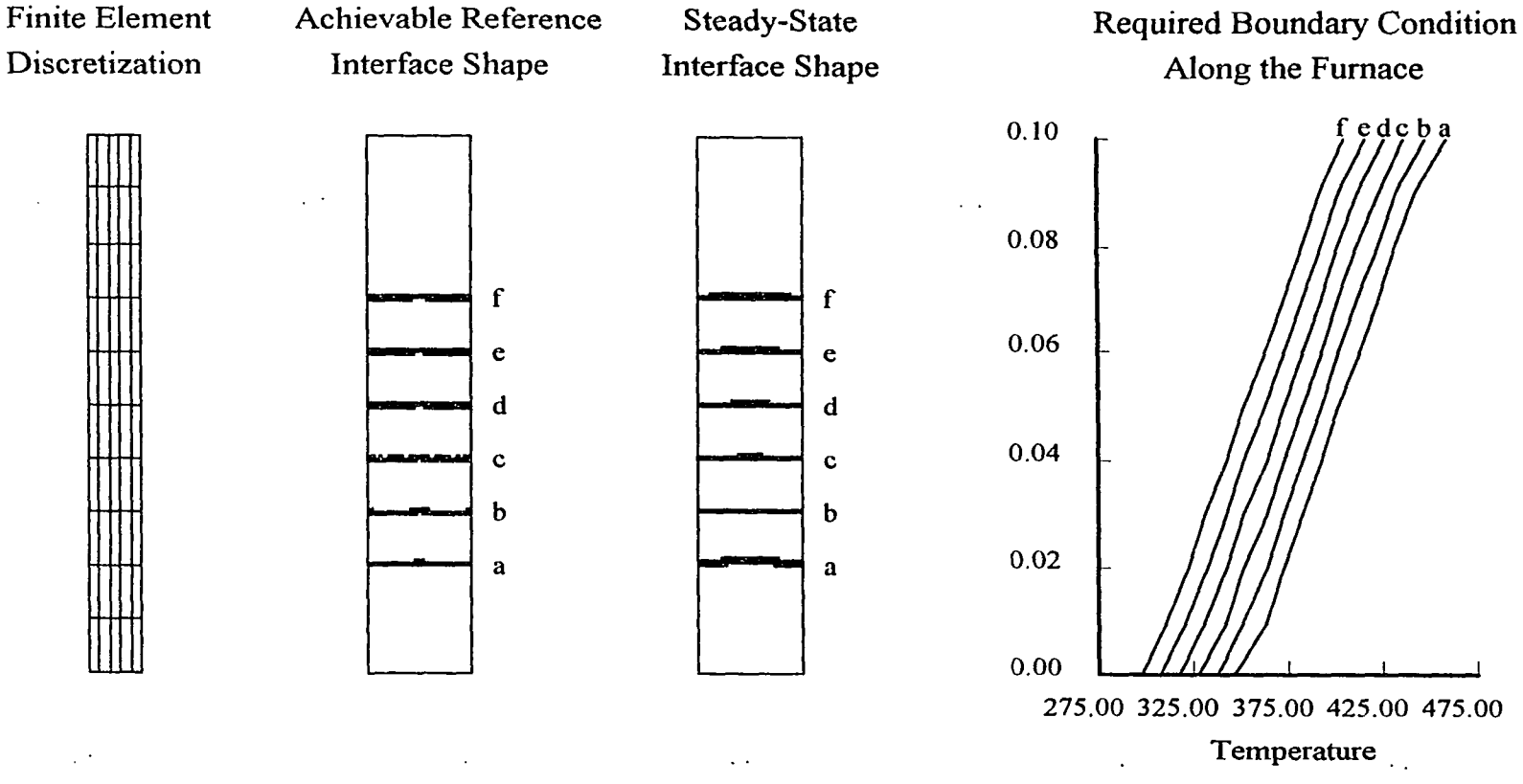

Times : a=32mins b=92mins c=152mins d=212mins e=272mins f=332mins

Figure 7.42 Steady-state interface shape for achieving a flat interface and moving it at the rate of 1 cm/hr. Here, the nodal temperatures on the outer surface of the material are measured.

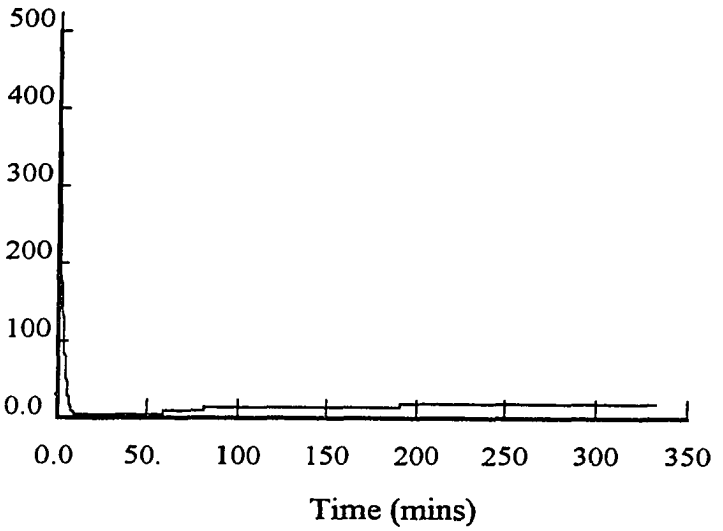

Figure 7.43 Plot of 2-norm of tracking error as a function of time.

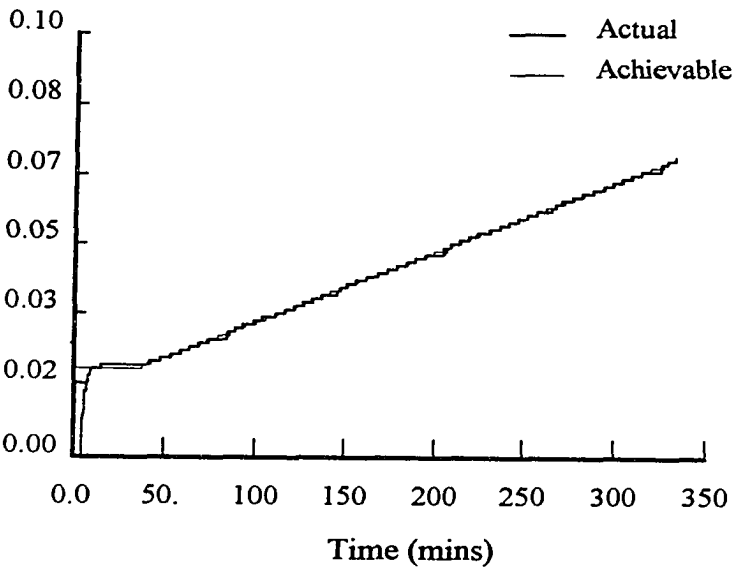

Figure 7.44 Interface height at the surface r=0.0 as a function of time. Note that there is undershoot/overshoot during startup. Over-shoot does not occur once the estimator converges.

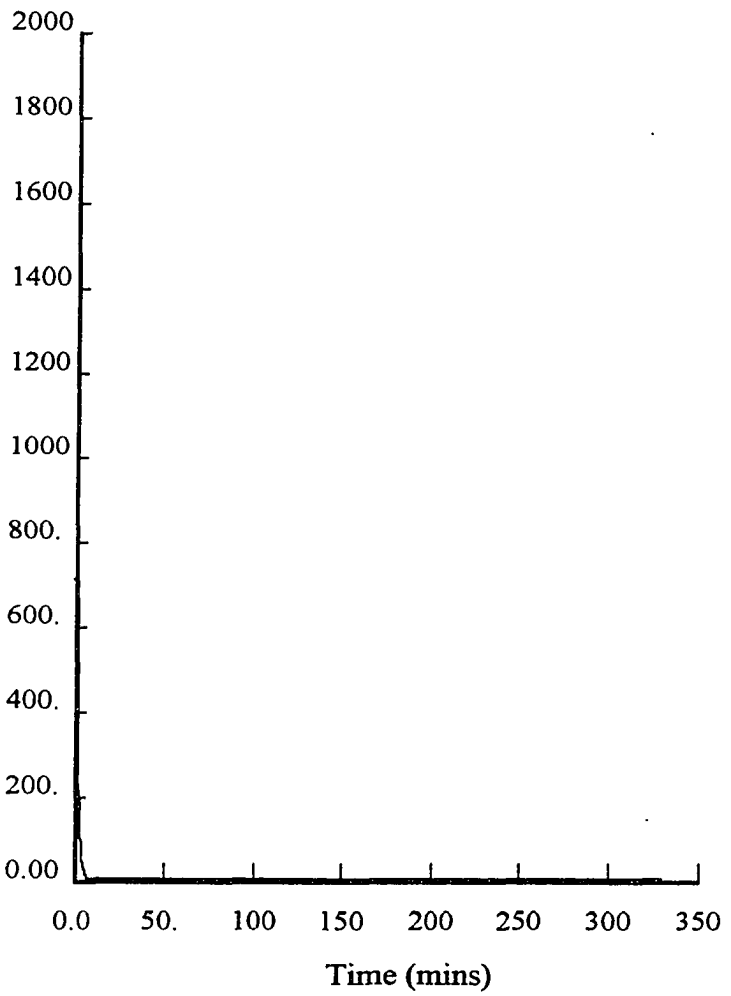

Figure 7.45 Plot of estimator error 2-norm as a function of time during crystal. Note that the error asymptotically decreases to zero.

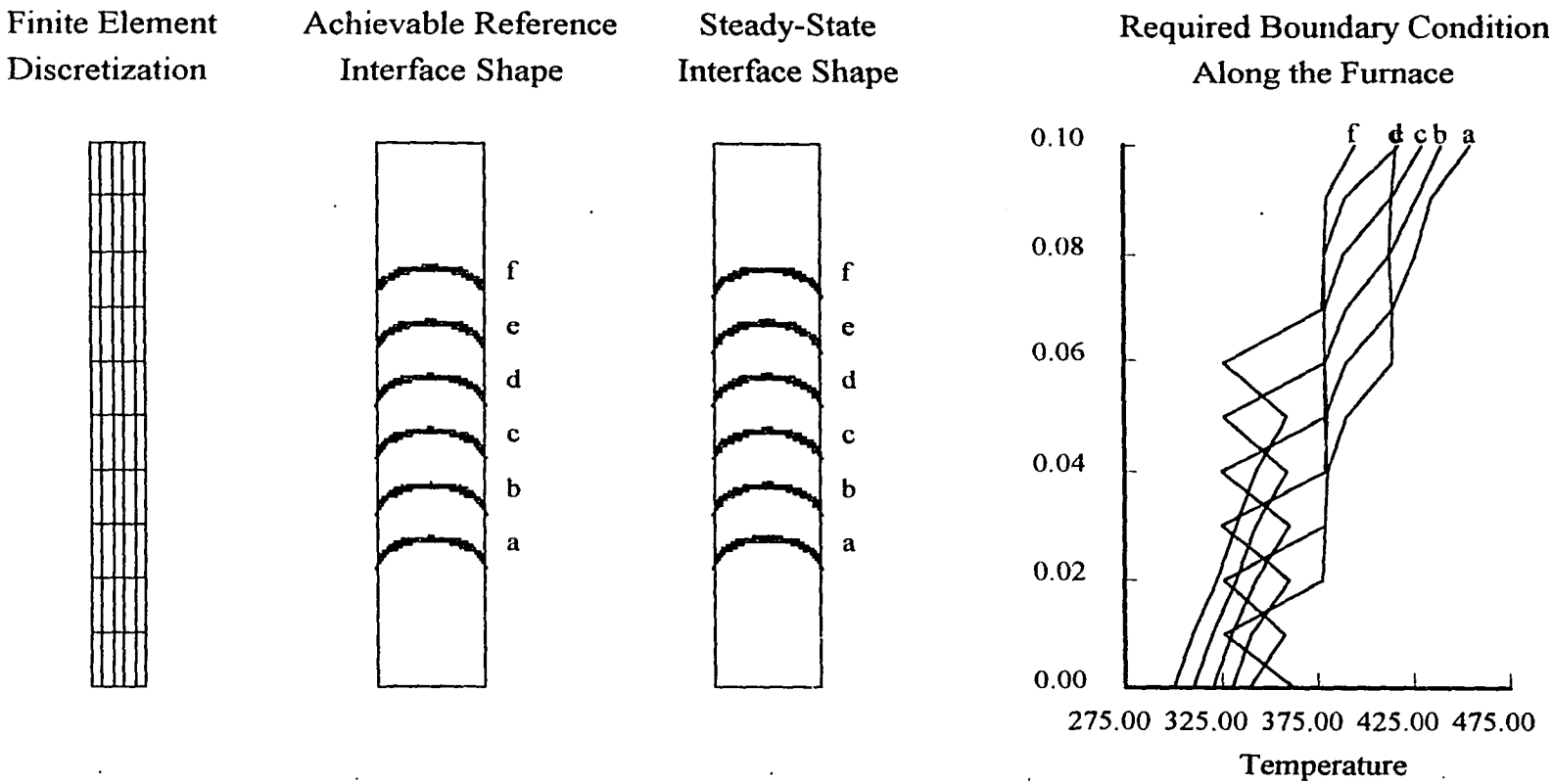

Times : a=14mins b=74mins c=134mins d=194mins e=254mins f=314mins

Figure 7.46 Steady-state interface shape for achieving a convex interface and moving it at the rate of 1 cm/hr. Here, the nodal temperatures on the outer surface of the material are measured.

CHAPTER VIII

SUMMARY AND CONCLUSIONS

This dissertation deals with the problem of controlling the solid-liquid interface shape during solidification of molten material inside an ampoule. The necessary boundary conditions that would achieve the desired interface shape and translation rate is found using the developments in the "Controls" area.

The finite element method is used to approximate the governing PDE found using apparent heat capacity formulation by a finite number of ODEs. A general methodology is proposed to obtain a state-space model of the heat-conduction system by appropriately parametrizing the boundary conditions. This procedure is used to obtain a state-space model of the heat-conduction system.

The state-space model is used to design a controller to improve the transient response and to establish arbitrary temperature distributions inside the material by altering the parameterized boundary conditions. The standard LQR / LQG procedure is used to design the controller. The tracking of reference temperatures is achieved through the bias input determined using the model. A set of necessary and sufficient conditions are derived to characterize the set of all achievable temperature distributions inside the material in the steady-state.

The heat conduction problem with no phase change is initially considered to gain insights into the modeling and control aspects. The reduced-order lumped state-space model obtained by balanced truncation method is used to design controllers for four different sets of measurements. In each case, a state-feedback controller is designed as LQR and if there is a need, an observer is designed through the LQG design procedure.

The robustness of the controllers are analyzed by finding the multi-variable gain and phase margins. As reported in the literature, it is found that there are no guaranteed margins for the LQG controllers and an arbitrary design may produce unstable controllers. It is proposed to use the LTR technique to design stable controllers that have the robustness properties of a standard LQR based controllers. In the current design, the bias input is found using the model and the output measurements are not utilized in determining them. Therefore, we propose to use a generalized version of integral-control that would guarantee zero steady-state error at all measurement locations.

The heat-conduction with phase change problem is treated in a similar fashion as the linear heat conduction fashion. The control problem is divided into four main design problems: establishing a desired interface shape assuming all nodal temperatures are measured, moving the interface at desired rate while maintaining the desired interface shape when temperatures at all nodes are measured, establishing a desired interface when only a partial set of temperatures are measured, moving the interface at a desired rate when only a few nodal temperatures are measured. In each of the four control design problems, two sets of desired interface shape are considered: flat interface, convex interface.

Initially, a linearized model to represent the dynamics of the interface shape during crystal growth is obtained by performing open-loop simulations using the non-linear FE model with appropriate boundary conditions. The linearized model is used to design the state-feedback gain by minimizing appropriately chosen costs. To determine the bias inputs, the designer is required to specify a temperature distribution that would represent the desired interface shape reasonably. The theorems developed in Chapter V are used to check if this desired temperature distribution can be achieved by any boundary temperatures. As observed during design exercises, it is very rare that the specified temperature distribution can be established by a boundary temperature. Therefore, the

desired temperature distribution is achieved in a weighted least-squares sense by finding appropriate control inputs. The weights are chosen so that temperatures around the interface region are given more emphasis than other locations. It is also observed that the success of achieving a desired interface shape is dependent on the choice of weight, especially for the convex interface shape.

The desired interface is translated by moving the desired temperature at all times. The bias input is determined in a similar fashion as in the case of simply establishing the interface at a specific location except that the translated desired temperatures are used instead of the desired temperatures. This strategy successfully moved the interface at the desired rate.

In the situation where only a few nodal temperatures are measured, an estimator is designed to reconstruct the nodal temperatures from the measured temperatures. The estimated nodal temperatures are used to implement the state-feedback controller. The linearized model is selected to be the same as the state-feedback case (all nodal temperature measured). However, from the Hankel singular value plot, it is found that some states are weakly controllable\observable. Hence a reduced-order model is found by eliminating the weakly controllable\observable modes. The reduced-order model is used to design the controller. The control design with the reduced-order model is very similar to that of the state-feedback case. Simulation results showed that the observer based state-feedback controller has similar performance except during initial start-up. A similar result is obtained while moving the interface in the presence of the partial measurements.

8.1 Future Directions

8.1.1 Modeling Aspects

The current model is obtained for a very simplified growth conditions. For example, the model has no ampoule built into it. It is reported in literature [42] that the

ampoule plays an important role in determining the radial temperature distribution. So leaving the ampoule out of the model will change the dynamics of the interface shape during crystal growth. Therefore, incorporating the ampoule into the model will bring the model closer to reality.

The current model considers heat-conduction as the sole governing phenomena to determine the shape of the interface. There are other heat-transfer phenomena such as convection, and radiation that may play an important role in determining the interface shape. In the future, implementing these dynamics will make the model more accurate.

There are several variables such as h, k_l, k_s, L, c_p and ρ. As one may expect, the model is sensitive on the choice of these variables. However, these variables are known only approximately in real life. Therefore, choosing these variables as close to reality will make the model more accurate.

8.1.2 Discretization and Other Numerical Issues

The FE model used in this dissertation is obtained by a discretizing the domain very coarsely. It is very well known that too coarse discretization would result in erroneous solutions. This is one of the main short-comings of this dissertation. Conceptually, the proposed solution can be applied on a finer meshed model without any change. In the future, it is required to see how the proposed algorithm works on models obtained by discretizing the domain into very small regions.

In the current implementation, the banded structure of the mass, stiffness matrices have not been exploited while simulating the system. This would not only increase the speed of computation but also would increase the accuracy. Other standard tricks such as nodal re-numbering to reduce the band-width of the mass and stiffness matrices would also result in increased speed and accuracy.

The model is simulated using the explicit Euler scheme. In order to obtain reasonably accurate results, very small time-steps must be used. This results in increased number of computations. There are several implicit schemes that would increase the speed and accuracy of simulation. Also variable time-steps can be used to further increase the simulation speed. Other approximations such as lumped mass choice can also increase speed while trading accuracy. These approaches must be considered, especially, while discretizing the domain very finely.

8.1.3 Control Issues

One of the improvements that would increase speed in the computation of the control is to use Descriptor systems theory to design a controller without inverting the rather large matrix M. The LQR and LQG gain computation did not take advantage of the special structures in the mass, stiffness matrices. This is essential if one needs to compute controllers for a system that has a large number of states. Actually, this is one of the primary reason for the coarse discretization of the domain.

For the present model, it is found that a single controller based on a single linearized model is sufficient to establish the desired interface shape and move the same at the desired rate. However, for some other material, it may so happen that one may need more than one controller to achieve the desired objective. This is a challenging problem, especially, during the transition, when one controller takes over from the other.

There are several uncertainties in system brought about through the inexact knowledge of physical parameter, unmodeled dynamics, non-linearities, etc. Robust control design methodologies can account for these uncertainties. However, this would result in a very sluggish controller. If some information on the structure of the uncertainty can be gathered either by performing simulation experiments, or through experience, robust control techniques can design controllers that are not too conservative, and that can

yield the desired performance in presence of these uncertainties. In the future, the application of robust control techniques to the crystal growth problem must be examined.

In the current design, the bias input that establish non-zero steady-state is designed in an open-loop manner. To realize the full benefits of feedback, one has to determine bias input using feedback. Methods such as pseudo-integral control can tune the bias input using the feedback and establish the desired distribution in presence of constant disturbances. These approach should be researched in the future.

8.2 Concluding Remarks

Overall, this dissertation provided a new approach to solving the inverse heat-conduction problem during crystal growth. Several new results have been obtained. The simulation results presented in this dissertation demonstrate the capability of the proposed methods. There are several improvements that have been suggested in Section 8.1 to improve the proposed technique. Hopefully, the results in this dissertation together with the developments in the sensor technology will pave way to the production of crystals with improved quality.

REFERENCES

[1] J. A. Dantzig and D. A. Tortorelli, "Optimal design of solidification processes", Proceedings of the Conference on Inverse Design Concepts and Optimization in Engineering Sciences III, pp 213-226, Washington, DC, Oct., 1991.

[2] S. Rajendran, R. H. Mellen, "Advances toward intelligent processing of electronic materials", Journal of Crystal Growth, Vol. 85, pp. 130-135, 1987.

[3] C. Batur, R.B. Sharpless, W.M.B. Duval, B.N. Rosenthal and N.B. Singh, "Adaptive temperature profile control of a multi-zone crystal growth furnace," ASME Publication PED, Vol. 44, pp. 335-348, edited by S.Y. Liang, T.C. Tsao, 1990.

[4] C. Batur, R.B. Sharpless, W.M.B. Duval, B.N. Rosenthal and N.B. Singh, , "Identification and control of a multi-zone crystal growth furnace," Journal of Crystal Growth, Vol. 119, pp. 371-380, 1992.

[5] R. B. Sharpless, Intelligent Control of Crystal Growth, Master's Thesis, The University of Akron, Akron, Ohio, 1991.

[6] A. Srinivasan, C. Batur, R. J. Veillette, B.N. Rosenthal and W.M.B. Duval, "Projective control design for multi-zone crystal growth furnace", IEEE Transaction on Control System Technology., Vol. 2, No. 2, 1994.

[7] A. Srinivasan, Projective Control Design For Multi-zone Crystal Growth Furnace, Master's Thesis, The University of Akron, Akron, Ohio, 1993.

[8] C. E. Chang and W. R. Wilcox, "Control of interface in the vertical Bridgman-Stockbarger technique", Journal of Crystal Growth, Vol. 21, pp 135-140, 1974.

[9] N. B. Singh, W. M. B. Duval and B. N. Rosenthal, "Characterization of directionally solidified lead chloride", Journal of Crystal Growth, Vol. 89, pp 80-85, 1988.

[10] K. Taghavi and W. M. B. Duval, "Inverse heat transfer analysis of Bridgman crystal growth", International Journal of Heat and Mass Transfer, Vol. 32, No. 9, pp 1741-1750, 1989.

[11] J. Crank, Free and Moving Boundary Problems, Clarendon Press, Oxford, 1984.

[12] C. Mennetrier, M. A. Chopra and H. C. de Groh III, "Effect of thermal convection on the shape of a solid-liquid interface", ASME Publication FED-Vol. 111, pp 5-10, edited by A. Hashemi, B.N. Antar and I. Tanasawa, 1991.

[13] J. A. Dantzig, "Modeling liquid-solid phase changes with melt convection", International Journal for Numerical Methods in Engineering, Vol. 28, pp 1769-1785, 1989.

[14] V. R. Voller, C. R. Swaminathan, B. G. Thomas, "Fixed grid techniques for phase change problems: a review", International Journal for Numerical Methods in Engineering, Vol. 30, pp 875-898, 1990.

[15] H. S. Carslaw and J. C. Jaeger, Conduction of Heat in Solids, Clarendon Press, Oxford, 1959.

[16] J. C. Muehlbauer and J. E. Sunderland, "Heat conduction with freezing or melting", Applied Mechanics Review, Vol. 18, pp 951-959, 1965.

[17] P. C. Sukanek, "Deviation of freezing rate from translation rate in the Bridgman-Stockbarger technique I: very low translation rates", Journal of Crystal Growth, Vol. 58, pp 208-218, 1982.

[18] P. C. Sukanek, "Deviation of freezing rate from translation rate in the Bridgman-Stockbarger technique II: Moderate translation rates", Journal of Crystal Growth, Vol. 58, pp 219-228, 1982.

[19] D. L. Sikarskie and B. A. Boley, "The solution of a class of two-dimensional melting and solidification problems", International Journal of Solids and Structures, Vol. 1, pp 207-234, 1965.

[20] H. Budhia and F. Kreith, "Heat transfer with melting and freezing in a wedge", International Journal of Heat and Mass Transfer, Vol. 16, pp 195-211, 1973.

[21] N. Shamsundar, E. M. Sparrow, "Analysis of multidimensional conduction phase change via the enthalpy model", Journal of Heat Transfer, Vol. , pp 333-340, 1975.

[22] H. M. Ettouney and R. A. Brown, "Finite element methods for steady solidification problems", Journal of Computational Physics, Vol. 49, pp 118-150, 1983.

[23] A. Lazaridis, "A numerical solution of the multidimensional solidification (or melting) problem", International Journal of Heat and Mass Transfer, Vol. 13, pp 1459-1477, 1970.

[24] A. B. Crowley, "Numerical solutions of phase change problems, International Journal of Heat and Mass Transfer, Vol. 21, pp 215-219, 1978.

[25] R. M. Furzeland, "A comparative study of numerical methods for moving boundary problems", Journal Inst. Math. Applications, Vol. 26, pp 411-429, 1980.

[26] M. Yao and A. Chait, "An alternative formulation of the apparent heat capacity method for phase change problems", Numerical Heat Transfer, 1992. (in review).

[27] C. Bonacina, G. Comini, A. Fasano and M. Primicerio, "Numerical solution of phase-change problems", Heat and Mass Transfer, Vol. 16, pp 1825-1832, 1973.

[28] M. Yao and A. Chait, "Application of the homographic approximation in the enthalpy method for phase change problem, International Journal of Numerical Methods in Heat and Fluid Flow, Vol. 3, pp , 1993.

[29] Q. T. Pham, "A fast, unconditionally stable finite-difference scheme for heat conduction with phase change", International Journal of Heat and Mass Transfer, Vol. 28, pp 2079-2084, 1985.

[30] E. C. Lemmon, "Phase change technique for finite element conduction codes", Proceedings of the Conference on Numerical Methods in Thermal Problems, Editors, R.W. Lewis and K. Morgan, pp 149-158, 1979.

[31] K. Morgan, R. W. Lewis and O. C. Zienkiewicz, "An improved algorithm for heat conduction problems with phase change", International Journal of Numerical Methods in Engineering, Vol. 12, pp 1191-1195, 1978.

[32] G. Comini, S. Del Giudice and O. Saro, "A conservative algorithm for multidimensional conduction phase change", International Journal of Numerical Methods in Engineering, Vol. 30, pp 697-709, 1990.

[33] V. R. Voller and C. R. Swaminathan, "General source-based method for solidification phase change", Numerical Heat Transfer, Part B, Vol. 19, pp 175-189, 1991.

[34] V. R. Voller, "A fast implicit finite difference method for the analysis of phase change problems", Numerical Heat Transfer, Part B, Vol. 17, pp 155-169, 1990.

[35] J. V. Beck, Inverse Heat Conduction: Ill Posed Problem, John Wiley and Sons, New York, 1985..

[36] P. K. C. Wang, " Control of distributed parameter system", In the Advances in Control Systems: Theory and applications (ed. C. T. Leondes), Vol. 1, pp 75-172, 1964.

[37] M. J. Balas, "Trends in large space structure control theory: Fondest hopes, wildest dreams", IEEE Transaction on Automatic Control, Vol. 27, No. 3, 1982.

[38] R. E. Goodson, M. P. Polis", Parameter identification in distributed systems: a synthesizing overview", in Identification of Parameters in Distributed Systems (eds. R. E. Goodson, M. P. Polis), The ASME, 1974.

[39] S. G. Tzafestas and P. Stavroulakis, "Recent advances in the study of distributed parameter systems", Journal of the Franklin Institute, Vol. 315, pp 285-305, 1983.

[40] A.G. Butkowskiy, Structural Theory of Distributed Systems, Ellis Horwood Limited, Chichester, England, 1983.

[41] W. F. Ames, Numerical Methods for Partial Differential Equations, Academic press Inc, Boston, 1992.

[42] P. M. Adornato and R. A. Brown, "Convection and segregation in directional solidification of dilute and non-dilute binary alloys: Effects of ampoule and furnace design", Journal of Crystal Growth, Vol. 80, pp 155-190, 1987.

[43] R. E. Goodson, "Distributed system simulation using infinite product expansions", Simulation, Vol. 15, No. 6, pp. 255-273, 1970.

[44] S. Matsumoto and M. Yoshida, "A method of design for a controller for a parabolic-type distributed-parameter system. Application to one-dimensional thermal conduction", Int. Chem. Eng., Vol. 29, No. 1, 1989.

[45] M. J. Balas, "Feedback control of flexible systems", IEEE Transaction on Automatic Control, Vol. 23, No. 4, 1978.

[46] K. Glover, R. F. Curtain, J. R. Partington, "Realization and approximation of linear infinite-dimensional systems with error bounds", SIAM Journal of Control and Optimization, Vol. 26, No. 4, pp 862-898, 1988.

[47] B. A. Finlayson, The Method of Weighted Residuals and Variational Principles, Academic Press, New York, 1972.

[48] O. C. Zienkiewicz, The Finite Element Method, McGraw-Hill, London, 1977.

[49] T. Kailath, Linear Systems, Prentice-Hall Inc., Englewood Cliffs, NJ, 1980.

[50] J. V. Ramakrishnan, S.V. Rao, L. R. Koval, "Control of large space structures using reduced order modes", Control-Theory and Advanced Technology, Vol. 7, No. 1, pp 73-100, 1991.

[51] L. A. Zadeh and C. A. Desoer, Linear System Theory, McGraw-Hill, New York, 1963.

[52] J. L. Melsa and D. G. Schultz, Linear Control Systems, McGraw-Hill, New York, 1969.

[53] K. Ogata, Modern Control Engineering, Prentice-Hall Inc., Englewood Cliffs, NJ, 1970.

[54] M. Vidyasagar, "Control of distributed parameter systems using coprime factorization approach", Recent Advances in Control of Nonlinear and Distributed Parameter System, Robust Control and Aerospace Control Applications, Presented at the Winter Annual meeting of the ASME, pp 1-10, 1988.

[55] R. F. Curtain and A. J. Pritchard, Infinite Dimensional Linear System Theory, Lecture Notes in Control and Information Science, Vol. 8, Springer-Verlag, Berlin, 1978.

[56] C. A. Desoer and Y. T. Wang, "On the generalized Nyquist stability criterion", IEEE Transactions on Automatic Control, Vol. 25, pp 187-196, 1980.

[57] Y. Chait, C.R. Maccluer and C. J. Radcliffe, "A Nyquist stability criterion for distributed parameter systems", IEEE Transactions on Automatic Control, Vol. 34, pp 90-92, 1989.

[58] F. Pourki and R. Shoureshi, "A Lyapunov approach to finite order control for stabilization of distributed parameter systems", Recent Advances in Control of Nonlinear and Distributed Parameter System, Robust Control and Aerospace Control Applications, Presented at the Winter Annual meeting of the ASME, pp 45-50, 1988.

[59] F. Pourki and R. Shoureshi, "Stability of a class of distributed parameter systems with application to MPD thrusters", Recent Advances in Control of Nonlinear and Distributed Parameter System, Robust Control and Aerospace Control Applications, Presented at the Winter Annual meeting of the ASME, pp 189-194, 1988.

[60] M. C. Delfour and S.K. Mitter, "Controllability and observability for infinite-dimensional systems", SIAM Journal of Control, Vol. 10, pp 329-333, 1972.

[61] J. L. Lions, "Exact controllability, stabilization and perturbations for distributed systems", SIAM Review, Vol. 30, pp 1-68, 1988.

[62] A. El Jai and A. J. Pritchard, "Sensors and actuators in distributed systems", International Journal of Control, Vol. 46, pp 1139-1153, 1987.

[63] C. A. Jacobson and C. N. Nett, "Linear state-space systems in infinite dimensional space: The role and characterization of joint stabilizability/detectability, IEEE Transaction on Automatic Control, Vol. 33, No. 6, 1988.

[64] R. Rebarber and G. J. Knowles, "Conditions for stabilizability of distributed parameter systems", Proceedings of the 27th IEEE Conference on Decision and Control, pp 369-372, 1988.

[65] R. E. Goodson and R. E. Klein, "A definition and some results for distributed system observability", IEEE Transactions on Automatic Control, Vol. 15, pp 165-174, 1970.

[66] J. P. Gauthier and C. Z. Xu, "H^{∞} control of a distributed parameter system with non-minimum phase", International Journal of Control, Vol. 53, No. 1, pp 45-79, 1991.

[67] H. Ozbay, "H^{∞} optimal controller design for a class of distributed parameter systems", Submitted to Automatica for publication.

[68]. S. A. Pohjolainen, "Robust multivariable PI-controller for infinite dimensional systems", IEEE Transactions on Automatic Control, Vol. 27, pp 17-30, 1982.

[69] A. J. Pritchard and D. Salamon, "The linear quadratic optimal control problem for infinite-dimensional systems with unbounded input and output operators", SIAM Journal of Control and Optimization, Vol. 25, pp 121-144, 1987.

[70] A. Chicatelli, Methods for Developing Linear Reduced Models of Internal Flow Propulsion System, M. S. Thesis, University of Akron, Akron, 1990.

[71] C. C. Ih and S. J. Wang and C. T. Leondes, "Application of adaptive control to space stations", Proceedings of the AIAA Guidance, Navigation and Control Conference, pp 709-724, 1985.

[72] M. J. Balas, "Feedback control of flexible systems", IEEE Transactions on Automatic Control, Vol. 23, pp 673-679, 1978.

[73] J. Bontsema and R. F. Curtain, "A note on spillover and robustness for flexible systems", IEEE Transactions on Automatic Control, Vol. 33, pp 567-569, 1988.

[74] M. Athans, "Toward a practical theory for distributed parameter system", IEEE Transactions on Automatic Control, Vol. 15, pp 245-247, 1970.

[75] K. Glover, R. F. Curtain, J. R. Partington, "Realization and approximation of linear infinite-dimensional systems with error bounds", SIAM J. Control and Optimization, Vol. 26, No. 4, pp 862-898, 1988.

[76] M. A. Erickson, R. S. Smith and A. J. Laub, "Calculating finite-dimensional approximations of infinite-dimensional linear systems", Proceeding of the 1992 American Control Conference, pp 157-161, 1992.

[77] T. J. R. Hughes, The Finite Element Method, Prentice-Hall Inc., Englewood Cliffs, NJ, 1987.

[78] B. C. Moore, "Principal component analysis in linear systems: controllability, observability, and model reduction", IEEE Transactions on Automatic Control, Vol. 26, pp 17-31, 1981.

[79] M. G. Safanov and R. Y. Chiang, "A Schur method for balanced-truncation model reduction", IEEE Transactions on Automatic Control, Vol. 34, No. 7, pp 729-733, 1989.

[80] B. Friedland, Control System Design: An Introduction to State-Space Methods, McGraw-Hill Book Company, New York, 1986.

[81] M. G. Safanov, M. Athans, "Gain and phase margin for multiloop LQG regulators", IEEE transactions on Automatic Control, Vol. 22, No.2, pp 173-179, 1977.

[82] N. A. Lehtomaki, N. R. Sandell, Jr., M. Athans, "Robustness results in linear-quadratic Guassian based multivariable control designs", IEEE transactions on Automatic Control, Vol. 26, No. 1, 1981.

[83] J. C. Doyle, G. Stein, "Robustness with observers", IEEE transactions on Automatic Control, Vol. 24, No.4, pp 607-611, 1978.

[84] L. Pernebo, L. M. Silverman, "Model reduction via balanced state space representation", IEEE transactions on Automatic Control, Vol. 27, pp 382-387, 1982.

[85] D. S. Bernstein and I. G. Rosen, "An approximation technique for computing optimal fixed-order controllers for infinite-dimensional systems", Proc. of the 27th IEEE Conf. on Decision and Control, pp 2023-2028, 1988.

[86] R. K. Cavin III and S. C. Tandon, "Distributed parameter system optimum control design via finite element discretization", Automatica, Vol. 13, pp. 611-614, 1977.

[87] B. D.O. Anderson and J. B. Moore, Optimal Control: Linear Quadratic Methods, Prentice-Hall Inc., Englewood Cliffs, NJ, 1990.

[88] R. F. Stengel, Stochastic Optimal Control: Theory and Application, John Wiley and Sons, New York, 1986.

[89] J. Young, Personal Communication, Department of Mathematics, The University of Akron, Akron, OH, 1994.